Characterizing the WRN DNA Helicase in Prostate Cancer and Implications for Microsatellite Unstable Metastatic Prostate Cancers

Emily A. Kohlbrenner

A dissertation

submitted in partial fulfillment of the

requirements for the degree of

Doctor of Philosophy

University of Washington

2021

Reading Committee:

Peter S. Nelson, Chair

Raymond Monnat

Colin Pritchard

Program Authorized to Offer Degree:

Molecular Medicine and Mechanisms of Disease

University of Washington

Abstract

Characterizing the WRN DNA Helicase in Prostate Cancer and Implications for Microsatellite Unstable Metastatic Prostate Cancers

Emily A. Kohlbrenner

Chair of the Supervisory Committee:
Peter S. Nelson, Professor
Department of Medicine, Genome Sciences and Lab Medicine & Pathology

Prostate cancer is the most common non-skin malignancy in men worldwide and the second most common cause of cancer mortality in men. Metastatic prostate cancer (mPC) is highly heterogenous and enriched for aberrations in genes involved in DNA repair, the loss of which generates further genetic alterations and genomic instability that ultimately promotes tumorigenesis. The DNA Helicase-Exonuclease RECQL2 protein, commonly referred to as WRN, plays an integral role in DNA repair by regulating the dynamics of the replication fork. *WRN* is lost along the 8p chromosomal arm in 10% of prostate cancers; however, the role of WRN in mPC remains unclear. WRN has also been established as a promising target for synthetic lethality in mismatch repair deficient (MMRd) cancer cells with microsatellite instability (MSI), an aggressive subtype of metastatic disease that promotes oncogenesis via genome hypermutability.

We aimed to identify the prognostic value of *WRN*-specific copy loss in mPC patient tumors as well as investigate the sensitivity of MSI-mPC cell models to engineered WRN knockdown. We first showed that adverse outcomes are associated with *WRN* copy number status in mPC, and connect mutual exclusivity between loss of *WRN* and mismatch repair deficient tumors using large scale clinical datasets. Then, we tested the sensitivity to WRN inhibitor NSC 19630 in the LUCaP PDX xenograft lines, and found marked sensitivity in tumor lines with DNA Repair Deficiency (DRD). Further, we demonstrated that MSI prostate cancer cells are indeed sensitive to WRN loss over time. Finally, using quantified confocal imaging, we showed that tertiary DNA secondary structures at GC rich regions, known as G-Quadruplexes, are associated with replicative stress in MMRd-MSI cells and are themselves a promising target for chemotherapeutics. Together, this work expands the knowledge of DRD heterogeneity in mPC and provides novel insight into the molecular mechanisms of WRN sensitivity in MSI cells.

TABLE OF CONTENTS

List of Figures

Acknowledgements

The following work could not have been completed without the help and support of my mentors, friends, and family.

I would like to thank Pete and my committee members Ray Monnat, Liz Swisher, Colin Pritchard and Kathi Malone for their input and support over the years as this thesis has grown and shifted in different directions. This project also would not have manifested in the way that it did without the insight of the late Alan Herr, who was a wonderful mentor and friend to all who knew him and to whom, alongside all cancer patients and the people who love them, this work is dedicated.

I would like to thank the members of the Nelson lab who have stepped in and helped me with new ideas, assays and directions in lab, brought me to endless coffee and lunch vent-sessions, and above all made five years of (sometimes tedious) lab work entertaining every day.

I would like to thank everyone in the M3D graduate program for your endless support, laughs, kindness and community you've fostered that has made Washington feel like home during this chapter of my life.

Thank you to my family for supporting me through it all and believing in everything I do, and to my friends near and far for making my life outside of lab adventurous, enriching and endlessly funny.

Most especially, thank you to Kevin. I am continually grounded by your love, support and scientific insight, and can't wait for our next adventure together.

Introduction

Prostate cancer is the most common non-skin malignancy in men worldwide and the second most common cause of cancer mortality in men[1]. With advancements in screening and early detection strategies, the majority of men are diagnosed with localized disease and have a five-year survival rate that approaches 100%; however, in men who present with metastatic disease, the five-year survival rate plummets to 30% and is ultimately lethal (https://seer.cancer.gov/statfacts/html/prost.html).

The standard of care for metastatic prostate cancer (mPC) centers on the suppression of the androgen receptor (AR) activity. Surgical or chemical suppression of androgen production or signaling via androgen deprivation therapy (ADT) is the most effective initial treatment for mPC, and though initially successful, often progresses to a therapy-resistant subtype known as castration resistant prostate cancer (CRPC). The predominant mechanism of this resistance to ADT is the cellular reactivation of AR and the synthesis of intracrine AR ligands that promote growth and treatment resistance, and once established, prognosis is poor. Identifying mechanisms of resistance, determining the optimal combination of therapies, and utilizing molecular subtypes and biomarkers to drive personalized medicine remain the current clinical challenges and priority for research development[2].

As with other malignancies, the accumulation of mutational aberrations and increasing genetic instability underlies mPC. mCRPC is characterized by recurrent somatic mutations including *AR* mutation or amplification, and the loss of *TP53*, *PTEN*, *RB1*, *BRCA1* or *BRCA2* and *CDK12*, largely altering the AR, PI3K and WNT signaling

pathways as well as the ability to regulate the cell cycle and accurately coordinate DNA repair during replication[3–5]. DNA repair protein machinery is central to a cancer cell's ability to generate and maintain the genomic instability that ultimately promotes tumorigenesis. Importantly, it is now recognized that men with inherited mutations in genes involved in DNA repair have an increased susceptibility to aggressive PC[6–8]. Loss of DNA repair proteins such as BRCA2, ERCC2 or MSH2 increase the buildup of alterations in the DNA, increasing genomic instability and ultimately activating tumor promoting mechanisms[9].

Fortunately the usage of clinical genomics in tandem with treatment advancements have been able to define further subtypes that can be clinically targeted, often with dramatic responses. Recent developments in precision oncology, specifically matching the administration of poly (ADP-ribose) polymerase inhibitors (PARPi) with those tumors having the specific type of DNA repair deficiency involving homologous recombination repair (HRR), exploit tumor-promoting defects in DNA repair mechanisms to cause synthetic lethality and tumor regression[9]. In 2015, a small clinical study of the PARPi Olaparib found that men with mPC harboring pathogenic DNA repair gene variants such as mutations in *BRCA1/BRCA2* had life-extending responses to PARPi, whereas those without such defects had no benefit[10]. The more recent PROfound trial in CRPC further supported these findings in a larger cohort, demonstrating response to Olaparib from men harboring germline or somatic aberrations in *BRCA1/BRCA2* as well as a larger cohort of genes involved in the DNA damage response (DDR)[11].

Mechanistically, it was originally proposed that PARP-1 inhibition increased single strand breaks in the DNA that were toxic to a homologous recombination repair-

deficient (HRRd) system, but new experimental evidence suggests that replication fork obstruction, caused by PARP-1 trapping on the DNA, may contribute more to the ultimately lethal genotoxic stress[12]. Current research suggests that pharmacologically inducing stalling and collapse of the replication fork may be a promising therapeutic avenue in DNA repair deficient tumors, and increasing our understanding of replication fork dynamics will help to expand synthetic lethal approaches across many tumor subtypes. Additionally, as many therapeutic agents both induce DNA breaks and target the DDR, it is critical to better understand the different molecular subtypes of DNA repair aberrations, as well as corresponding therapeutic susceptibilities, in order to better target the intra-patient tumor burden.

One such protein upstream of PARP1 that also predominantly functions at the replication fork is DNA helicase RECQL2, better known as Werner syndrome protein (WRN). WRN is comprised of a 3'-5' DNA helicase and exonuclease domains and is utilized during DNA replication and repair to unwind DNA and to resolve DNA secondary structures that may arise and impede the replication fork. WRN has been most extensively studied in the context of its associated autosomal recessive genetic disease, Werner syndrome, which manifests in premature aging and susceptibility to myocardial infarction, cancer predispositions and ultimately decreased lifespan[13–16].

WRN has been established as a functional tumor suppressor, lost predominantly in tumors via promoter methylation, mutation or loss of heterozygosity[17–19]. WRN is located along the chromosome 8p arm, which in itself is commonly lost in prostate cancer[20]. 8p arm loss has been associated in aggressive disease onset[21,22]. In *in vitro* models, 8p arm loss has been demonstrated to act as a tumor suppressive circuit that

drives progression early on when lost by altering lipid metabolism, though the clinical associations and outcomes of WRN-specific loss along this arm is not known[23].

Loss of WRN protein has also been shown to increase tumor sensitivity to topoisomerase I inhibitors, though the functional utility of WRN as a biomarker for topoisomerase inhibitor treatment remains disputed[17,24–26]. Due to its involvement in DNA replication and the DDR, WRN itself has been the focus of therapeutic development targeting the DDR in tumors[27,28]. WRN has also been proposed as a promising target for selective toxicity in mismatch repair deficient (MMRd) and microsatellite unstable (MSI) cancer cells, as large scale CRISPR knock-out and RNAi knock-down screens have demonstrated WRN loss as a unique synthetically lethal target for cancer cells with MSI[29–31]. Though this mechanism is not yet well understood, experimental evidence suggests that WRN is required to mediate the resolution of DNA-secondary structures that form at repeat regions that are expanded in MSI cancer cells, causing replication fork blockage, DNA damage, irreparable genotoxic stress and ultimately cell death[32].

Loss of MMR capability over time leads to the rapid accumulation of mutations and the loss of genomic fidelity during the replication cycle, often resulting in somatic hypermutation and the expansion of existing microsatellite repeat regions, generating MSI. Regardless of histology or tumor origin, patients with MSI tumors have exhibited promising clinical outcomes to immune checkpoint blockade, and as such, diagnosed MMRd/MSI solid tumors are the first molecular subgroup to be approved for pembrolizumab. Men with MMRd or MSI mPC present with a high Gleason score and advanced disease, and similar to patients with other MMRd or MSI-high cancers, also

had a successful response to immune checkpoint blockade treatment[33]. However, not all patients have seen universal success from this treatment, and further optimizing patient response by targeting a protein such as WRN is a promising avenue forward.

In the following study, we characterize *WRN* status in mPC and investigate the utility of targeting WRN in *in vitro* models. We found a chromosomal homozygous deletion along the 8p arm drives *WRN* loss in mPC, and mutual exclusivity between this genetic loss, driver mutations in mismatch repair genes and tumors with microsatellite instability. Characterizing WRN-loss in *in vitro* mPC cell lines, we found significant sensitivity to WRN knockdown in cell lines with MSI. Finally, we proposed a mechanism of MSI cancer sensitivity to WRN loss, centralizing on the essentiality of the WRN protein to resolve G-quadruplex DNA secondary knots formed from expanded GC repeats in MSI genomes. This work expands the characterization of WRN status in mPC and provides promising evidence for its therapeutic targeting in MMRd/MSI tumors.

Chapter 1. Characterizing WRN DNA Helicase in Prostate Cancer

Emily Kohlbrenner[1], Lisa Ang[2], Ilsa Coleman[2], Navonil deSarkar[2], Sander Frank[2], Peter S. Nelson[1,2*]

[1] Department of Pathology, University of Washington School of Medicine, Seattle WA

[2] Fred Hutchinson Cancer Research Center, Seattle, WA

1.1 Abstract

The Werner Syndrome DNA Helicase, WRN, has been well characterized for its loss of function via germline mutation leading to the premature ageing phenotype known as Werner Syndrome. However, the functional consequence of WRN loss via copy number variation (CNV), as seen in 10% of prostate cancers, along the 8p chromosomal arm has not been investigated. Though the loss of chr.8p has been well documented to occur in carcinomas arising in many different organs, and believed to contain putative tumor suppressors, the prognostic value of WRN-specific copy loss in metastatic prostate cancer (mPC) remains unexplored. In this study we investigated the clinical variables associated with WRN copy number status in mPC and identify mutual exclusivity between loss of WRN and mismatch repair deficiency and hypermutation in both prostate and across all TCGA PANCANCER datasets. Finally, to extend the range of mPC patients who may benefit from WRN inhibitors, we used LuCaP PDX xenografts

to test sensitivity to WRN inhibitor NSC 19630 in LuCaP lines with DNA Repair Deficiency (DRD) and microsatellite instability (MSI).

1.2 Introduction

Prostate cancer (PC) is the second most prevalent cancer diagnosis and cause of cancer related mortality in men. Identifying clinically useful prognostic biomarkers, targeted treatment for metastatic disease, more diverse molecular stratification subtypes, and more accurate surrogate biomarkers that predict overall survival are all central to improving the standard of care for metastatic PC (mPC)[1].

Similar to other malignancies, the accumulation of mutational aberrations and increasing genetic instability[5,34,35] underlies mPC and men with mutations in DNA repair genes are particularly susceptible to aggressive disease progression[9,34]. Recent developments in precision oncology exploit these tumor-promoting defects in DNA repair through targeted therapeutics that cause tumor regression, most notably, by the successful utilization of poly (ADP-ribose) polymerase inhibitors in tumors with homologous recombination deficiency [36]. However, the use of targeted approaches by subgrouping mPC patient population based on specific molecular phenotypes to improve clinical outcomes in patients with PC remains elusive. Expanding and redefining clinically actionable subtypes of DNA Repair Deficiency (DRD) has the potential to expand the number of patients that may benefit from alternative targeted therapeutics.

Many genes that reside on chromosomal arm 8p, commonly lost in mPC, are considered to be putative tumor suppressors with well-characterized tumor promoting effects [21,22,37,38] . One such gene, *WRN*, is found on this arm and thus frequently lost in advanced disease. Werner's syndrome protein, WRN, has been extensively studied in for its critical role in replication and genomic maintenance[16,39,40]. Though WRN mutational or epigenetically controlled loss has been described in other cancers, the clinical outcomes of this protein-specific copy loss from the 8p deletion remains to be demonstrated[24,41,42]. This question is especially relevant in the context of developing WRN-targeting therapeutics for mismatch repair deficient (MMRd) and microsatellite unstable (MSI) tumors, which have been shown to be especially sensitive to the loss of WRN[30,43,44].

It is a priority to determine if MMRd and MSI patient tumors, largely more complex than cell lines, may also be vulnerable to WRN therapeutic targeting[27]. With clinical testing farther away, large genomic clinical datasets may be able to provide a necessary intermediate step to determine if this observed dependent relationship can be exploited beyond cell lines and into human tumors. Given that functional WRN expression is required for successful therapeutic targeting by a WRN-inhibitor, it is imperative to determine what type, and within which tumors, genomic aberrations alter WRN expression. To determine if *WRN* copy number status had an influence on transcriptional regulation or associated with adverse clinical outcomes, we used the Stand Up To Cancer (SU2C) metastatic prostate cancer (mPC) clinical dataset to characterize *WRN* status in mPC. We then utilized an established mPC LuCaP PDX

cohort, paired with corresponding genomic sequencing, to test sensitivity to established WRN inhibitor, NSC 19630, by genomic subtype.

1.3 Materials and Methods

Sequencing Datasets, Clinical Variables and Mutual Exclusion Analysis

Oncoplots were generated from sequenced datasets from cBioPortal (http://cbioportal.org) as previously described[45,46]. Associated clinical variables were downloaded for each dataset, categorized into groups by genetic alteration or expression status, and graphed accordingly. Survival plots within each clinical dataset were graphed displaying tumor samples grouped by the presence or absence of the selected alteration. Mutual exclusivity between genetic alterations in the same tumor sample was analyzed as previously described [47]. Whole transcriptome sequencing (RNAseq) and analysis was performed and analyzed as previously described[48].

Ex vivo tissue culture and treatment assays

Harvested LuCaP PDX tumors were excised and disassociated within 1 hr of removal as previously described[49,50]. Tumors were digested in 10% serum containing media (1 mg/mL collagenase+1 mg/ml dispase) for 1 hr followed by 10 min in TrypLE and passed through a by a 0.45-mm filter. Individual cells were seeded at 8k cells per well in a 96-well black-bottomed plate (Corning) and luminescence was measured on a Synergy H1 microplate reader by Cell Titer Glo, as per the manufacturer's instructions (Promega), to determine cell viability. A doxycycline-inducible Tet-LNCaP^{BRCA2} knockdown line was generated as previously described[51]. WRN inhibitor NSC 19630

(Millipore) was used in this study. Cells were treated with chemotherapeutics for 72 hrs before confocal imaging.

Confocal microscopy

Cells were plated at 100k per well density on coverslips in 6-well dishes in growth media or treated with DMSO, 3uM or 6uM NSC 19630. After 72 hrs, cells were fixed with 4% paraformaldehyde for 30 min, permeabilized in 0.2% triton X-100 in PBS for 7 min and blocked in 3% FBS PBS-tx for 1 hr. Coverslips were immunostained in 53BP1 (Abcam ab175933) primary antibodies for 90 min followed by fluorescently conjugated secondary antibody AlexA Fluor goat anti-rabbit (Invitrogen) for 1 hr and counterstained with DAPI (Vector Laboratories). Slides were analyzed across multiple microscope fields at 63x oil on the confocal, and foci from 80-100 cells were counted per individual cell via Image J and plotted.

Immunohistochemistry

Cells were plated at 100k per well in 6-well dish and grown for 48 hr before isolation for western blotting. Cells were washed in PBS and covered in 200ul lysis solution (1% SDS, 1% NP-40, 2% Tween-20, 1.5 M Urea) and collected using a cell scraper. Lysates were boiled for 2 min, sheared by sonication and immunoblotted as described[52].

Statistical analysis

Knockdown comparisons were direct comparison of continuous variables, compared to non-targeting shNTC control using a Student's t-test on Graph-Pad Prism 6 to generate graphs and analyses. Two-sided P-values are presented with * $P < 0.05$, ** $P < 0.01$ and *** $P < 0.005$ as mean ± standard deviation (SD). At least three

independent experiments were used for each experimental group and analyzed in total as presented. Log rank test statistic was used for all Kaplan-Meier survival analysis and mutual exclusivity calculations.

1.4 Results

1.4.1 Alterations in the WRN Helicase in Primary and Metastatic Prostate Cancer

Of reported genomic aberrations, *WRN* was lost via homozygous deletion in 10% of primary (TCGA PRAD N=499) and 8% of metastatic (SU2C N=444) adenocarcinomas (Figure 1.1A, Supplemental figure 1.1). *WRN* copy number variation (CNV) status associated with RNA transcriptional expression in both primary and metastatic disease; notably tumors with homozygous (deep) and heterozygous (shallow) deletion of *WRN* correlated with low WRN transcription expression (Figure 1.1B-C).

1.4.2 Loss of WRN Associates with Adverse Metastatic Prostate Cancer Outcomes

Deep deletion of *WRN* was associated with significantly worse overall and disease-free survival (OS) in primary, but not in metastatic, PC (Figure 1.1D-E, Supplemental Figure 1.1C). However, mPC patients with *WRN* homozygous deletion had a higher AR score and lower neuroendocrine (NEPC) score as compared to diploid tumors, had a higher percent of tumors with Gleason Score 8 and were not associated with NEPC features. Tumors with a shallow deletion of *WRN* had a higher AR score,

lower age of diagnosis and presence of androgen receptor-V7 (ARV7) as compared to diploid. Patients with a gain in *WRN* were more likely to have received abiraterone (ABI) and enzalutamide (ENZA) and had a higher percent of tumors with ETS fusions. There was no observed enrichment for prostate-specific antigen (PSA), but *WRN*-homdel tumors had co-occuring loss of *TP53* and *PTEN*, and amplification of *MYC*, *AMER1* (WNT signaling), *PIK3CA* and *STK3* (HIPPO pathway) (Figure 1.2, Supplemental Figure 1.2). Interestingly, the deep deletion of *WRN* had an inverse correlation with the number of total tumor mutations (Figure 1.3A). To validate this observation, we looked at the number of tumor mutations by *WRN* copy number status across the entirety of the PAN-Cancer TCGA (PANCAN TCGA N= 10,953 patients from a combined study of 32 TCGA cancer cohorts) as well as PRAD, and observed the same inverse correlation (Figure 1.3B-C). Further, we looked at the quantity of microsatellite loci in the genome, calculated by MSisensor score, and observed an enrichment for low MSI-status in tumors with *WRN* deep deletion (Figure 1.3D-E).

1.4.3 Homozygous Deletion of *WRN* is Mutually Exclusive to Driver Mutations in Mismatch Repair Genes

To validate WRN essentiality in human MSI+ tumors, we determined the mutual exclusivity between driver mutations in mismatch repair (MMR) genes, the precursor and established diagnostic biomarker driving MSI+ tumors[53], and the loss of *WRN* via homozygous deletion. MMR gene driver mutations and *WRN* homozygous deletion were mutually exclusive in both PRAD and mPC datasets, as well as across all TCGA cancers (Figure 1.4A, Supplemental Figure 1.3 and Supplemental Figure 1.4A-C).

Notably, using the PANCAN TCGA datasets we observed that the total frequency of *WRN* homozygous deletion was higher in cancers where MSI is less common, such as prostate and liver cancers, as compared to endometrial or cervical cancer (Figure 1.4B, Supplemental Figure 1.4D). Further, across multiple TCGA cancers, we observed inverse up and down transcriptional regulation of WRN and individual MMR-genes (Figure 1.4C, Supplemental Figure 1.5).

1.4.4 The WRN inhibitor may be a therapeutic target for DNA repair deficient metastatic prostate cancer

WRN-selective inhibitor NSC 19630 has been determined to effectively suppress growth in cell models, though it's effect in MSI+ cells remains unknown[27]. We sought to ascertain if WRN could be therapeutically targeted in human tumors via disassociating and treating propagated xenograft PC models[49,50]. Notably, the LuCaP PDX series expresses WRN RNA and protein in MSI+ tumor samples, and WRN expression correlates with copy expression (Figure 1.5). PDX LuCaP tumors were disassociated, grown *in vitro* and treated with 3 or 6 µM NSC 19630, we observed that WRN inhibition was more effective reducing cell viability after 3 µM NSC 19630 in tumors with established DNA-repair deficiencies. In LuCaP 147 and 147CR, established mPC MSI+ lines, growth suppression was also observed (Figure 1.6). To further determine if HRRd tumors could be sensitive to WRN inhibition, we used an established dox-inducible LNCaP^{BRCA2} knockdown line to test both WRN protein and chemical inhibition in the context of BRCA2 loss. We observed a decrease in proliferation in the dox- LNCaP^{BRCA2} cells when given pooled siWRN RNAi as compared to the no dox cells, all normalized to

a scrambled non-targeting RNAi pool. Additionally, though there was not clinical mutual exclusivity between *BRCA1* or *BRCA2* genetic loss and *WRN* homozygous deletion in prostate tumors, dox-LNCaP^{BRCA2} cells displayed increased 53BP1 foci after 3 and 6 µM 19630 treatment as compared to control (Supplemental Figure 1.6).

1.5 Discussion

WRN is lost in about ~10% of both primary and metastatic disease, via a large chromosomal homozygous deletion along chromosome 8p. 8p arm loss has been associated with adverse outcomes, though the effects of individual protein loss via the large arm event has not been explored. We show that copy number variation is correlated with WRN transcriptional expression, and homozygous deletion results in loss of WRN expression. As this was universally seen across many cancers, it is clinically relevant for the future development of genetic biomarkers.

To justify the goal of eventually targeting WRN pharmacologically in MSI+ patients, we first sought determine if this observed synthetically lethal phenotype translated to clinical patient tumors. It has been previously demonstrated that WRN targeting therapeutics are less effective when WRN is not expressed[27,54], and as WRN itself is lost in a fraction of prostate tumors, it was essential to establish if the loss of *WRN* via homozygous deletion was mutually exclusive to the loss of MMR proteins via deleterious mutations, the established genetic precursor to MSI development [53,55]. Mutual exclusivity was present in both prostate and pan-cancer TCGA datasets, which provides evidence that WRN and mismatch repair protein loss do not frequently co-occur in clinical samples and MMR-status could be a potential biomarker for future WRN-targeting.

Additional research is required to determine the effect of WRN inhibitors in *in vivo* models, however, preliminary studies ex-vivo suggests that tumors with DNA repair deficiency may universally benefit from WRN therapeutic targeting. Further, as *WRN* is one gene of many lost in the 8p chromosomal deletion, we may not be capturing the full scope of clinical utility[20]. As *WRN* is not focally lost as a tumor suppressor, it is possible that the combinatory effects of 8p loss, or concurrent with 8q gain, are more significant than *WRN* loss itself. As such, future experiments will use CRISPR technology to selectively remove the 8p arm and repeat the cellular viability and metastatic potential experiments above. There may be additional putative tumor suppressors with higher penetrance than *WRN* residing on 8p, so future work will expand this methodology to compare these results to additional proteins, such as NEIL2. Importantly, the present study provides evidence that MSI+ PC patients should not be excluded from future investigations involving WRN-antagonizing agents.

We propose that the mutual exclusivity between MMR and *WRN* aberrations across cancer suggests that these biological phenomena could be translational to patients upon the advent of better WRN-inhibitors. This investigation proposes to add a broader context to the clinical value of the observed dependency of MSI cells on the WRN protein, using a systems-level genomic approach, and concludes with a clearer picture on how to stratify subtypes of targetable DRD.

1.6 List of Figures

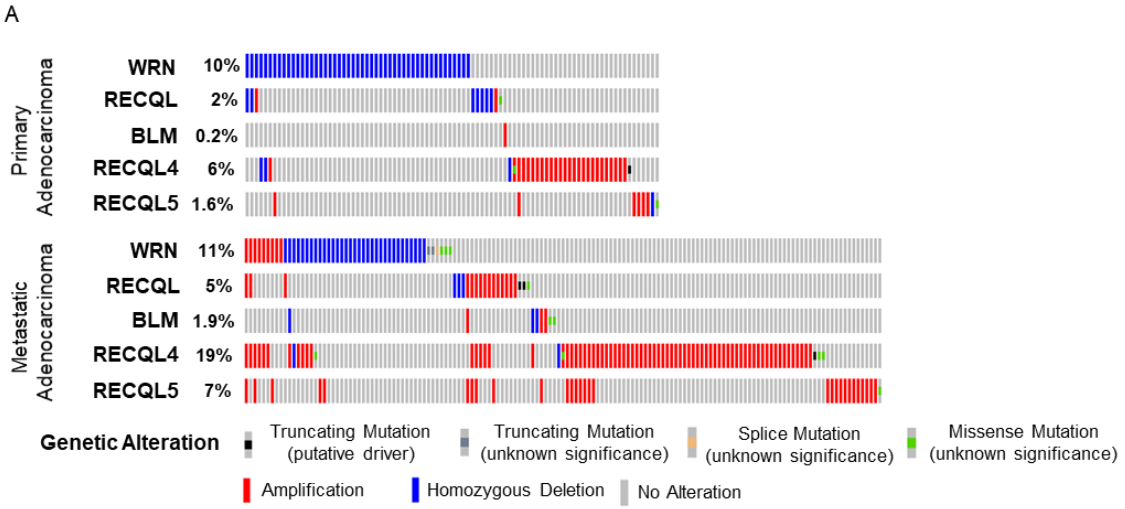

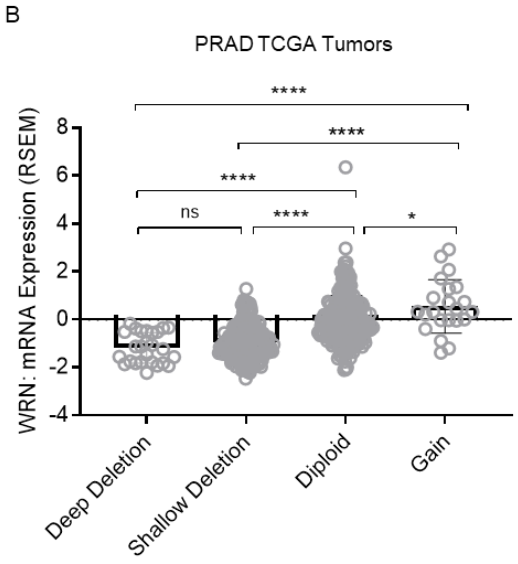

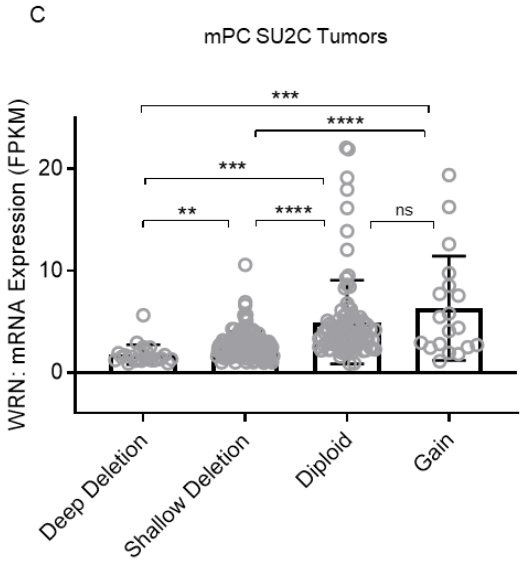

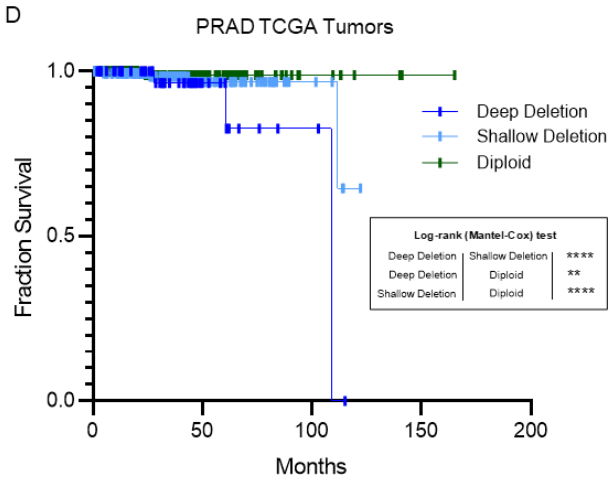

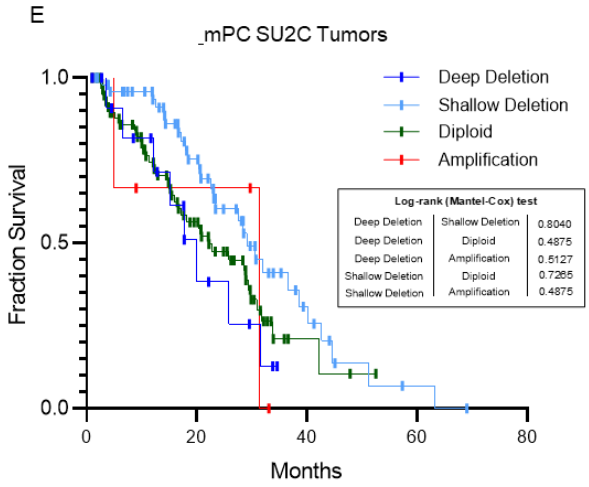

Figure 1.1.The WRN DNA helicase is altered in a subset of localized and metastatic prostate cancers. (A) Oncoplot (http://cbioportal.org) of *RECQL* aberrations in primary (PRAD TCGA firehose N=499) and metastatic (SU2C N=444) prostate cancer. (B-C) The correlation of WRN transcriptional expression (RNAseq) versus copy number status in both primary (PRAD)(B) and metastatic (SU2C)(C) prostate cancer. (D-E) Fraction of Primary (D) and Metastatic (E) Adenocarcinoma patient overall months survival based on *WRN* copy number status (log rank test).

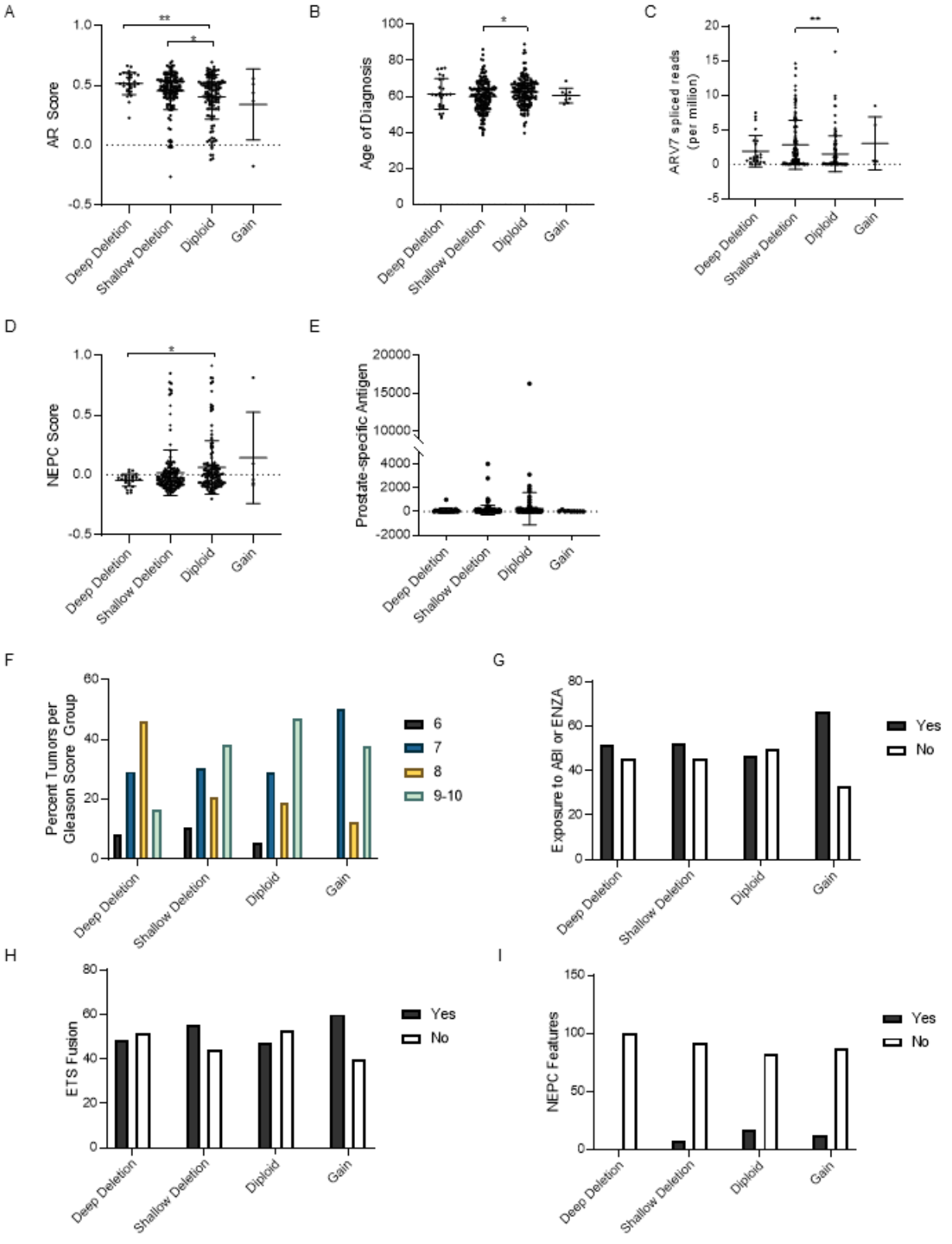
A
AR Score
1.0
0.5
0.0
-0.5
**
*
Deep Deletion
Shallow Deletion
Diploid
Gain
B
Age of Diagnosis
100
80
60
40
20
0
*
C
ARV7 spliced reads (per million)
20
15
10
5
0
-5
**
D
NEPC Score
E
Prostate-specific Antigen
20000
15000
10000
4000
2000
0
-2000
F
Percent Tumors per Gleason Score Group
60
40
20
0
6
7
8
9-10
G
Exposure to ABI or ENZA
80
60
40
20
0
Yes
No
H
ETS Fusion
I
NEPC Features
150
100
50

Figure 1.2. WRN loss in mPC is associated with clinical and genomic features. (A-I) Metastatic prostate cancer clinical data comparing tumors with *WRN* homozygous and heterozygous deletion as compared to tumors with diploid or copy gain of *WRN* (SU2C N=444). Plots display *WRN* status versus tumor (A)AR-score, (B) the age at diagnosis , (C) presence of androgen receptor ARV-7 variant, (D) neuroendocrine prostate score (NEPC) , (E) prostate-specific antigen, (F) Gleason Score group, (G) the percent of tumors exposed to abiraterone and enzalutamide, (H) the percent of tumors with ETS-fusions, (I) and the percent of tumors classified having neuroendocrine features. **P < 0.01 by One Way ANOVA.

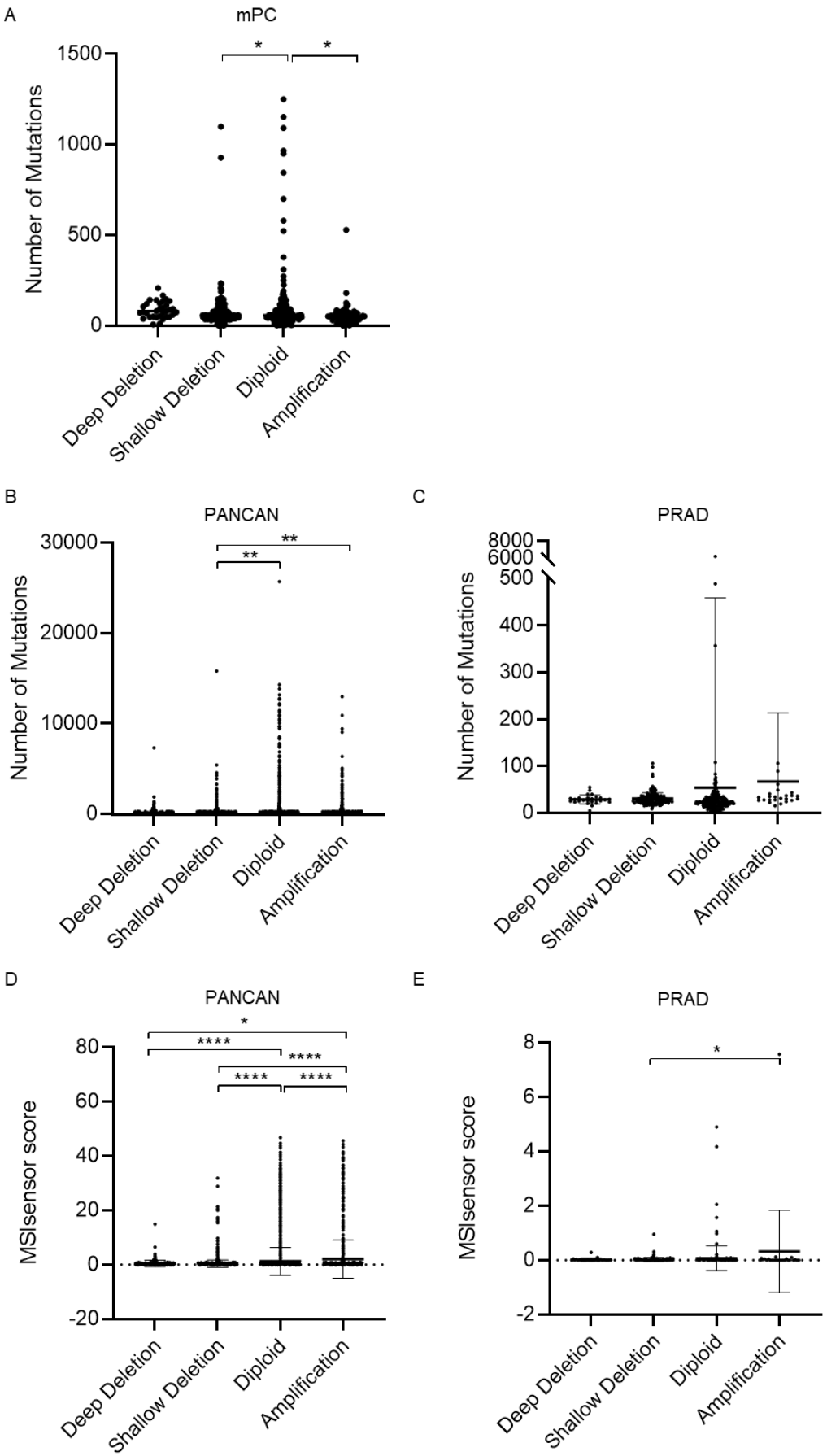
A
mPC
Number of Mutations
1500
1000
500
0
*
*
Deep Deletion
Shallow Deletion
Diploid
Amplification
B
PANCAN
Number of Mutations
30000
20000
10000
0
**
**
Deep Deletion
Shallow Deletion
Diploid
Amplification
C
PRAD
Number of Mutations
8000
6000
500
400
300
200
100
0
Deep Deletion
Shallow Deletion
Diploid
Amplification
D
PANCAN
MSIsensor score
80
60
40
20
0
-20
*
****
****
****
****
Deep Deletion
Shallow Deletion
Diploid
Amplification
E
PRAD
MSIsensor score
8
6
4
2
0
-2
*
Deep Deletion
Shallow Deletion
Diploid
Amplification

Figure 1.3. Homozygous deletion of *WRN* does not associate with hypermutation or microsatellite instability. (A) *WRN* CNA status in mPC (SU2C N=444) by number of total mutations. (B-C) CNA status of *WRN* and the associated corresponding number of mutations across (B) PAN-Cancer TCGA and (C) PRAD TCGA. (D-E) CNA status of *WRN* as compared to tumor MSIsensor score across (D) PAN-Cancer TCGA and (E) PRAD TCGA

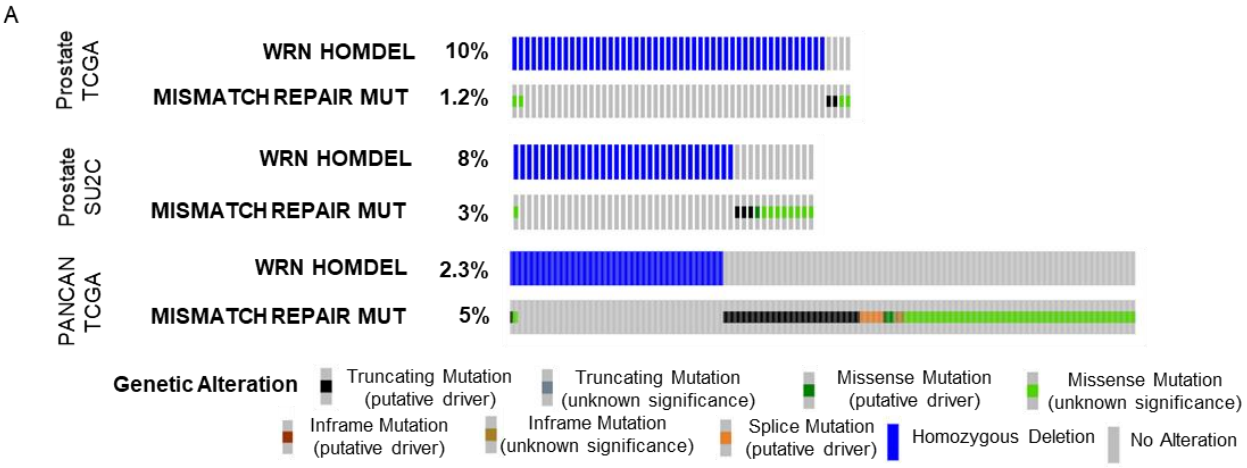
A
Prostate TCGA
WRN HOMDEL 10%
MISMATCH REPAIR MUT 1.2%
Prostate SU2C
WRN HOMDEL 8%
MISMATCH REPAIR MUT 3%
PANCAN TCGA
WRN HOMDEL 2.3%
MISMATCH REPAIR MUT 5%
Genetic Alteration
Truncating Mutation (putative driver)
Truncating Mutation (unknown significance)
Missense Mutation (putative driver)
Missense Mutation (unknown significance)
Inframe Mutation (putative driver)
Inframe Mutation (unknown significance)
Splice Mutation (putative driver)
Homozygous Deletion
No Alteration

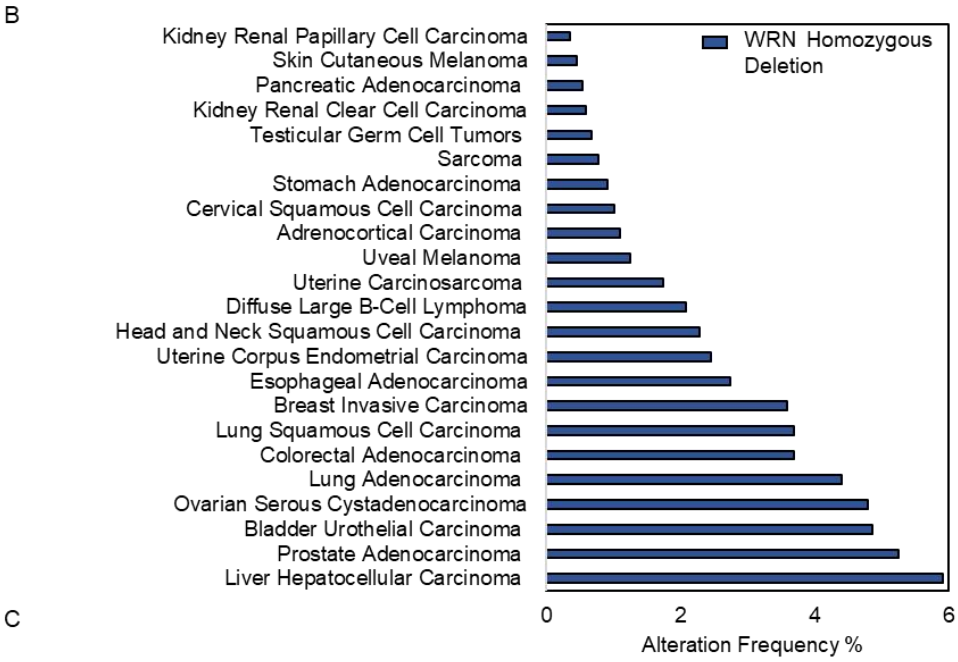
B
WRN Homozygous Deletion
Kidney Renal Papillary Cell Carcinoma
Skin Cutaneous Melanoma
Pancreatic Adenocarcinoma
Kidney Renal Clear Cell Carcinoma
Testicular Germ Cell Tumors
Sarcoma
Stomach Adenocarcinoma
Cervical Squamous Cell Carcinoma
Adrenocortical Carcinoma
Uveal Melanoma
Uterine Carcinosarcoma
Diffuse Large B-Cell Lymphoma
Head and Neck Squamous Cell Carcinoma
Uterine Corpus Endometrial Carcinoma
Esophageal Adenocarcinoma
Breast Invasive Carcinoma
Lung Squamous Cell Carcinoma
Colorectal Adenocarcinoma
Lung Adenocarcinoma
Ovarian Serous Cystadenocarcinoma
Bladder Urothelial Carcinoma
Prostate Adenocarcinoma
Liver Hepatocellular Carcinoma
0
2
4
6
Alteration Frequency %

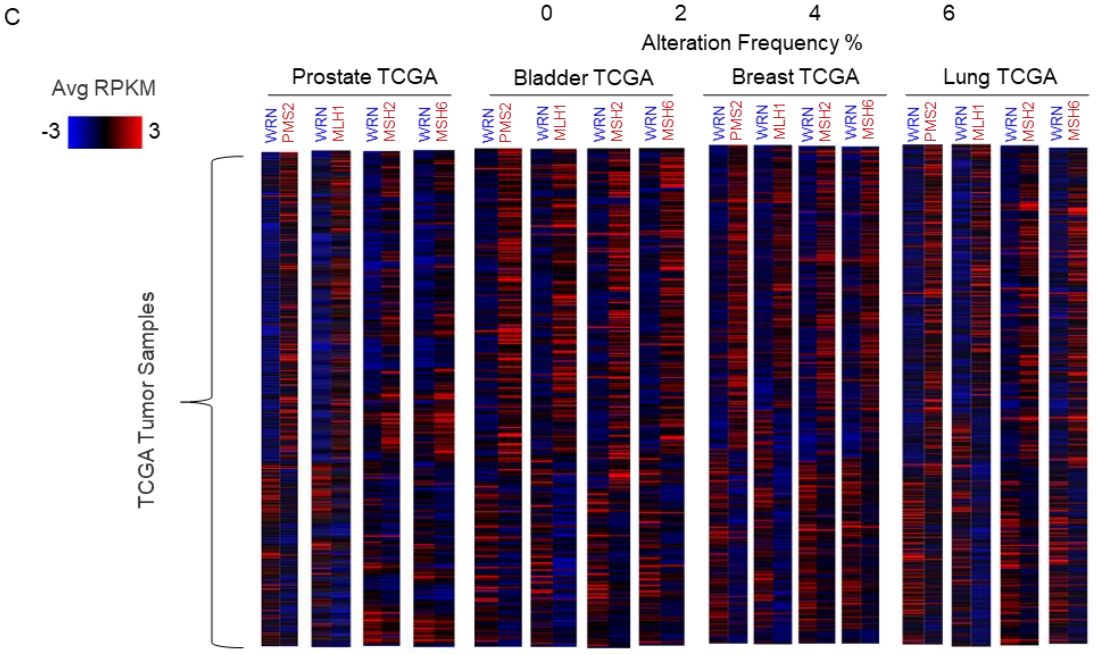
C
Avg RPKM
-3
3
Prostate TCGA
Bladder TCGA
Breast TCGA
Lung TCGA
WRN PMS2
WRN MLH1
WRN MSH2
WRN MSH6
TCGA Tumor Samples

Figure 1.4. *WRN* copy loss is mutually exclusive to MMR driver mutation. (A) Oncoplot of mutations in mismatch repair genes versus *WRN* homozygous deletion across PRAD TCGA, mPC SU2C and PANCAN TCGA, datasets. Tumors without alterations are omitted to save space. (B) The percent alteration frequency of *WRN*-specific homozygous deletion across TCGA PANCAN tumors. (C) transcriptional expression (RNAseq average RPKM) of *WRN* and mismatch repair genes across prostate adenocarcinoma (N = 499), bladder urothelial carcinoma (N = 411), breast invasive carcinoma (N = 1084) and lung adenocarcinoma (N = 566) TCGA individual tumors. Each column represents an individual tumor expression.

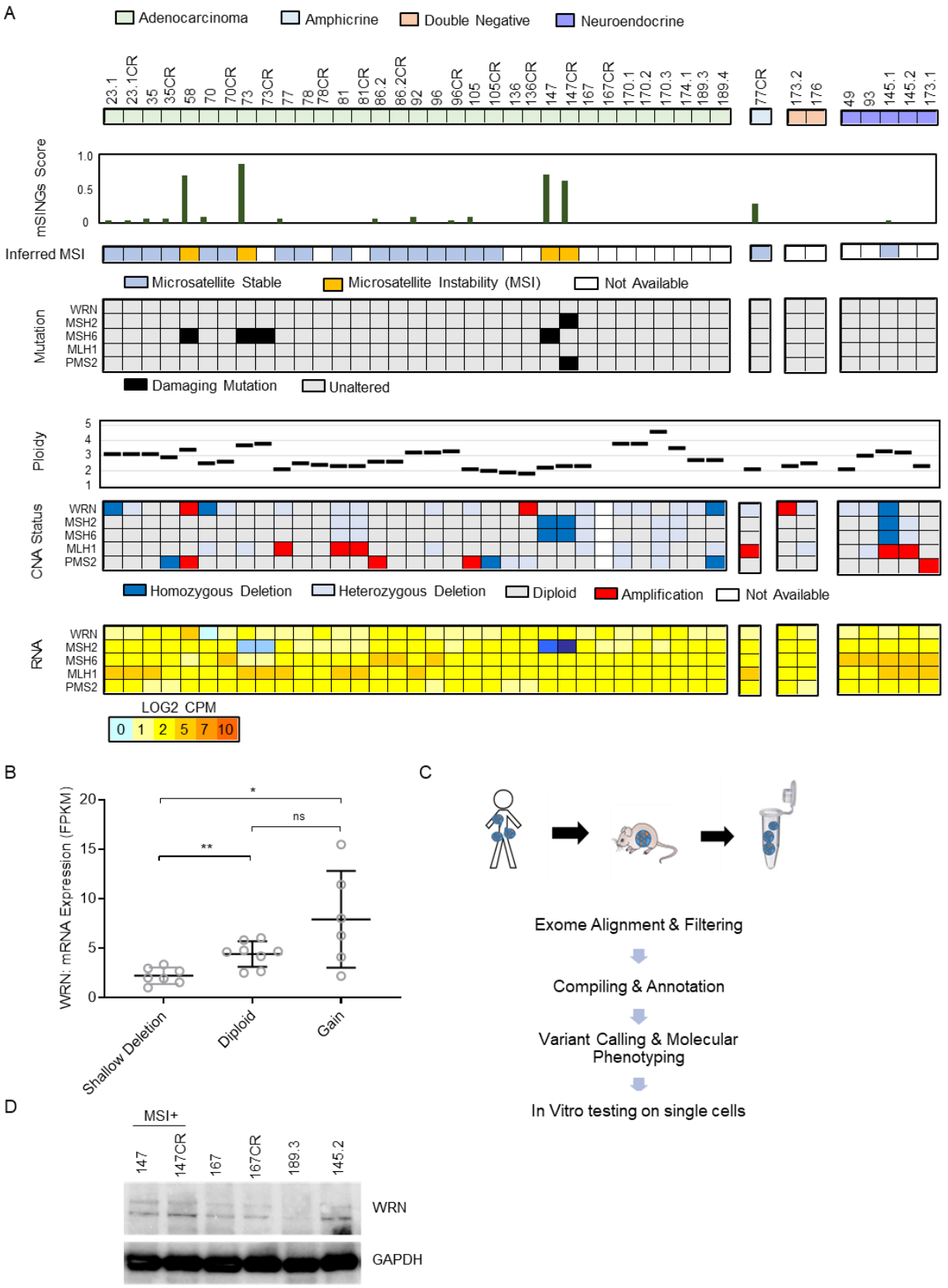
A
Adenocarcinoma
Amphicrine
Double Negative
Neuroendocrine
23.1
23.1CR
35
35CR
58
70
70CR
73
73CR
77
78
78CR
81
81CR
86.2
86.2CR
92
96
96CR
105
105CR
136
136CR
147
147CR
167
167CR
170.1
170.2
170.3
174.1
189.3
189.4
77CR
173.2
176
49
93
145.1
145.2
173.1
mSINGs Score
1.0
0.5
0
Inferred MSI
Microsatellite Stable
Microsatellite Instability (MSI)
Not Available
Mutation
WRN
MSH2
MSH6
MLH1
PMS2
Damaging Mutation
Unaltered
Ploidy
5
4
3
2
1
CNA Status
Homozygous Deletion
Heterozygous Deletion
Diploid
Amplification
Not Available
RNA
LOG2 CPM
0
1
2
5
7
10
B
WRN: mRNA Expression (FPKM)
20
15
10
5
0
*
ns
**
Shallow Deletion
Diploid
Gain
C
Exome Alignment & Filtering
Compiling & Annotation
Variant Calling & Molecular Phenotyping
In Vitro testing on single cells
D
MSI+
147
147CR
167
167CR
189.3
145.2
WRN
GAPDH

Figure 1.5. *WRN* and MMR gene characterization in LuCaP PDX tumors .

(A) Genomic characterization table of established PDX lines quantifying subtype, mSINGs MSI score and status, damaging mutations, ploidy, CNA status as well as RNA transcriptional status of *WRN* and mismatch repair genes. (B) WRN transcriptional expression (average FPKM) in LuCaP PDX tumors based on *WRN* copy number status. **P < 0.01 by Unpaired, Two-tailed T-Test. (C) LuCaP PDX experimental schematic. (D) WRN protein expression in MSI+ versus non-MSI LuCaP tumors via western blot.

A

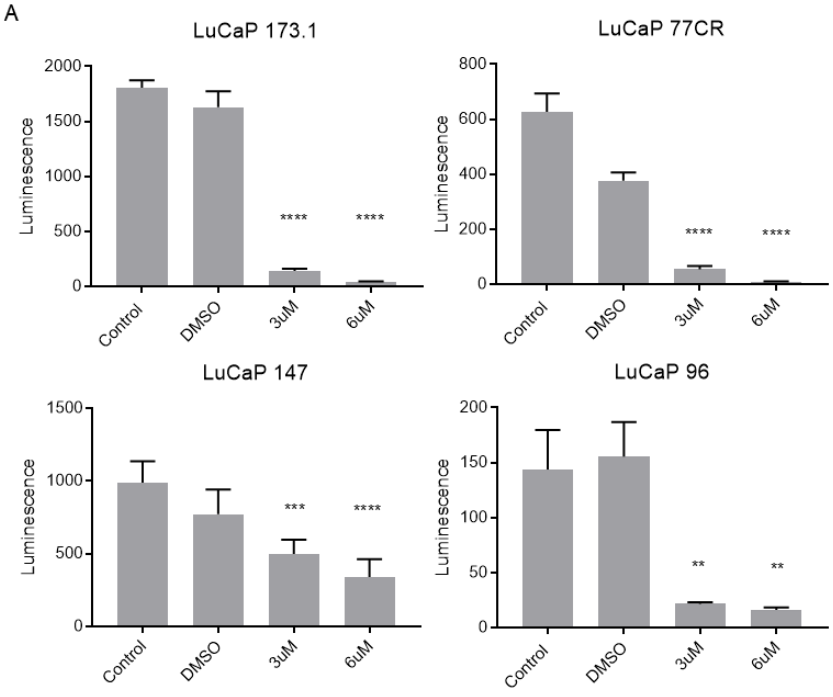

B

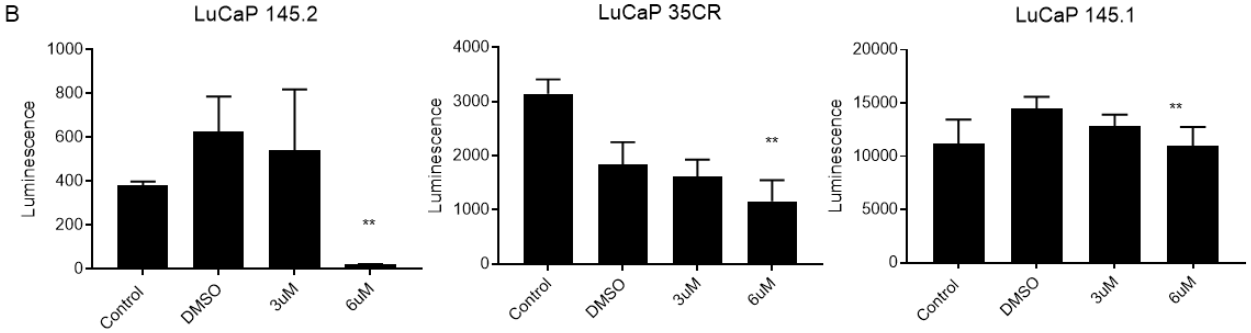

C

Responders	Frac. Unstable Loci (mSINGS)	MSI	Tumor Type	DNA Repair Status
LuCaP 173.1	n/a	n/a	Neuroendocrine	Unknown; COSMIC Signature MMR Defect
LuCaP 77CR	0.27775	Mixed	Adenocarcinoma	MSH3 Copy Loss; COSMIC Signature Unknown
LuCaP 147	0.7059	MSI+	Adenocarcinoma	MSH2 Homozygous Deletion; COSMIC Signature MMR Defect
LuCaP 96	0	No	Adenocarcinoma	BRCA2 Mutant; COSMIC Signature HR Defect

Non Responders	Frac. Unstable Loci (mSINGS)	MSI	Tumor Type	DNA Repair Status
LuCaP 35CR	0.0556	No	Neuroendocrine	MSH3 Copy Loss; COSMIC Signature Unknown
LuCaP 145.1	0.0278	No	Adenocarcinoma	MSH2 Copy Loss; ATM Mutant; No COSMIC Signature DNA Repair Deficit
LuCaP 145.2	n/a	n/a	Adenocarcinoma	MSH2 Copy Loss; ATM Mutant; COSMIC Signature HR Defect

Figure 1.6. WRN inhibitor NSC 19630 is an effective therapeutic in DRD tumors. (A) Cell viability of disassociated LuCaP PDX xenograft tumors sensitive (A) or resistant (B) to growth media, DMSO, 3 µM or 6 µM WRN inhibitor NSC 19630. (C) LuCaP PDX xenograft summary table of tumor lines and respective DNA repair signature. **P < 0.01 by Unpaired, Two-tailed T-Test.

A

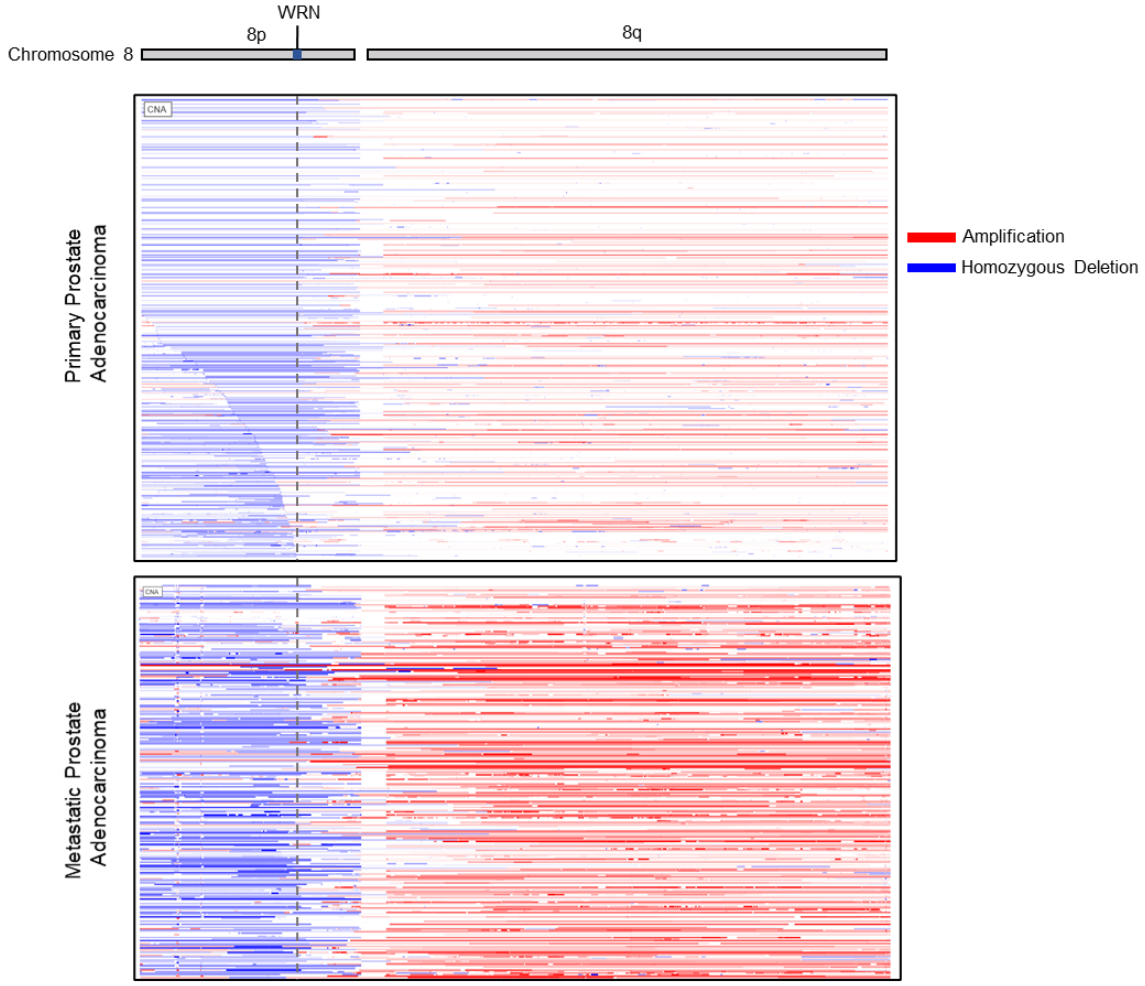

B

8p genes			
ADAM28	EXTL3	NAT1	SH2D4A
AGPAT5	FAM160B2	NAT2	SLC39A14
ASAH1	FAM167A	NEIL2	SLC7A2
ATP6V1B2	FAM86B1	NKX3-1	SORBS3
BIN3	FAM86B2	NUDT18	SPAG11B
BNIP3L	FBXO16	PBK	STC1
C8orf48	FDFT1	PCM1	STMN4
C8orf58	FGL1	PDGFRL	TNFRSF10A
CCDC25	FUT10	PDLIM2	TNFRSF10B
CHMP7	FZD3	PEBP4	TNFRSF10C
CHRNA2	GSR	PHYHIP	TNKS
CSGALNACT1	GTF2E2	PNMA2	TRIM35
CLU	HMBOX1	POLR3D	TUSC3
CNOT7	INTS10	PPP1R3B	UBXN8
DCTN6	INTS9	PPP2CB	VPS37A
DEFB4A	KCTD9	PPP2R2A	WRN
DLC1	KIF13B	PPP3CC	XPO7
DOCK5	LEPROTL1	PSD3	ZDHHC2
DPYSL2	LONRF1	PTK2B	ZNF395
DUSP4	LPL	R3HCC1	
EGR3	MCPH1	RBPMS	
ELP3	MSRA	REEP4	
ENTPD4	MTMR7	RHOBTB2	
EPHX2	MFHAS1	SCARA3	
ERI1	MTMR9	SCARA5	
	MTUS1	SFTPC	
	MYOM2		

C

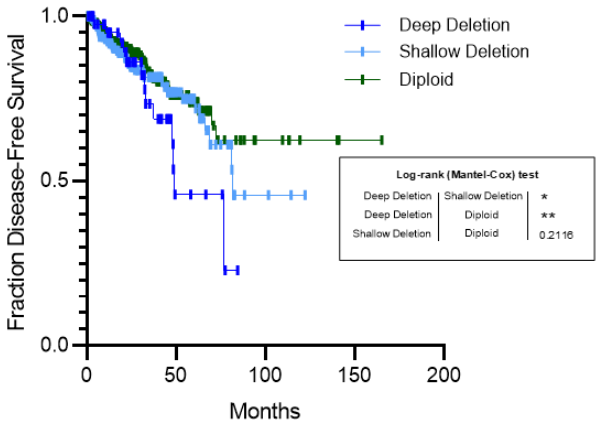

Supplemental Figure 1.1. *WRN* Homozygous Deletion along the Chromosome 8p arm loss. (A) Representative CNA of PRAD and mPC tumor datasets along chromosome 8. (B) homdel genes lost via the 8P deletion and included in the “8P Genes” subgroup. (C) Fraction of Primary Adenocarcinoma (TCGA) patient fraction of disease-free survival based on *WRN* copy number status (log rank test).

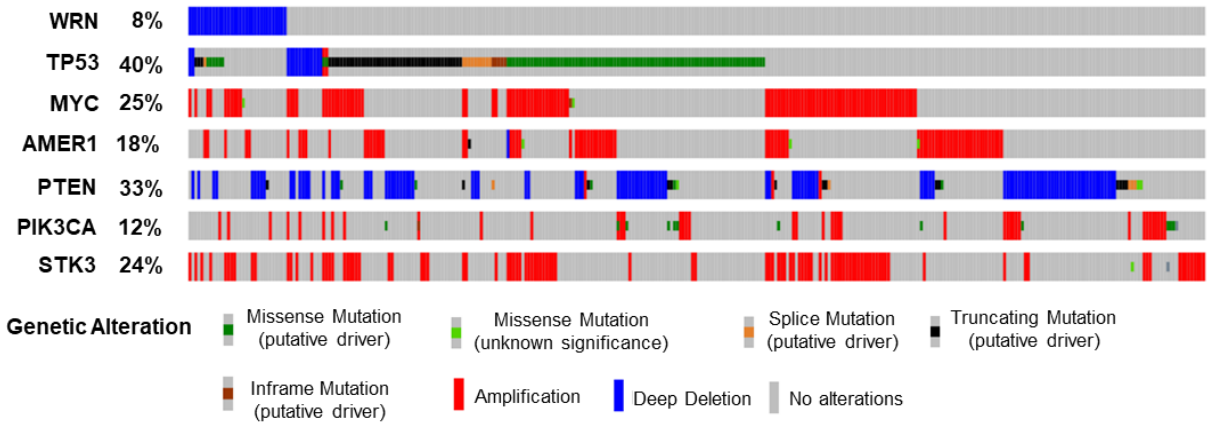

Supplemental Figure 1.2. Co-occurring alterations with *WRN* HOMDEL. Oncoplot of mPC (SU2C) tumors (columns) with *WRN* homozygous deletion with major pathway co-occurring alterations: *TP53*, *MYC*, *AMER1* (WNT signaling), *PTEN*, *PIK3CA* and *STK3* (HIPPO pathway) alterations. Grey bars without alterations are omitted for space.

A

		***	***	**	*		
	Mutual Exclusivity P-Value	<0.001	0.002	0.027	0.054		
PANCAN Tumors		**MSH2**	**MSH3**	**MSH6**	**MLH1**	**PMS2**	**WRN**
	MSH2	**66**	6	6	4	1	1
	MSH3		**59**	4	2	6	0
	MSH6			**59**	5	5	2
	MLH1				**55**	1	1
	PMS2					**33**	1
	WRN			PANCAN Tumors			**251**

B

TCGA Tumors P-Value = 0.096

TCGA Tumors	WRN Homdel	MMR Mut	HyperMut
WRN Homdel	**26**	0	0
MMR Mut		2	2
HyperMut			**4**

C

SU2C Tumors P-Value = 0.82

SU2C Tumors	WRN Homdel	MMR Mut	HyperMut
WRN Homdel	**20**	0	0
MMR Mut		3	2
HyperMut			**13**

Supplemental Figure 1.3. Pan-cancer *WRN* and MMR gene mutual exclusivity. (A-C) The number of tumors with clinically pathogenic mutations in mismatch repair genes versus *WRN* homozygous deletion of WRN and the mutual exclusivity probability analysis of a mutation in each gene co-occurring in the same tumor across PANCAN TCGA (N= 10,953 patients from a combined study of 32 TCGA cancer cohorts), TCGA PRAD (N=499) and SU2C mPC (N=444). **P < 0.01 by one-sided Fisher Exact Test.

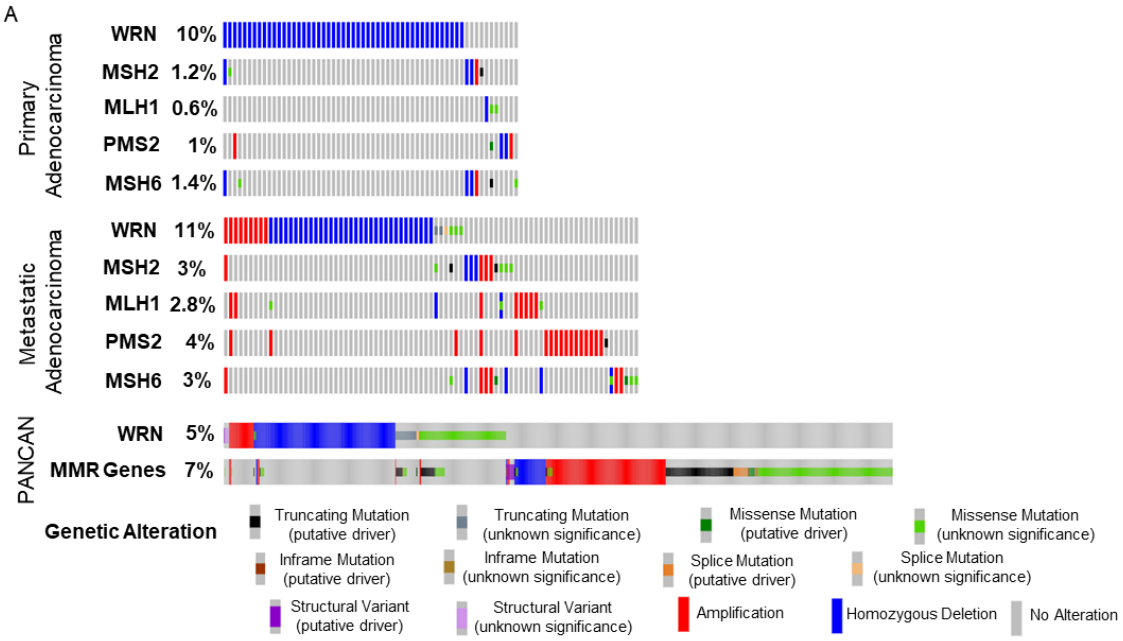

B

PANCAN TCGA

A	B	Neither	A not B	B not A	Both	Log2 Odds Ratio	P-value	Q-value	Tendency
MMR Truncating Mutations	8P Genes	9532	204	449	4	-1.264	0.042	0.042	Mutual Exclusivity

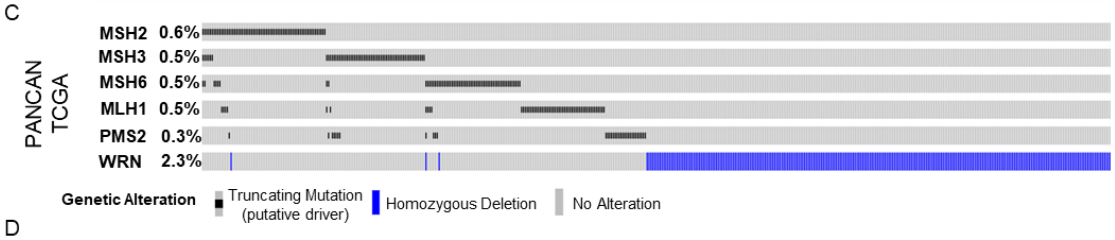

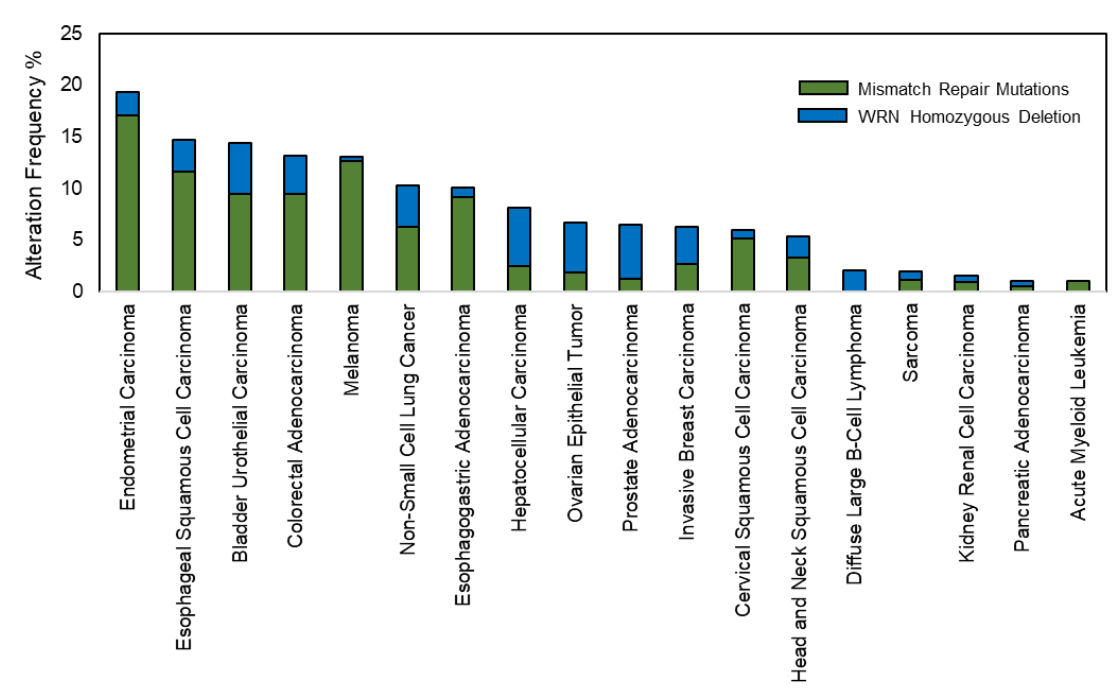

Supplemental Figure 1.4. *WRN* HOMDEL and MMR driver mutations mutual exclusivity across prostate and pan-cancer cancer clinical datasets. (A) Oncoplot of all alterations of mismatch repair genes and *WRN* across PRAD (TCGA N=499), mPC (SU2C N=444) and PANCAN TCGA (N= 10,953 patients from a combined study of 32 TCGA cancer cohorts) (B) PANCAN TCGA (mutual exclusivity analysis table utilizing the log rank test. (C) Oncoplot of pathogenic mutations in mismatch repair genes versus *WRN* homozygous deletion across PANCAN TCGA datasets. Blue or grey columns represent patients with or without homozygous deletion, respectively. Black dots represent pathogenic mutation (A, C). Most of the unaltered grey bars are omitted to save space (C). (D) Alteration distribution across TCGA cancers of damaging mismatch repair mutations and homozygous deletion of *WRN*.

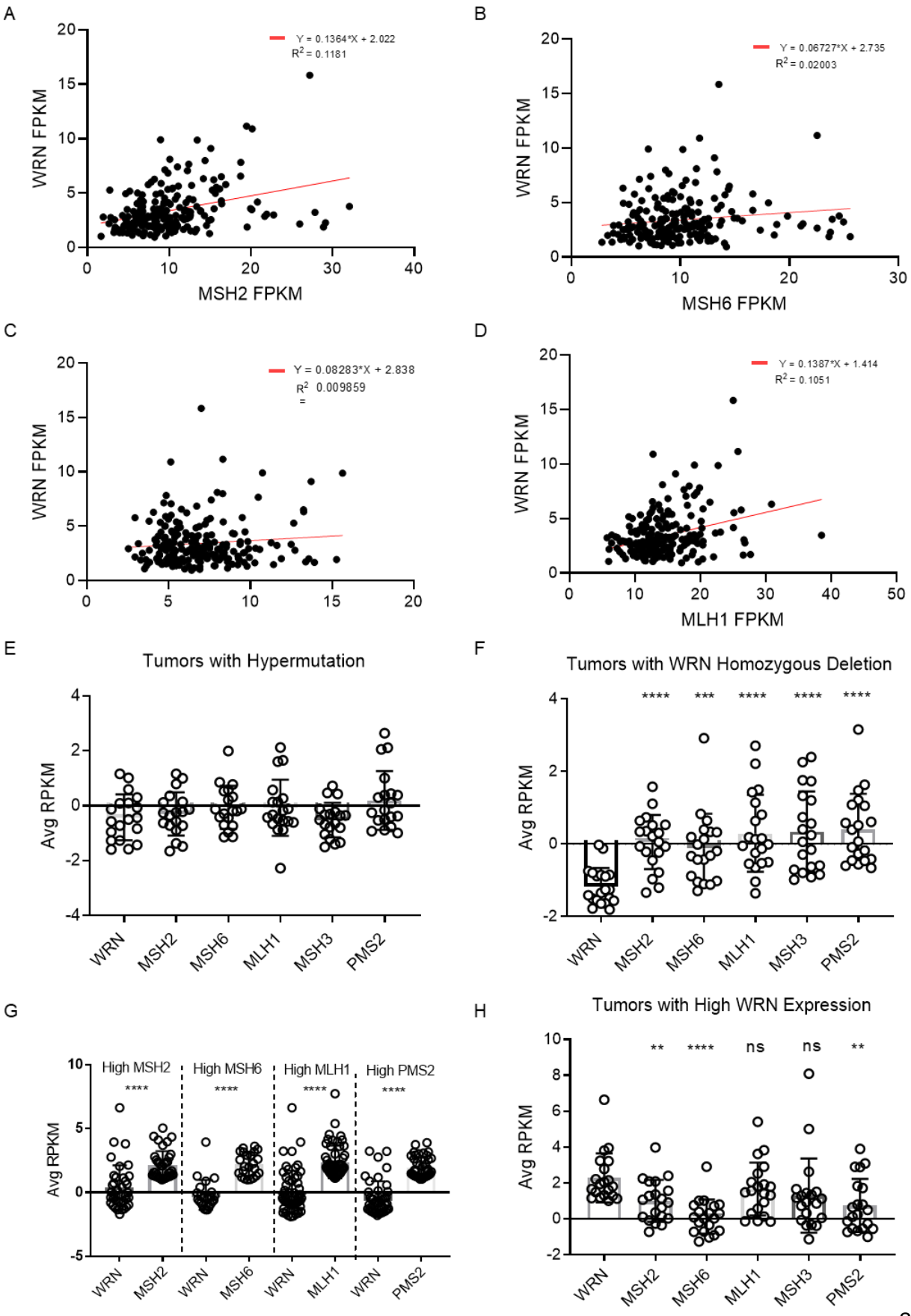
A
Y = 0.1364*X + 2.022
R2 = 0.1181
WRN FPKM
MSH2 FPKM
B
Y = 0.06727*X + 2.735
R2 = 0.02003
WRN FPKM
MSH6 FPKM
C
Y = 0.08283*X + 2.838
R2 0.009859
=
WRN FPKM
D
Y = 0.1387*X + 1.414
R2 = 0.1051
WRN FPKM
MLH1 FPKM
E
Tumors with Hypermutation
Avg RPKM
WRN
MSH2
MSH6
MLH1
MSH3
PMS2
F
Tumors with WRN Homozygous Deletion
Avg RPKM
****
***
****
****
****
G
High MSH2
High MSH6
High MLH1
High PMS2
Avg RPKM
H
Tumors with High WRN Expression
Avg RPKM
**
****
ns
ns
**

Supplemental Figure 1.5. Transcriptional expression of WRN and MMR genes. (A-D) WRN transcriptional expression (FPKM) versus mismatch repair genes *MSH2* (A), *MSH6* (B), *PMS2* (C) and *MLH1* (D) expression from the mPC SU2C dataset, fit to linear regression slope. (E-H) transcriptional expression of WRN and mismatch repair genes in mPC tumors that are hypermutated (E), have *WRN* homozygous deletion (F), have high mismatch repair expression (G), or high WRN expression (H). **P < 0.01 by Unpaired, Two-tailed T-Test.

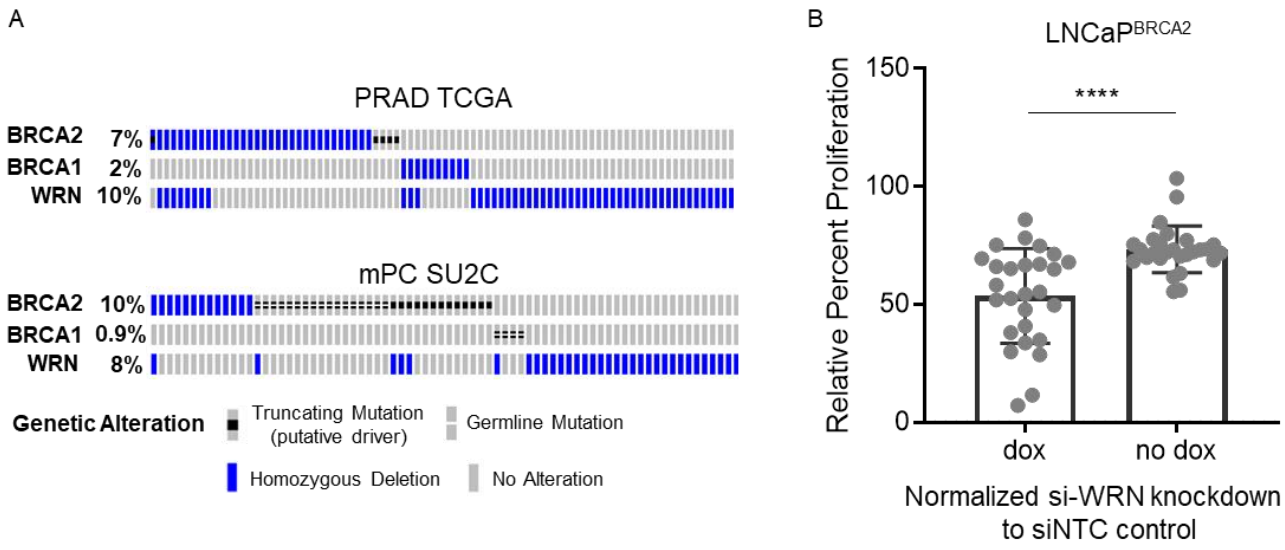
A
PRAD TCGA
BRCA2 7%
BRCA1 2%
WRN 10%
mPC SU2C
BRCA2 10%
BRCA1 0.9%
WRN 8%
Genetic Alteration
Truncating Mutation (putative driver)
Germline Mutation
Homozygous Deletion
No Alteration
B
LNCaP^BRCA2
****
Relative Percent Proliferation
150
100
50
0
dox
no dox
Normalized si-WRN knockdown to siNTC control

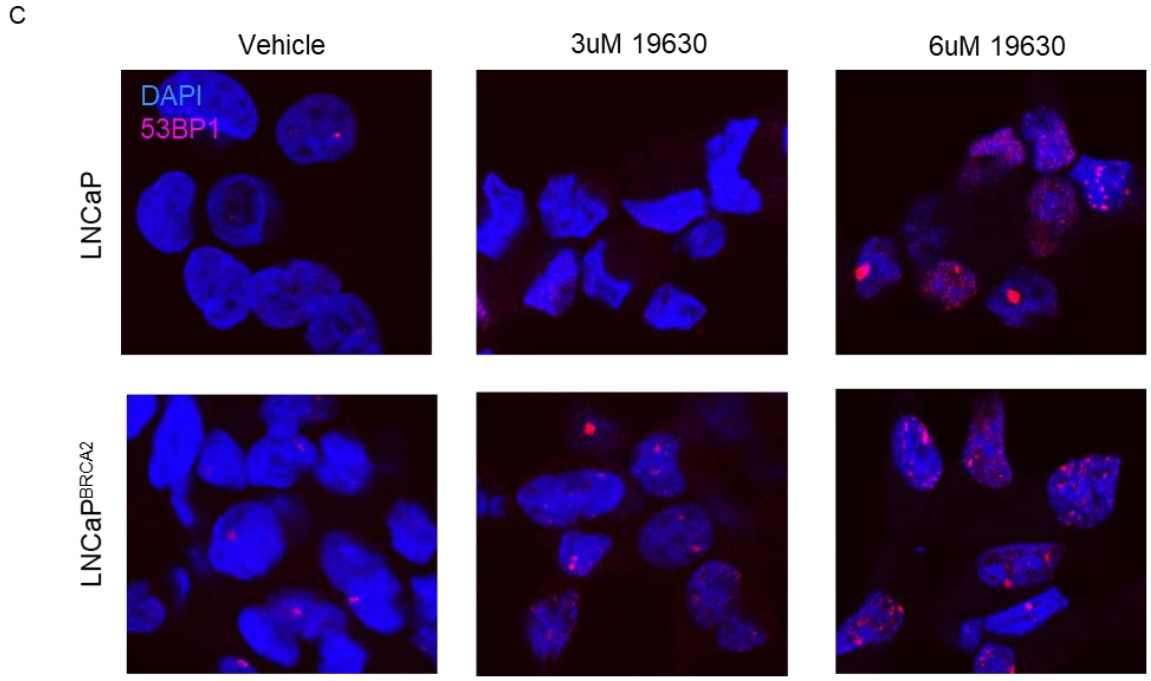
C
Vehicle
3uM 19630
6uM 19630
DAPI
53BP1
LNCaP
LNCaP^BRCA2

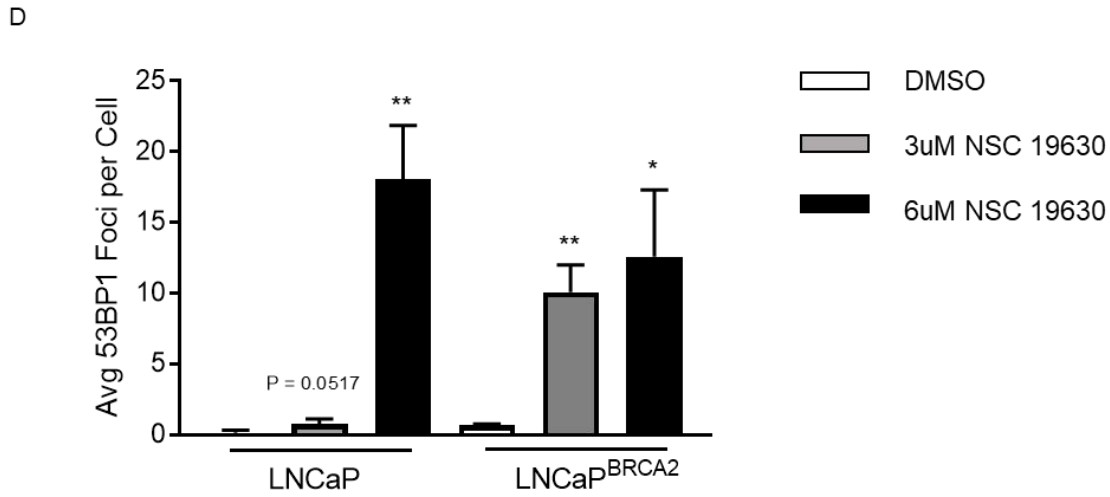
D
Avg 53BP1 Foci per Cell
25
20
15
10
5
0
**
**
*
P = 0.0517
LNCaP
LNCaP^BRCA2
DMSO
3uM NSC 19630
6uM NSC 19630

Supplemental Figure 1.6. LNCaP^{BRCA2} is sensitive to WRN-knockdown and susceptible to increased DNA damage post NSC 19630. (A)Oncoplot of mPC tumors *BRCA2* loss via homozygous deletion or deleterious mutation as well as the homozygous deletion of *WRN* (B)Relative percent proliferation of dox-inducible LNCaP^{BRCA2} after siWRN knockdown as compared to siNTC control. (C)Confocal microscopy (63x) and quantification (D) of LNCaP and LNCaP^{BRCA2} cells post treatment with DMSO, 3uM or 6uM NSC 19630. **P < 0.01 by Unpaired, Two-tailed T-Test.

Chapter 2. WRN DNA Helicase sensitivity in Metastatic Prostate Cancer and Implications for Cancer Treatment

Emily Kohlbrenner[1], Peter S. Nelson[1,2]

[1]Department of Pathology, University of Washington School of Medicine, Seattle WA
[2]Fred Hutchinson Cancer Research Center, Seattle, WA

2.1 Abstract

The WRN DNA helicase has been established as a promising target for therapeutic development based on the observed synthetic lethality shown in mismatch repair deficient (MMRd) cancer cells with microsatellite instability (MSI)[29,31,56]. WRN has been shown to be essential to the resolution of TA-dinucleotide non-B DNA secondary structures that accumulate in MSI cells, resulting in lethal DNA damage and cell death when WRN is lost[32]. However, this proposed mechanism is limited to cell lines from cancers where MSI tumors more commonly occur, such as colorectal, gastric and endometrial cancers, and has not yet been investigated in cancers with less overall MSI prevalence, such as prostate cancer. We aimed to characterize WRN, mismatch repair and MSI status in available prostate cancer cell lines, and show that MSI prostate cancer cells are indeed sensitive to WRN loss over time, despite not displaying immediate synthetic lethality as seen in other cancers. We also indicate that the G-Quadruplexes, DNA secondary structures formed by GC-repeat regions and mediated by the RecQ family of DNA

helicases, notably WRN, also contributes to the observed irreparable replicative stress in MMRd-MSI cells, and are a promising target for chemotherapeutics themselves in the context of low or loss of WRN expression. These findings broaden the understanding of WRN-sensitivity in MSI cells in a lesser-studied subtype of prostate cancer, and support the inclusion of prostate cancer tumors in future research regarding WRN therapeutic targeting in MSI-high tumors.

2.2 Introduction

Tumor mutational burden is a known driver of oncogenesis, and if driven by mismatch repair (MMR) or DNA polymerase loss, can generate a state of genomic tumor hypermutability. The inability to repair mismatched nucleotide gains and losses over time within microsatellite regions in the genome can lead to the generation of novel, replicatively unstable microsatellite alleles, known as microsatellite instability (MSI)[57,58]. MSI status is clinically diagnostic and most common in colorectal, gastric and endometrial cancers, but still occurs at less frequency in cancers such as prostate[59–61]. Due to the lesser prevalence of MSI diagnosis, the research and mechanistic understanding regarding how MSI-high prostate cancer tumors compare to other MSI high cancers remains limited[29,62] .

Recent large-scale RNAi/CRISPR screens have revealed that that mismatch repair deficient (MMRd) and MSI cell lines across cancer types are dependent on the DNA helicase and 3’ exonuclease RECQL-2; more commonly referred to as Werner Syndrome protein (WRN) [29,31,39,56]. WRN plays multiple roles in DNA replication,

contributing to the maintenance of genomic stability by functionally interacting with other proteins at the replication fork[40]. Notably, MMRd or MSI-diagnosed solid tumors have been approved treatment with anti-PD1 blockade[61,63–65]; however, this treatment is not effective in all patients and the usage of a synergistic agent to reduce therapeutic toxicity and augment tumor sensitivity with administered synthetic lethality is promising. These previous studies support the development of WRN-targeting therapeutics but are limited by the translational bounds of early pre-clinical, large-scale cell line knock down studies[66,67]. Importantly, the biological mechanism underlying WRN-dependency in cancer types where MSI is less prevalent, such as prostate cancer, remains unknown[61].

Therefore, we aimed to characterize WRN and the drivers of MMRd, notably MSH2 and MSH6, in cellular models of metastatic prostate cancer (mPC) and investigate the mechanism behind the observed biological dependency of WRN and MSI-high, MMRd cell lines. We generated isogenic shWRN and shMSH2/shMSH6 knock down models to further study this relationship in mPC, and aimed to model the potential applicability of WRN therapeutic targeting. This investigation proposes to add a broader context to future research on MSI-high tumor subtypes and WRN therapeutic targeting by including a model of WRN-sensitivity in available mPC cell lines.

2.3 Materials and Methods

Characterization

Cell line characterization data was downloaded from the cancer cell line encyclopedia[68]. Whole transcriptome sequencing (RNAseq) data was isolated in triplicate, sequenced and analyzed as previously described[48].

Cell culture and treatment

PC cell lines were obtained from the American Type Culture Collection (ATCC). All cells were confirmed negative for mycoplasma. LNCaP, 22RV1 and PC3 shRNA non-targeting control (shNTC) and shWRN knockdown cell lines were maintained in RPMI medium (Gibco, ThermoFisher, USA) supplemented with 10% FBS (Gibco). HCT116 and HEK293T cell lines were grown in Dulbecco's modified Eagle medium (Gibco, ThermoFisher) supplemented with 10% FBS (Gibco); transfection of 293T was performed using Lipofectamine. Lentiviruses were produced by co-transfecting pLVC.2 plasmid containing WRN, MSH2 (22RV1 and PC3), MSH6 (LNCaP) or scrambled non-targeting gDNA, with psPAX2 and pMD.2 into 293T cells as previously described[48,52]. Virus was harvested 48 and 72 hr post transfection, filtered and pooled. shNTC, shWRN, shMSH2 or shMSH6 knockdown lines were selected under 1ug/ml puromycin. Olaparib (Sellek Chemical), carboplatin (Sigma, C2538), irinotecan (Sellek Chemical), cisplatin (Sellek Chemical), docetaxel (Sellek Chemical), pyridostatin trifluoroacetate salt (Selleck Chem) and NSC 19630 (Millipore) were used in this study. Cells were treated with

chemotherapeutics for 72 hr for cell death and survival assays, 48 hr for G-quadruplex (G4) RNAi confocal imaging and 72 hr for yH2ax drug confocal imaging.

WRN	sgRNA +	caccgGTAAATTGGAAAACCCACGG	Forward	GCGACATGAACAAACAGTTGAC
	sgRNA -	aaacCCGTGGGTTTTCCAATTTACc	Reverse	TGCATCAGTCTGTGTGTGTG
MSH2	sgRNA +	caccgTCAAAATAGATAATTCAAAG	Forward	AAAGAGTTGTTACCGTTGGGAC
	sgRNA -	aaacCTTTGAATTATCTATTTTGAc	Reverse	CAGCACTATTCATCTGCTCTCC
MSH6	sgRNA +	caccgATCACCACCTCCACTAACGT	Forward	AAGCCAGACACTAAGGAGGAAGG
	sgRNA -	aaacACGTTAGTGGAGGTGGTGATc	Reverse	TAATCTGCCACCACTTCCTCATC

Table 2.1. shRNA sequences and corresponding validation primers used to generate knockdown constructs.

Growth Assays

LNCaP, 22RV1 and PC3 shNTC, shWRN, shMSH6 (LNCaP) and shMSH2 (22RV1 and PC3) cell lines were plated at 50,000 cells or 25,000 cells in a 12 well dish for 7-day or 10-day growth, respectively, following 48hr puromycin selection and measured for percent viable untreated or treated cells via the vicell cell counter (Beckman Coulter, Atlanta, GA) after 3-10 days. Cells were seeded as above for siRNA double knockdown screens, with siRNA transfected with Lipofectamine RNAiMax (Invitrogen) 48hr before each timepoint. The following Dharmacon siRNA pools were used: Human WRN siRNA Smartpool, OnTargetplus MSH2 siRNA Smartpool, MSH6 siRNA Smartpool and non-targeting scrambled control siRNA (Dharmacon).

Drug Response Assays

The percentage of viable cells was determined following 72 hr of growth in chemotherapeutic containing media (olaparib, carboplatin, docetaxel, irinotecan, pyridostatin, NSC 19630) treatment via the vicell (Beckman Coulter, Atlanta, GA) cell

counter and normalized to either the non-targeting or shWRN knockdown grown in DMSO. Cell viability assays was determined by Cell Titer Glo, as per the manufacturer's instructions (Promega, cat#G7572) and luminescence was measured on a Synergy H1 microplate reader (Biotek). Cells were seeded at 8k cells per well in a 96 well plate (corning) in growth media, then treated 24 hr following with chemotherapeutics (Olaparib, carboplatin, docetaxel, enzalutamide, pyridostatin, NSC 19630) and grown for 72 hr before assay. Drugs were diluted in growth media and added at a total volume of 100uL per well.

RT-qPCR

RNA was extracted from 6-well cell culture plates using RNEasy extraction kit (Qiagen) according to the manufactures protocol. Real time PCR was performed in triplicate using SYBR green master mix (Invitrogen) by the fast real-time PCR system (Applied Biosystems 7900). IDT primers were used and normalized to the GAPDH housekeeping gene (Table 2).

WRN	Forward	GCATGTGTTCGGAAGAGTGTTT
	Reverse	TGACATGGAAGAAACGTGGAA
MSH2	Forward	TGGATCAGGTGGAAAACCAT
	Reverse	ATCCAAACTGTGCACTGGAA
MSH6	Forward	TTTTGGTAAGCGGCTCCTAA
	Reverse	TCAGGGGAGACCCAACATTA
RECQL	Forward	TGAAGCAGGCAGAGGAACTG
	Reverse	AGCCACAACACCTGCTACTC
BLM	Forward	GAGTCTGCGTGCGAGGATTA
	Reverse	AGTGTTCTGGCTGAGTGACG
RECQL4	Forward	TCACAGTGAGGTCCCAGATT
	Reverse	CTGACTTCTTGGAAGGCTGA
RECQL5	Forward	GCTCAGGAAGACGGGAGAAG
	Reverse	AGAACAGCTTGGAGAACGGG
GAPDH	Forward	CATGAGAAGTATGACAACAG
	Reverse	ATGAGTCCTTCCACGATA

Table 2.2 Forward and reverse primers used for RT-qPCR studies.

Confocal microscopy

Cells were plated at 100k per well density on coverslips in 6-well dishes in growth media or treated with DMSO, 5uM Olaparib, 5uM Carboplatin, 1uM Irinotecan or 0.1uM Pyridostatin. After 72 hrs, cells were fixed with 4% paraformaldehyde for 30 min, permeabilized in 0.2% triton X-100 in PBS for 7 min and blocked in 3% FBS PBS-tx for 1 hr. Coverslips were immunostained in primary antibodies for 90 min: rabbit anti-WRN (Novus), anti-ser 139 yH2ax (Millipore) or anti-gquadruplex (Millipore) followed by fluorescently conjugated secondary antibodies Alexa Fluor 555 donkey anti-mouse or AlexA Fluor goat anti-rabbit (Invitrogen) for 1 hr and counterstained with DAPI (Vector Laboratories). Slides were analyzed across multiple microscope fields at 63x oil on the confocal, and foci from 80-100 cells were counted per individual cell via Image J and plotted.

Immunohistochemistry

Cells were plated at 100k per well in 6-well dish and grown for 48 hr before isolation for western blotting. Cells were washed in PBS and covered in 200ul lysis solution (1% SDS, 1% NP-40, 2% Tween-20, 1.5 M Urea) and collected using a cell scraper. Lysates were boiled for 2 min, sheared by sonication and immunoblotted as described[52].

Ab92471 Rb mAb MSH6 EPR3945 (abcam)
Ab70270 Rb pAb MSH2 (abcam)
MABE1126 anti DNA G-quadruplex clone 1H6 mAb mouse (EMD Millipore)
MABE324 mAb mouse anti-MSH3 clone 1F6 (EMD Millipore)
Ab92312 Rb mAb MLH1 EPR3894 (abcam)
Ab110638 Rb mAb PMS2 EPR3947 (abcam)
Anti-Phospho-histone H2A.x Ser139 mouse Clone JBW301 (EMD Millipore)
NB100-472 Rb anti-WRN pAb (Novus)
Goat anti-Rabbit IgG (H+L), horseradish peroxidase conjugated (Thermo)
Goat anti-Mouse IgG (H+L), horseradish peroxidase conjugated (Thermo)
Goat anti-mouse IgG (H+L) Alexa fluor plus 555 (Invitrogen)
Goat anti-rabbit IgG (H+L) Alexa fluor plus 488 (Invitrogen)

Table 2.3.Antibodies used for immunohistochemistry.

Senescence Assay

SA-β-gal activity was detected using the β-galactosidase staining kit (Cell Signaling Technology) in shNTC or shWRN knockdown LNCaP, 22RV1 or PC3 cells according to the manufacturer's protocol. 100k Cells were plated in a 6-well dish for 72 hr, fixed and stained. SA-β-gal+ staining was visualized under brightfield and quantified as percent stained cells of total cells analyzed, across 10 fields (~50 cells per field) at 40x.

Colony Formation Assay

LNCaP, 22RV1, PC3 and all derived shNTC, shWRN and shMSH6 (LNCaP) or shMSH2 (22RV1 or PC3) were plated at 1k (22RV1 and PC3) or 2k (LNCaP) cell density in 10-cm dishes and grown in RPMI + 10% FBS media for 21 (LNCaP and 22RV1) or 14

(PC3) days based on clonal growth. Colonies with fewer than 50 cells were counted after 0.1% crystal violet staining.

Statistical analysis

Knockdown comparisons were direct comparison of continuous variables, compared to non-targeting shNTC control using a Student's t-test on Graph-Pad Prism 6 to generate graphs and analyses. Two-sided P-values are presented with * $P < 0.05$, ** $P < 0.01$ and *** $P < 0.005$ as mean ± standard deviation (SD). At least three independent experiments were used for each experimental group and analyzed in total as presented. Log rank test statistic was used for all Kaplan-Meier survival analysis and mutual exclusivity calculations.

2.4 Results

2.4.1 Characterizing WRN and Mismatch Repair Genes in Prostate Cancer Cell Lines

Of established prostate cancer cell lines, 22RV1, DU145, MDAPCA2B and LNCaP have a high mutational burden and are inferred MSI, whereas PC3, NCIH660, VCAP, BPH1 and PWR1E cell lines have few mutations and MSI loci, and are considered microsatellite-stable (MSS)[68]. Interestingly, only MSS line NCIH660 has been previously categorized as WRN-sensitive in large scare CRISPR-RNAi screens[29]. Mutational data from Cancer Cell Line Encyclopedia was utilized to determine damaging mutation status for WRN and key driver genes as previously described[68]. We then performed RNAseq on available prostate lines 22RV1, DU145, LNCaP, PC3, NCIH660 and VCAP to determine the expression status of *WRN* and the mismatch repair genes,

and found stable transcriptional WRN expression across all lines, and lower expression of MSH2 in LNCaP lines and MLH1 in DU145 (Figure 2.1).

2.4.2 WRN Knockdown Results in Growth Suppression in MSI+ Prostate Cancer

To first replicate previous findings in available prostate cancer cells, we used WRN-targeting RNAi in 22RV1, LNCaP and PC3 cell lines as well as an established MSI+ positive control, HCT116 cells (Figure 2.2A, Supplemental Figure 2.1A-B). While we observed the lethality to short term loss of WRN in HCT116 cells in congruence with previous findings[29], the sensitivity of 22RV1 cells to WRN-RNAi suggests that there may be a broader spectrum of sensitivity to WRN in MSI+ cells. To better understand the effects of WRN loss in metastatic disease, we generated a WRN knockdown model in three mPC cell lines, 22RV1, LNCaP, and PC3. Knockdown of WRN was validated in these lines by qPCR and western blot following selection in puromycin. (Figure 2B, Supplemental Figure 2.1C-D). shWRN knockdown did not influence transcriptional expression of the other RECQL helicases (Supplemental Figure 2.1E). WRN knockdown suppressed growth in all three lines, most notably in 22RV1 cells with a high MSI score (Figure 2.2C).

As WRN plays a functional role in DNA repair, we utilized confocal microscopy and immunostaining to visualize and quantify phosphorylated H2AX (γH2AX) as a maker of DNA damage in the nucleus of our knockdown lines. WRN-knockdown increased the number of γH2AX foci in all lines, most notably in MSI+ 22RV1 cells (Figure 2.3A-B). WRN-knockdown also led to increased percent of endogenous beta-

galactosidase expressing cells, a biomarker for senescence, in both 22RV1 and LNCaP (Figure 2.3C, Supplemental Figure 2.2A). To confirm that the sensitivity to WRN was a factor of MSI+ status, we repeated the above experiments in MSI+ DU145 cells and observed significant growth repression, increased DNA damage and senescent staining in the DU145^{WRN} knockdown lines (Supplemental Figure 2.3).

2.4.3 WRN Inactivation Does not Universally Alter Susceptibility to Therapeutics

In order to test if WRN-loss increased sensitivity to commonly used chemotherapeutics, we quantified the number of shNTC or shWRN knockdown cells after growth in media containing common chemotherapeutics and normalized the results to the number of cells in each condition, grown in media with DMSO. We observed increased sensitivity to 1μM Irinotecan in both 22RV1^{WRN} and LNCaP^{WRN}, but not PC3^{WRN} cells. However, PC3^{WRN} were more sensitive to 5 μM Olaparib (Figure 2.3D). 22RV1^{WRN} cells were slightly more sensitive to 5uM Enzalutamide as compared to control, but no lines were more sensitive to cisplatin post WRN knockdown (Supplemental Figure 2.3B). DNA damage, as visualized and quantified by γH2AX foci, increased in 22RV1^{WRN} and LNCaP^{WRN} post-72 hr Olaparib (5 μM) and Docetaxel (1nM) exposure; both LNCaP^{WRN} and PC3^{WRN} had more γH2AX foci post-72 hr of growth exposure to Irinotecan (1nM) (Supplemental Figure 2.4-5).

2.4.4 MSH2/6 Knockdown Promotes Clonal Growth and is Sufficient to Induce Increased Sensitivity to Loss of WRN

To determine if the loss of mismatch repair proteins drives susceptibility to WRN knockdown, we generated MSH2+MSH6 complex knockdown models in available mPC lines. Driver mutations in MSH2 have been previously shown to have a more severe impairment of mismatch repair and occur the most frequently in hypermutated PC[53,55,61]. Utilizing mismatch repair deficient HCT116 cell line as a positive control, we identified MSH2 expression in PC3 and 22RV1 lines, but not LNCaP. LNCaP cells had protein expression of MSH6, the complimentary complex to MSH2, which was targeted for protein knockdown as an alternative (Figure 2.4A-B). Over ten days, shMSH2 increased the growth rate in 22RV2^{MSH2} cells (Figure 2.4C). Longitudinally, both shMSH2 (22RV1 and PC3) and shMSH6 (LNCaP) knockdowns had a greater number of colonies grow over 21 days. In comparison, shWRN knockdown was observed to significantly reduce clonal growth in 22RV1 and LNCaP lines (Figure 2.5A-B).

To determine if knockdown of the MSH2 complex increased sensitivity of these lines to WRN-depletion, we utilized either a scrambled non-targeting siRNA (NTC) or a pool of WRN-targeting siRNA (siWRN) to perform a double knockdown experiment. 22RV1^{MSH2}, PC3^{MSH2} and LNCaP^{MSH6} knockdowns were more sensitive to WRN-RNAi as compared to shNTC control lines, indicating that loss of MSH2 or MSH6 is sufficient induce increased sensitivity to WRN, but does not demonstrate complete lethality (Figure 2.5C).

2.4.5 G-quadruplex foci are a marker of MSI+ status and accumulate with loss of WRN

One possible mechanism of WRN-induced synthetic lethality in MSI + cell lines has recently been attributed to the inability to repair secondary cruciform structures that form at amplified TA-repeat regions, resulting in double strand breaks and genotoxic cell stress[32]. As WRN is known to selectively mediate and prevent DNA damage from the tension formed from tertiary G-quadruplexes (G4) in GC-rich regions of the genome[69], we sought to investigate if the resolution of these G-quadruplexes could be an additional mechanism of genomic stress. Utilizing a G4 specific antibody[70], and HCT116 as an MSI+ positive control [71], we observed increased G4 foci in MSI+ mPC lines 22RV1 and DU145 control cells as compared to non-MSI, PC3 lines. LNCaP cells are on the borderline of MSI+, as they are the PC line with the fewest MSI foci, and were observed to have more G4 staining as compared to PC3. Further, WRN knockdown also increased G4 foci across all cells, most notably in $PC3^{WRN}$ (Figure 2.6A-B, Supplemental Figure 2.6).

To determine if the presence of MSH2-MSH6 complex changes G4 foci concentration following WRN double knockdown, we performed the same experiment using the shMSH2 or shMSH6 knockdown lines treated with either siWRN or siNTC RNAi. $22RV1^{MSH2}$ and $LNCaP^{MSH6}$ MSI+ cells had more G4 foci than $PC3^{MSH2}$ following siWRN treatment, indicating an enrichment of G4 structures when both proteins are absent (Figure 2.6C-D). We then compared growth rates of the shWRN knockdown lines exposed to an established G4 inhibitor, pyridostatin[72], and observed an augmented sensitivity to the drug in the MSI+ $22RV1^{WRN}$ knockdown as compared to control. Treatment also suppressed growth to a lesser extent in PC3, but not LNCaP, shWRN knockdown lines (Figure 2.7A-C). More γH2AX foci were observed in both 22RV1 and

LNCaP shWRN knockdown models after 0.1 μM of pyridostatin, and PC3^{WRN} after 1 μM pyridostatin treatment (Figure 2.7D-G, Supplemental Figure 2.7).

2.5 Discussion

Recently, WRN, a mediator of DNA repair, has become centered in clinical relevance when targeting solid tumors with a high number of genomic microsatellite regions, classified as MSI. Across multiple cancer cell types, MSI status alone predicted synthetic lethality with WRN CRISPR and RNAi knock out/knock down, but did not exhibit sensitivity in PC cell models[29,31,56]. While the functionality of WRN at the replication fork is well characterized[15,16,40], its role in the context of hypermutated and MSI+ tumors remains unclear. Additionally, though the characterization of MSI pathology has predominantly been focused within cancers where MSI high tumors are more prevalent, research remains limited in cancers with a lower overall frequency, such as PC. As such, we sought to characterize the function of WRN and explore potential selective vulnerabilities in prostate cancer.

Using established MSI+ PC cell lines 22RV1 and DU145, borderline-MSI+ LNCaP cells, and MSS PC3 cells, we observed an increased growth inhibition post-shWRN knockdown in all MSI+ lines in comparison to PC3. Additionally, we observed MSI+ 22RV1 cells to be sensitive, albeit not lethal, to WRN-RNAi short term knockdown. These data suggest that MSI+ PC cell lines are not resistant to loss of WRN as previously described [29], a finding that is further supported by the observed increased DNA damage and pre-senescent staining in shWRN knockdown MSI+ prostate lines. Future

investigations will need to expand the scope of WRN targeting beyond MSI+ cancers with immediate synthetic lethality.

Further, we observed that MSH2-MSH6 complex knockdown promoted clonal growth in our cell models over time, suggesting that though mismatch repair mutations occur infrequently in PC overall, they have similar tumor suppressor properties as seen in other cancers[73–76]. It is possible that the frequency of mismatch repair deficient tumors remains low in prostate solid tumors, as compared to others, due to the high propensity for chromosomal instability and copy number alterations in PC, which is known to coincide and potentially drive genomic instability[77–80]. MSH2 knockdown was sufficient to increase the sensitivity to WRN RNAi, but did not induce synthetic lethality in PC cells. similar to previous results targeting mismatch repair machinery in other cancer studies [29]. This supports the hypothesis described in the literature that unique genomic scarring, possibly in the form of specific secondary structures, from MSI repeat regions rely on the WRN protein for resolution. In addition to the damage caused by TA-repeat cruciform structures[32], we propose that G-quadruplexes (G4) are an alternative location where WRN is required to mediate genotoxic stress. The visualization of increased G4 foci in MSI+ prostate and colorectal carcinoma MSI+ HCT116 cell lines, as well as the observed increase of foci post WRN knockdown, may hold potential as promising biomarkers of MSI+ disease in tumor samples. This introduces the possibility of additional chemotherapeutic targets with inhibitors that stabilize the G4 tertiary structure such as, pyridostatin, which we observed to augment the effects of WRN knockdown in 22RV1^{WRN} cells. As such, Cx5461 is currently undergoing clinical trials in homologous and non-homologous end joining-deficient tumors [81].

We speculate lethality of WRN-depletion in MMRd is due to the accumulation of MSI over time, and therefore when WRN is perturbed, the cells are unable to mediate the resulting accumulations of WRN-specific DNA secondary structures around the replication fork, ultimately leading to irreparable DNA damage. We have yet to explore the relationship with WRN and alternatively driven hypermutated tumors, such as ones driven by loss of DNA polymerases, and the therapeutic utility of pyridostatin as well as other g quadruplex inhibitors will be critical to establish moving forward.

2.6 Figures

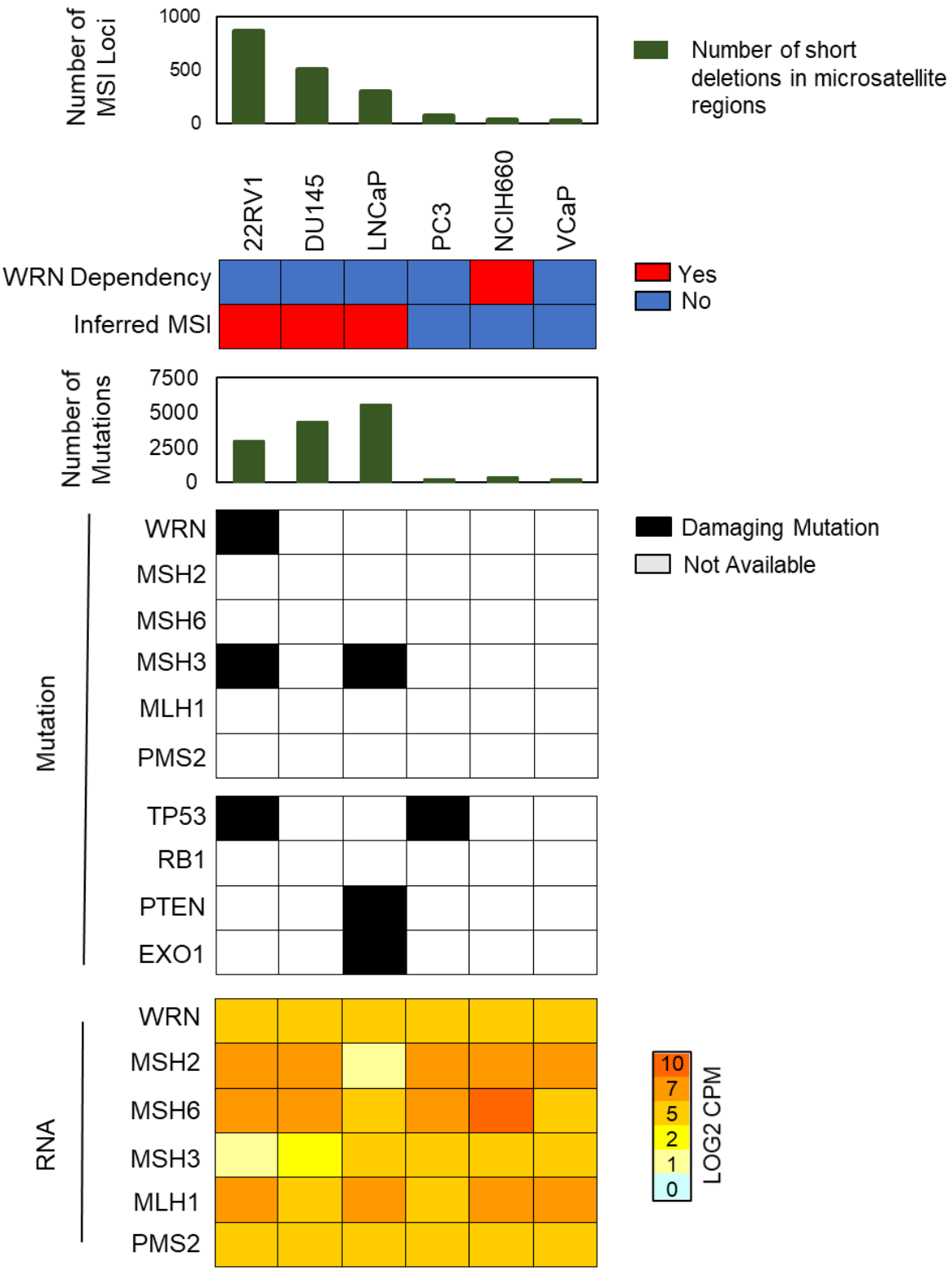
Number of MSI Loci
1000
500
0
Number of short deletions in microsatellite regions
22RV1
DU145
LNCaP
PC3
NCIH660
VCaP
WRN Dependency
Inferred MSI
Yes
No
Number of Mutations
7500
5000
2500
0
Mutation
WRN
MSH2
MSH6
MSH3
MLH1
PMS2
TP53
RB1
PTEN
EXO1
Damaging Mutation
Not Available
RNA
WRN
MSH2
MSH6
MSH3
MLH1
PMS2
10
7
5
2
1
0
LOG2 CPM

Figure 2.1. *WRN* and mismatch repair gene characterization in prostate cancer cell lines. Genomic characterization table of established prostate cancer cell lines quantifying number of MSI loci, WRN dependency, MSI status, number of mutations and damaging mutations (Cancer Cell Line Encyclopedia) as well as RNA transcriptional status of WRN and mismatch repair genes across cell lines from RNAseq.

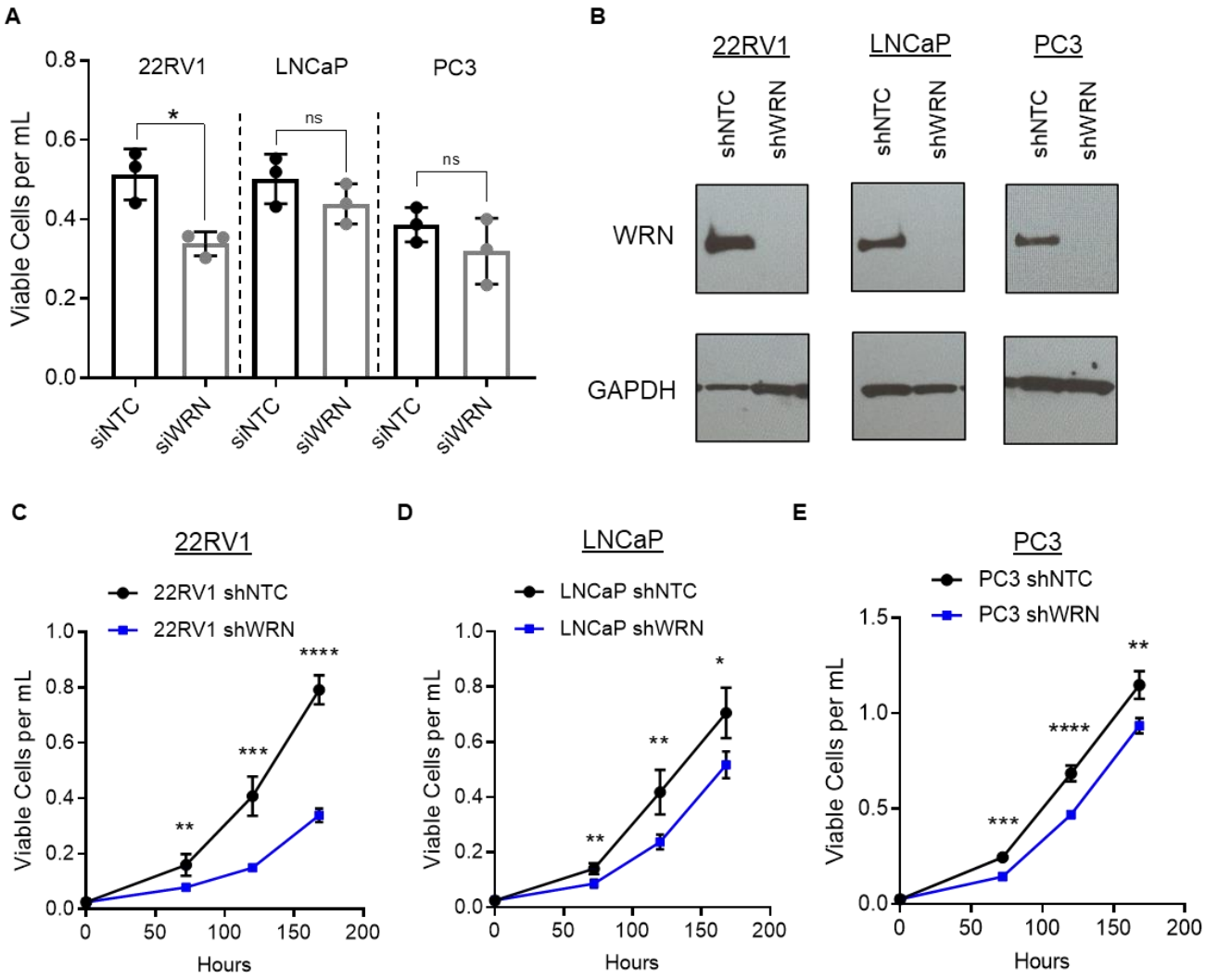

Figure 2.2. WRN knockdown results in growth suppression in MSI+ PC. (A) shNTC (Non-Targeting Control) and shWRN WRN and GAPDH protein expression across 22RV1, LNCaP and PC3 knockdown cell lines via western blot (B) Viable cell counts post RNAi treatment with either siWRN or scrambled si-Non-targeting control (siNTC). (C-E) Cell count growth curves over time of 22RV1, LNCaP and PC3 shNTC versus shWRN knockdown lines. **P < 0.01 by Unpaired, Two-tailed T-Test.

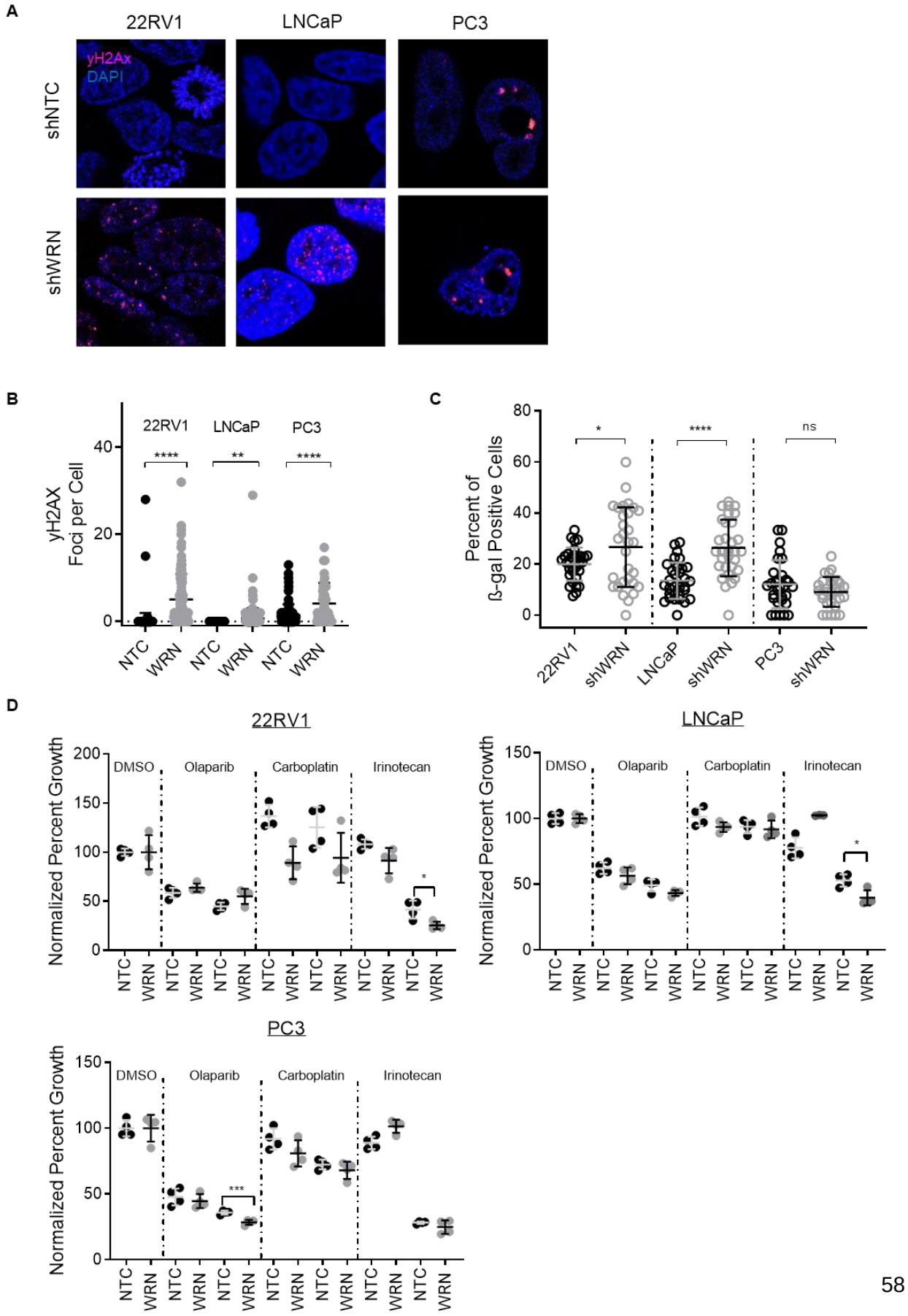
A
22RV1
LNCaP
PC3
yH2Ax
DAPI
shNTC
shWRN
B
22RV1
LNCaP
PC3
yH2AX
Foci per Cell
****
**
****
NTC
WRN
C
Percent of
ß-gal Positive Cells
*
****
ns
22RV1
shWRN
LNCaP
shWRN
PC3
shWRN
D
22RV1
LNCaP
PC3
Normalized Percent Growth
DMSO
Olaparib
Carboplatin
Irinotecan
NTC
WRN

Figure 2.3. WRN knockdown increases DNA damage and senescence staining but does not universally augment the effects of specific chemotherapeutics. (A) Confocal immunostaining (63x) and quantification (B) of γH2AX foci in 22RV1, LNCaP and PC3 shNTC versus shWRN knockdown cells (C) β-galactosidase staining in shWRN knock downs of cellular senescence after five days of growth (D) Normalized percent growth of shWRN knockdown lines vs non-targeting vector control, 48 hours after treatment with 3 or 5 μM Olaparib and Carboplatin, or 0.1 and 1μM Irinotecan, respectively. **P < 0.01 by Unpaired, Two-tailed T-Test.

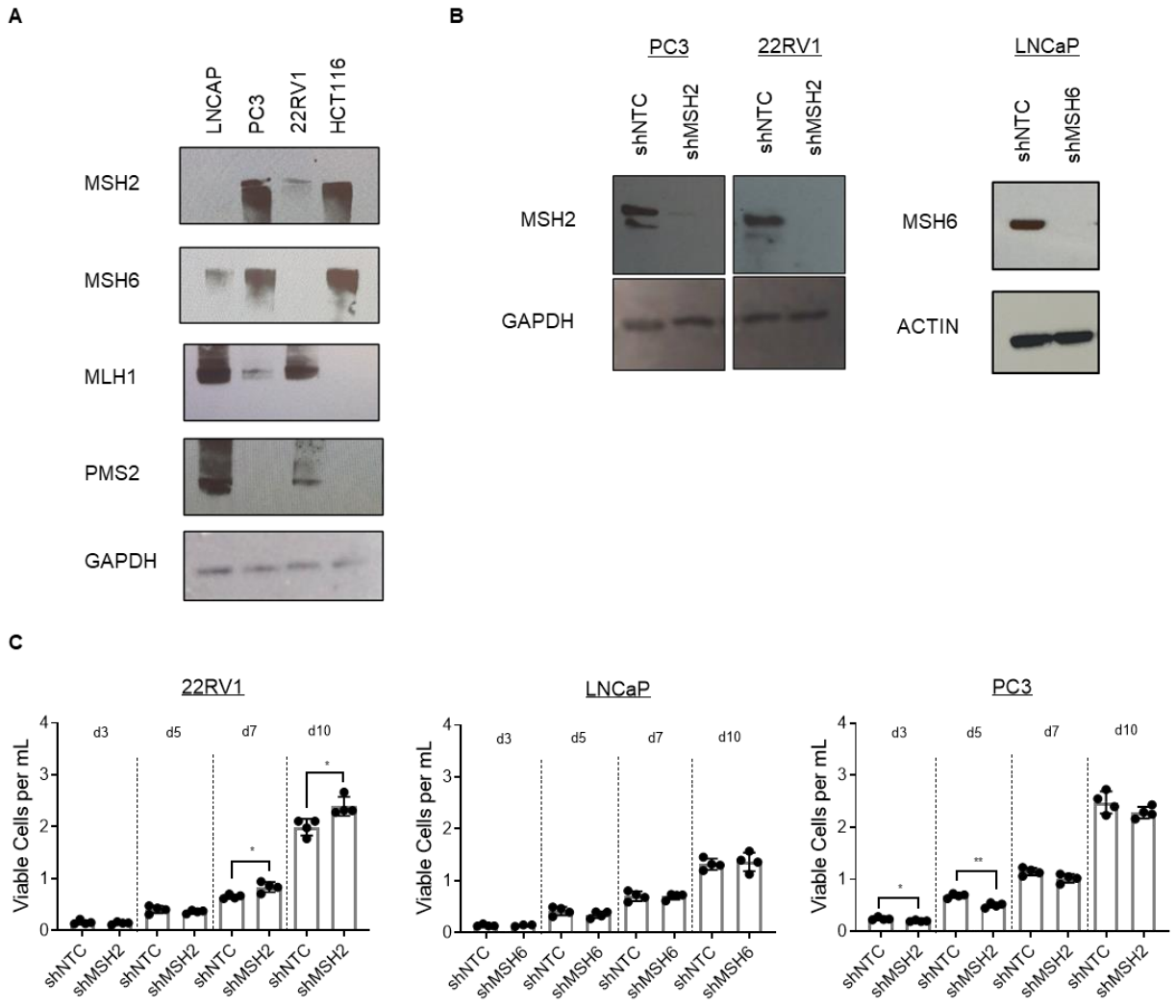

Figure 2.4. MSH2-MSH6 knockdown in prostate cancer cell lines. (A) Mismatch repair protein status in LNCaP, PC3, 22Rv1 and HCT116 by western blot. (B) MSH2 and NTC (Non-Targeting Control) knock down validation in PC3 and 22RV1 and MSH6 knock down validation in LNCaP by western blot. (C) Total cell counts of shMSH2 (PC3 and 22RV1) and shMSH6 (LNCaP) knockdown cells in selection media over 10 days.

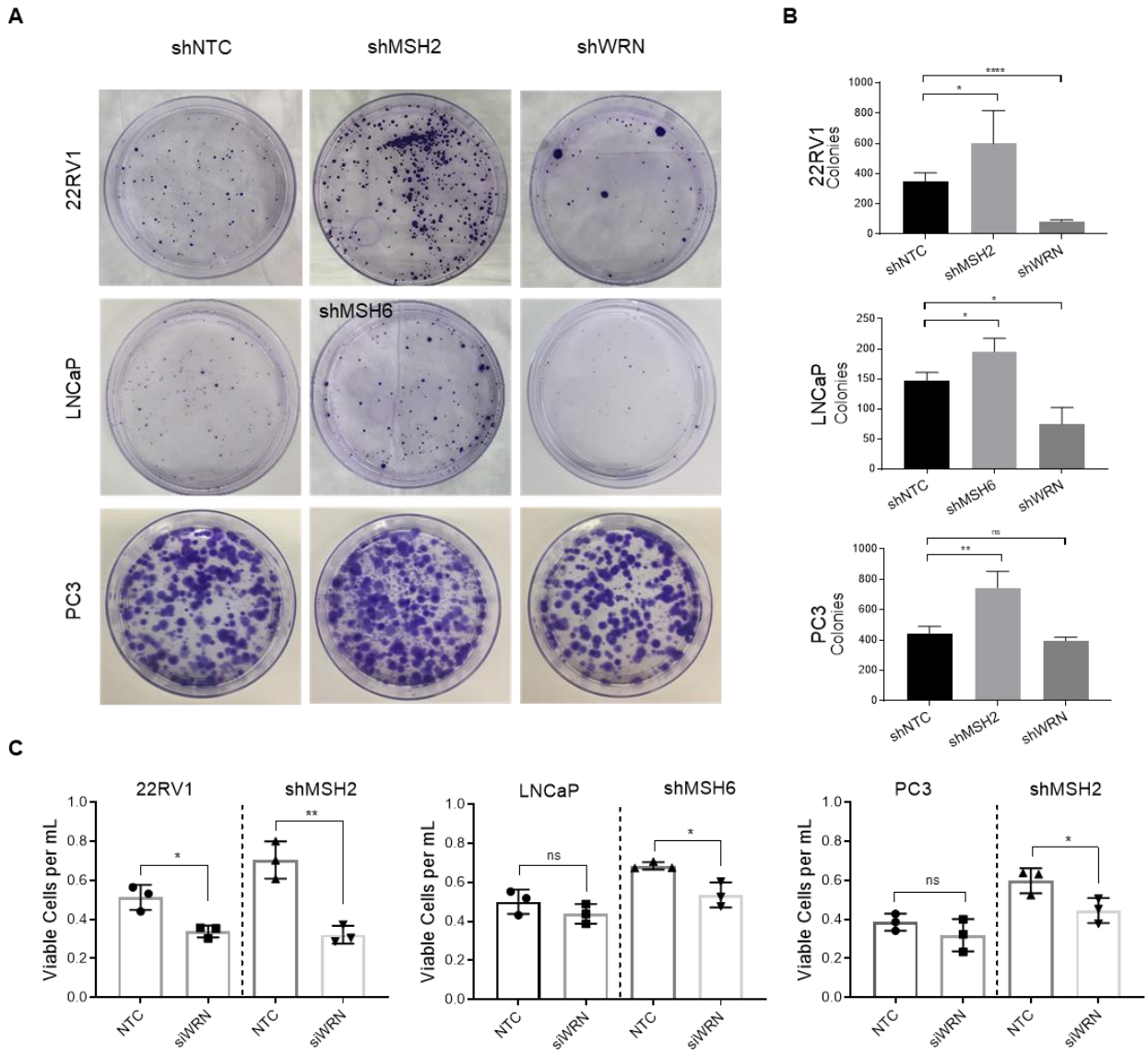

Figure 2.5. MSH2 knockdown promotes growth over time and is sufficient to induce sensitivity to WRN-double knockdown. (A-B) Clonogenic colony formation assay and quantification (B) over 21 days in shNTC, shMSH6 (LNCaP), shMSH2 (PC3 or 22RV1), or shWRN knockdown 22RV1, LNCaP and PC3 cells. (C) Double knockdown cell counts of 22RV1, LNCaP and PC3 cells post-48h of treatment with RNAi (siNTC or siWRN) as compared to RNAi-treated cell counts in the shMSH6 (LNCaP) and shMSH2 (PC3 and 22RV1) knockdowns. **P < 0.01 by Student's T-Test compared to control.

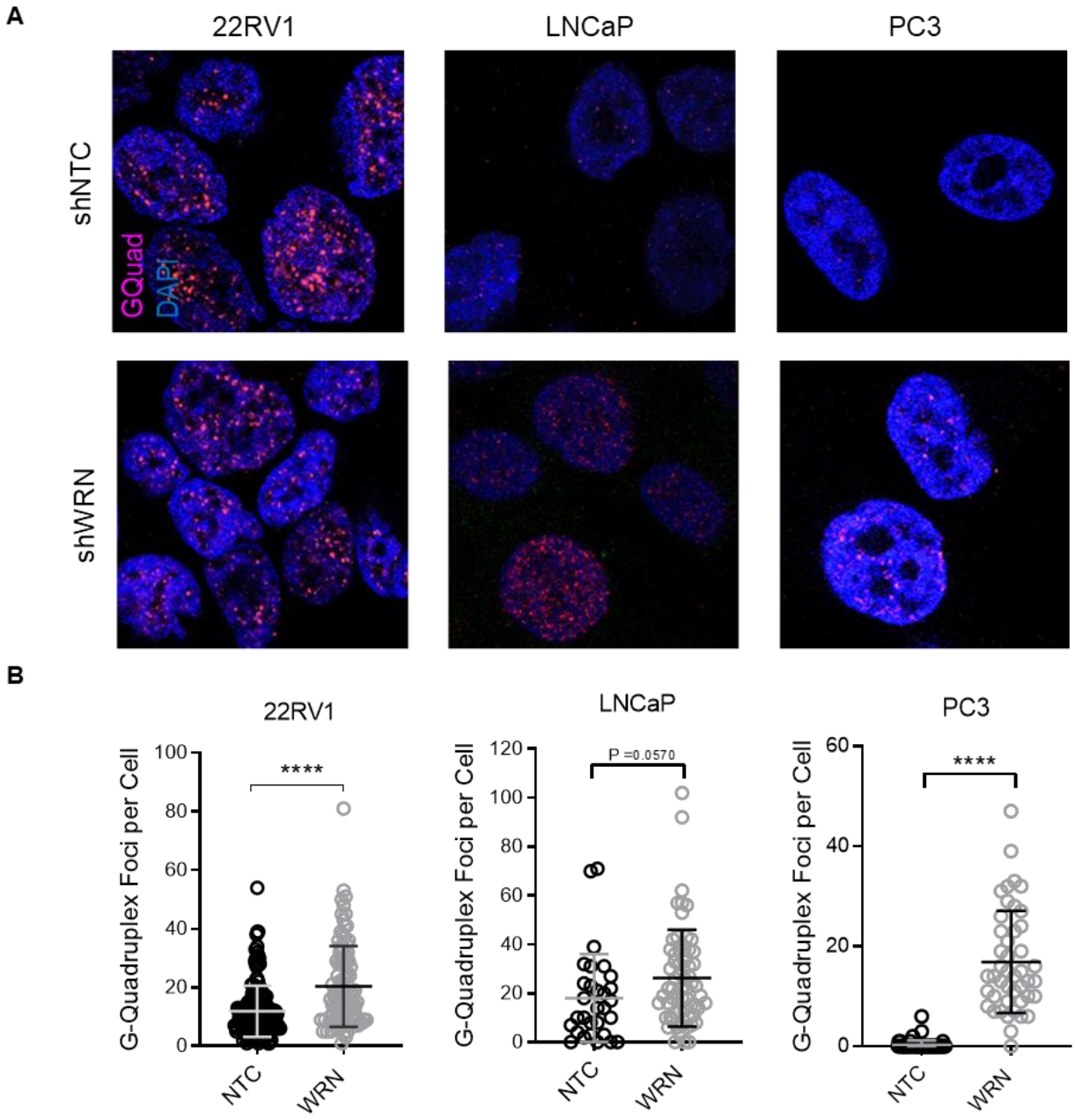
A
22RV1
LNCaP
PC3
shNTC
shWRN
GQuad
DAPI
B
22RV1
LNCaP
PC3
G-Quadruplex Foci per Cell
****
P =0.0570
NTC
WRN

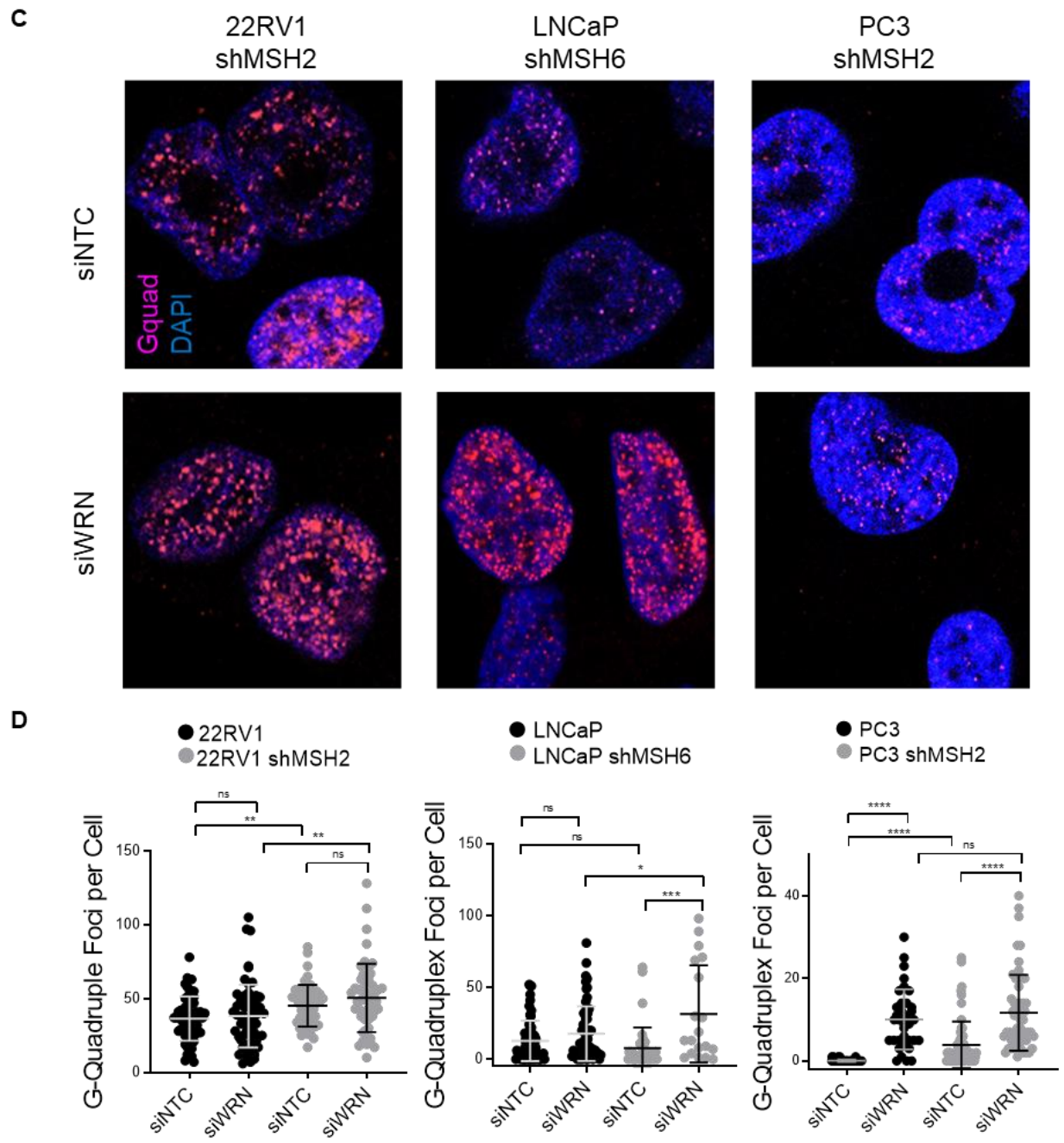

Figure 2.6. Both WRN and MSH2-WRN double knockdown increases G4 foci. (A-B) Confocal immunostaining (A) and quantification (B) of G-Quadruplexes in 22RV1, LNCaP and PC3 shWRN knockdown. (C-D) Confocal immunostaining (C) and quantification (D) of G-quadruplexes in 22RV1 shMSH2, LNCaP shMSH6 and PC3 shMSH2 knockdown cells after 48h exposure to control siNTC or siWRN RNAi. Original magnification for A and C: ×40. **P < 0.01 by Unpaired, Two-tailed T-Test.

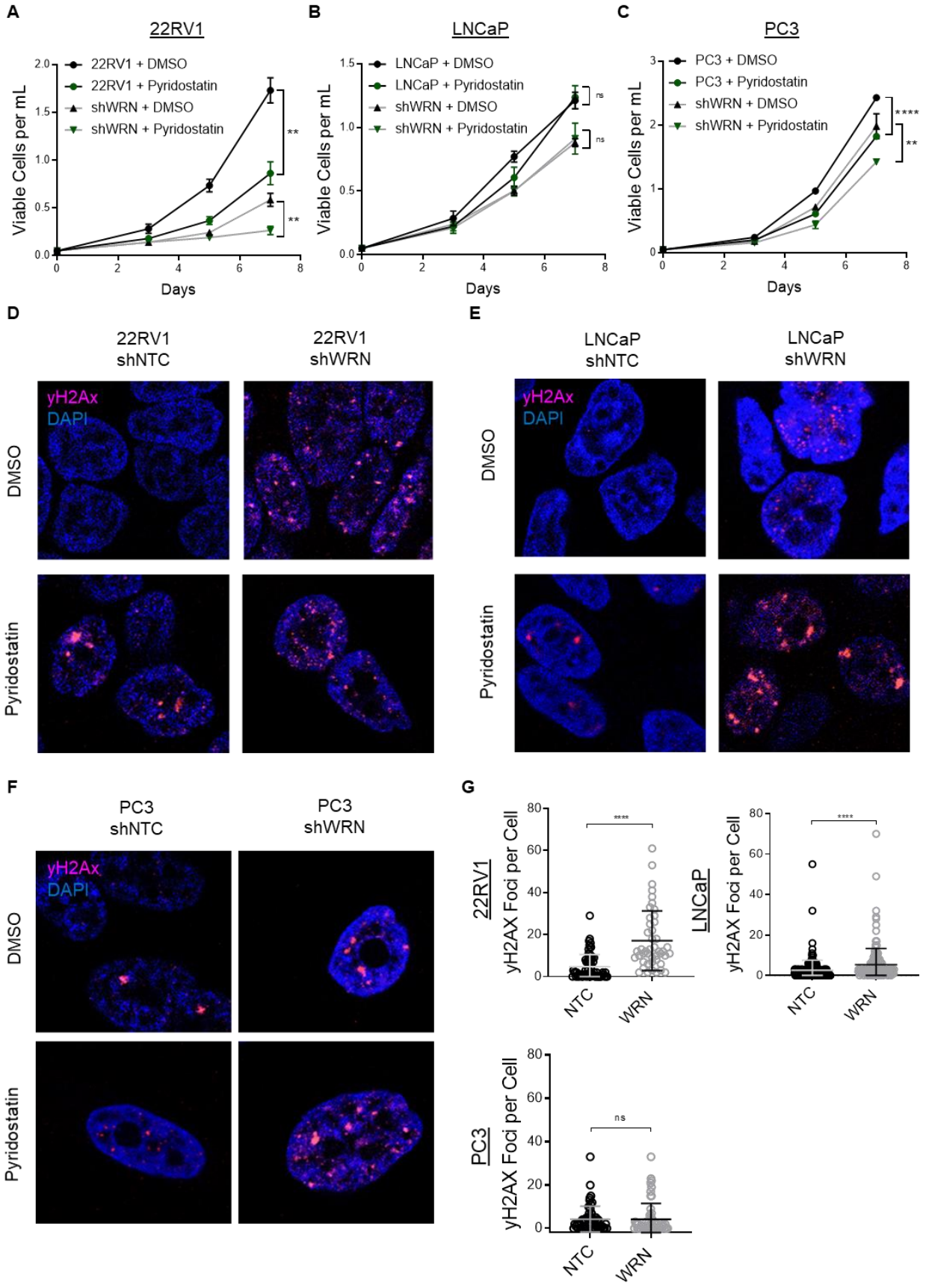
A
22RV1
Viable Cells per mL
Days
22RV1 + DMSO
22RV1 + Pyridostatin
shWRN + DMSO
shWRN + Pyridostatin
**
**
B
LNCaP
Viable Cells per mL
Days
LNCaP + DMSO
LNCaP + Pyridostatin
shWRN + DMSO
shWRN + Pyridostatin
ns
ns
C
PC3
Viable Cells per mL
Days
PC3 + DMSO
PC3 + Pyridostatin
shWRN + DMSO
shWRN + Pyridostatin
****
**
D
22RV1 shNTC
22RV1 shWRN
DMSO
Pyridostatin
yH2Ax
DAPI
E
LNCaP shNTC
LNCaP shWRN
DMSO
Pyridostatin
yH2Ax
DAPI
F
PC3 shNTC
PC3 shWRN
DMSO
Pyridostatin
yH2Ax
DAPI
G
22RV1
yH2AX Foci per Cell
****
NTC
WRN
LNCaP
yH2AX Foci per Cell
****
NTC
WRN
PC3
yH2AX Foci per Cell
ns
NTC
WRN

Figure 2.7. G4 stabilizer, pyridostatin, generates DNA damage in shWRN knockdown and growth suppression in MSI+ mPC. (A-C) Viable cells per mL of 22RV1, LNCaP and PC3 shNTC control and shWRN knockdown lines after 3, 5 or 7 days of growth in DMSO or 0.1 µM pyridostatin media. (D-F) Confocal immunostaining (63x) of γH2AX in 22RV1, LNCaP and PC3 shNTC versus shWRN cells, 72 hours after treatment with growth media containing DMSO, or 0.1 µM pyridostatin. (D) Quantitation of γH2AX foci counts per cell in 22RV1, LNCaP and PC3 shNTC and shWRN cell lines exposed to DMSO, or 0.1 µM pyridostatin. **P < 0.01 by Unpaired, Two-tailed T-Test.

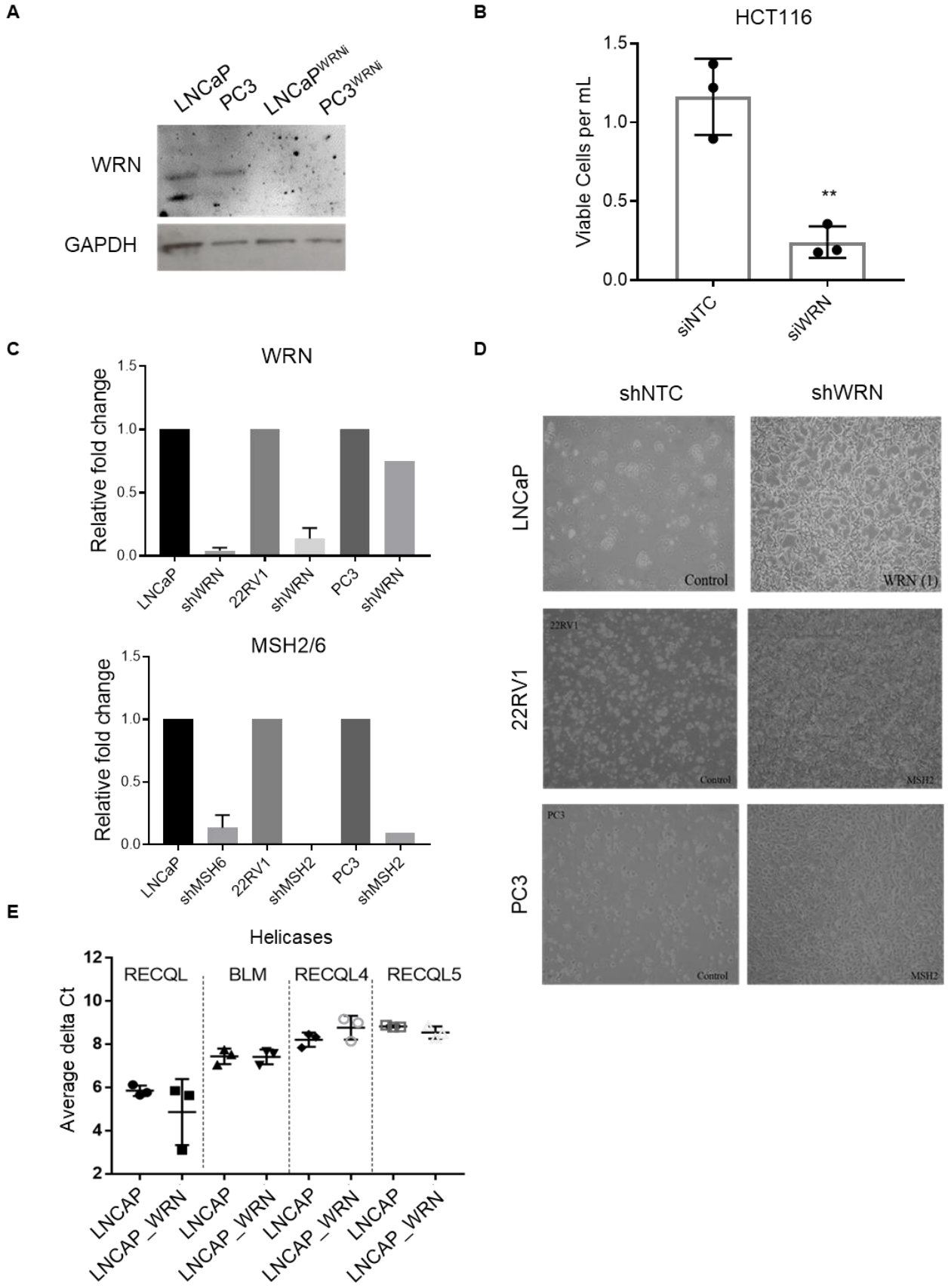
A
LNCaP
PC3
LNCaP^WRNi
PC3^WRNi
WRN
GAPDH
B
HCT116
Viable Cells per mL
1.5
1.0
0.5
0.0
**
siNTC
siWRN
C
WRN
Relative fold change
1.5
1.0
0.5
0.0
LNCaP
shWRN
22RV1
shWRN
PC3
shWRN
MSH2/6
Relative fold change
1.5
1.0
0.5
0.0
LNCaP
shMSH6
22RV1
shMSH2
PC3
shMSH2
D
shNTC
shWRN
LNCaP
22RV1
PC3
Control
WRN (1)
22RV1
Control
MSH2
PC3
Control
MSH2
E
Helicases
Average delta Ct
12
10
8
6
4
2
RECQL
BLM
RECQL4
RECQL5
LNCAP
LNCAP_WRN
LNCAP
LNCAP_WRN
LNCAP
LNCAP_WRN
LNCAP
LNCAP_WRN

Supplemental Figure 2.1. Generating a model of WRN knockdown in mPC. (A) RNAi knockdown validation in LNCaP and PC3 via western blot (B) Cell counts of HCT116 cells exposed to 48h treatment with siNTC or siWRN RNAi. (C) rtPCR validation of WRN knockdown (D) 20x magnification images of vector free control lines versus puromycin sh-WRN knockdown LNCaP, 22RV1 and PC3 cells. (E) RECQL helicase transcriptional expression (average delta ct) in LNCaP shNTC control versus shWRN knockdown.

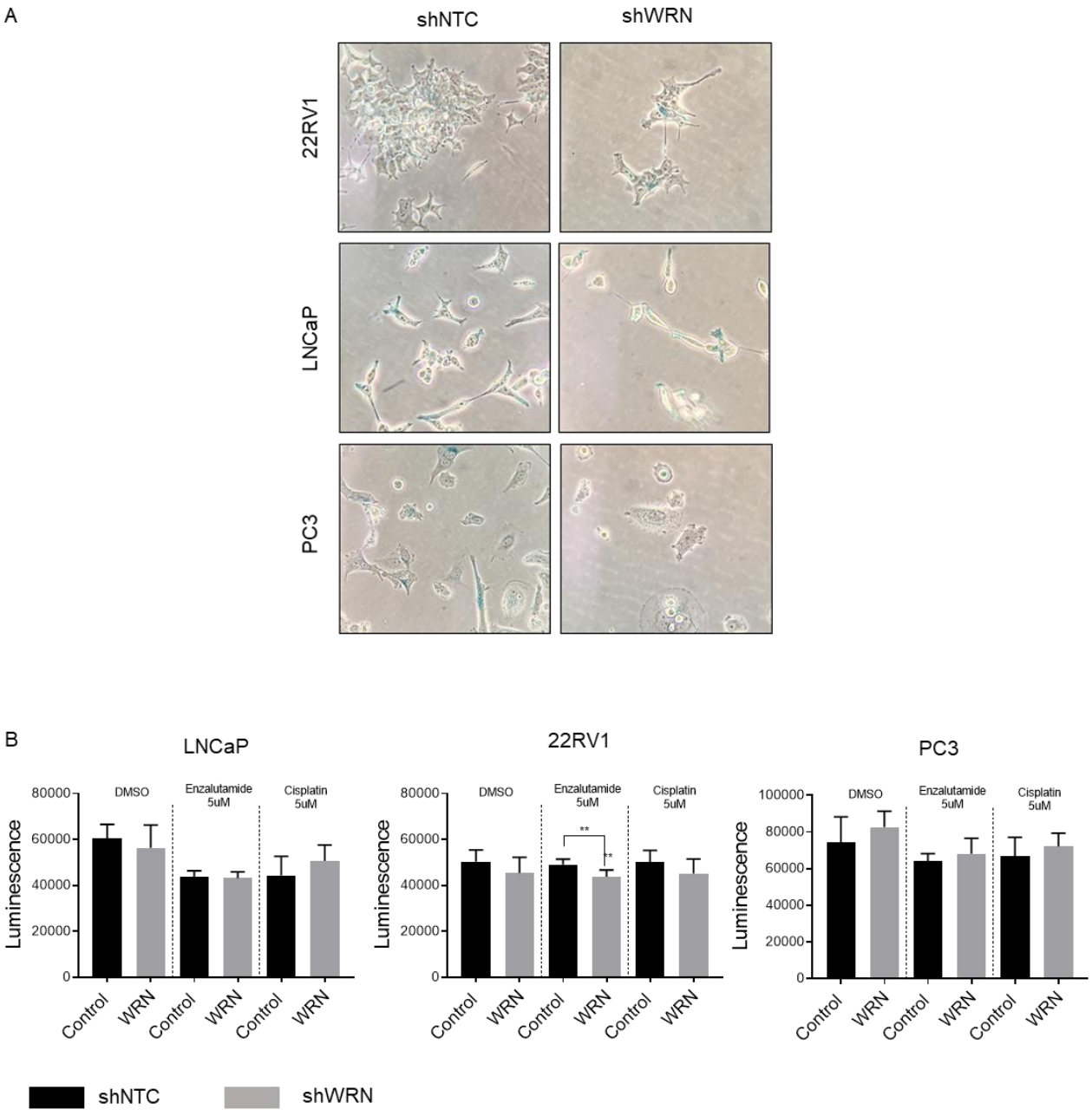
A
shNTC
shWRN
22RV1
LNCaP
PC3
B
LNCaP
22RV1
PC3
Luminescence
DMSO
Enzalutamide 5uM
Cisplatin 5uM
Control
WRN
shNTC
shWRN

Supplemental Figure 2.2. WRN knockdown increases senescent staining but does not alter drug sensitivity. (A) Representative images of β-galactosidase staining in shNTC control lines versus shWRN knockdown lines after five days of growth. Imaged under brightfield at 40x magnification. (B) Cell viability assay by cell titer glo quantification of shWRN knockdown lines vs non-targeting vector control, 48 hours after treatment with either enzalutamide or cisplatin (5uM). **P < 0.01 by Unpaired, Two-tailed T-Test to control.

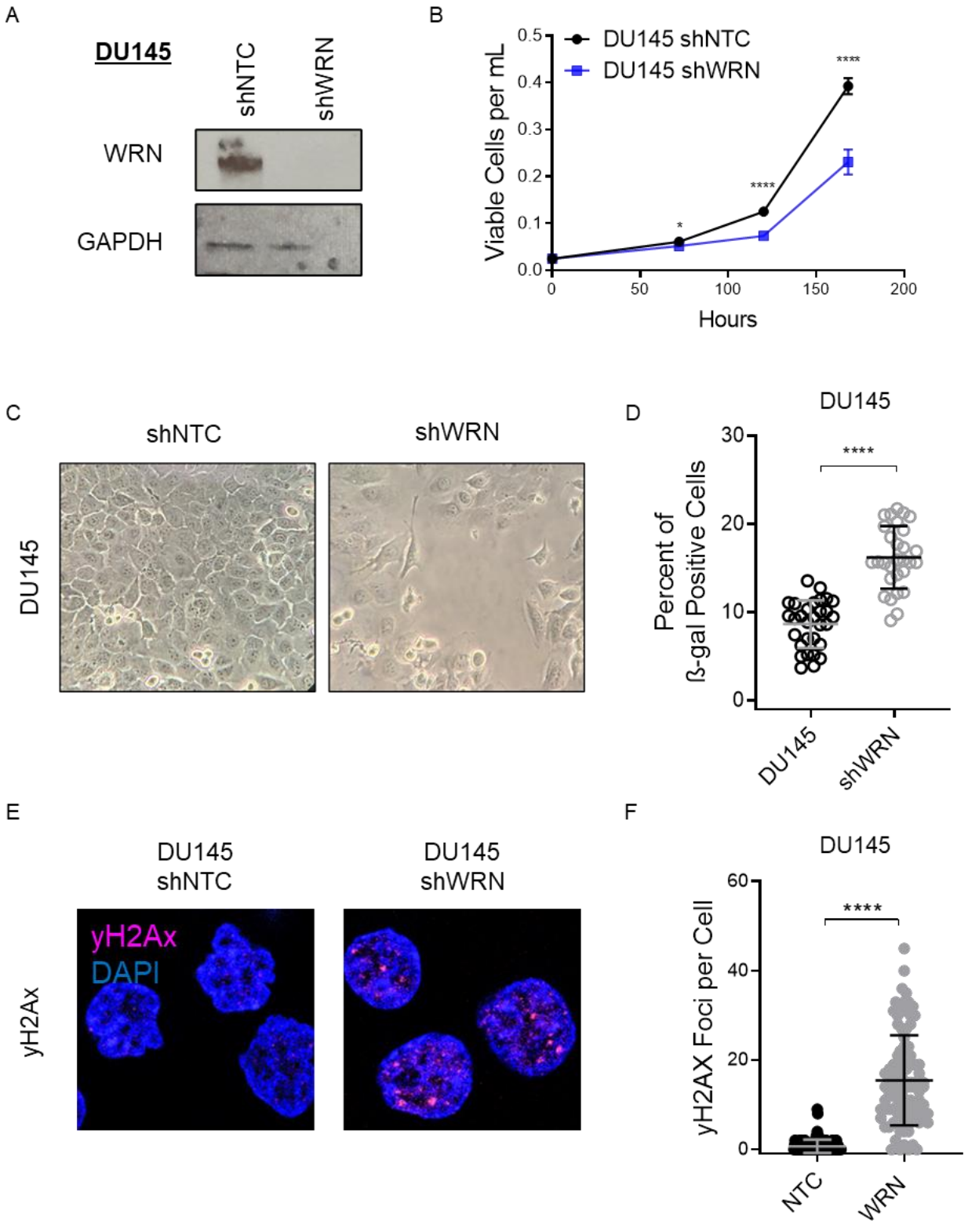
A
DU145
shNTC
shWRN
WRN
GAPDH
B
DU145 shNTC
DU145 shWRN
Viable Cells per mL
0.5
0.4
0.3
0.2
0.1
0.0
0
50
100
150
200
Hours
*
****
****
C
shNTC
shWRN
DU145
D
DU145
Percent of ß-gal Positive Cells
30
20
10
0
****
DU145
shWRN
E
DU145 shNTC
DU145 shWRN
yH2Ax
yH2Ax
DAPI
F
DU145
yH2AX Foci per Cell
60
40
20
0
****
NTC
WRN

Supplemental Figure 2.3. MSI+ DU145 cells exhibit growth repression, senescence and DNA damage post WRN knockdown. (A) shNTC and shWRN knockdown WRN and GAPDH protein expression in DU145 cell lines via western blot. (B) Cell count growth curves over time of DU145 shNTC versus shWRN knockdown lines. (C) Representative images of β-galactosidase staining in shNTC control lines versus shWRN knockdown DU145 cells after five days of growth. Imaged under brightfield at 40x magnification. (D) β-galactosidase staining in shWRN knock downs of cellular senescence after five days of growth. (E) Confocal immunostaining (63x) and quantification (F) of γH2AX in DU145 shNTC versus shWRN knockdown cells **P < 0.01 by Unpaired, Two-tailed T-Test

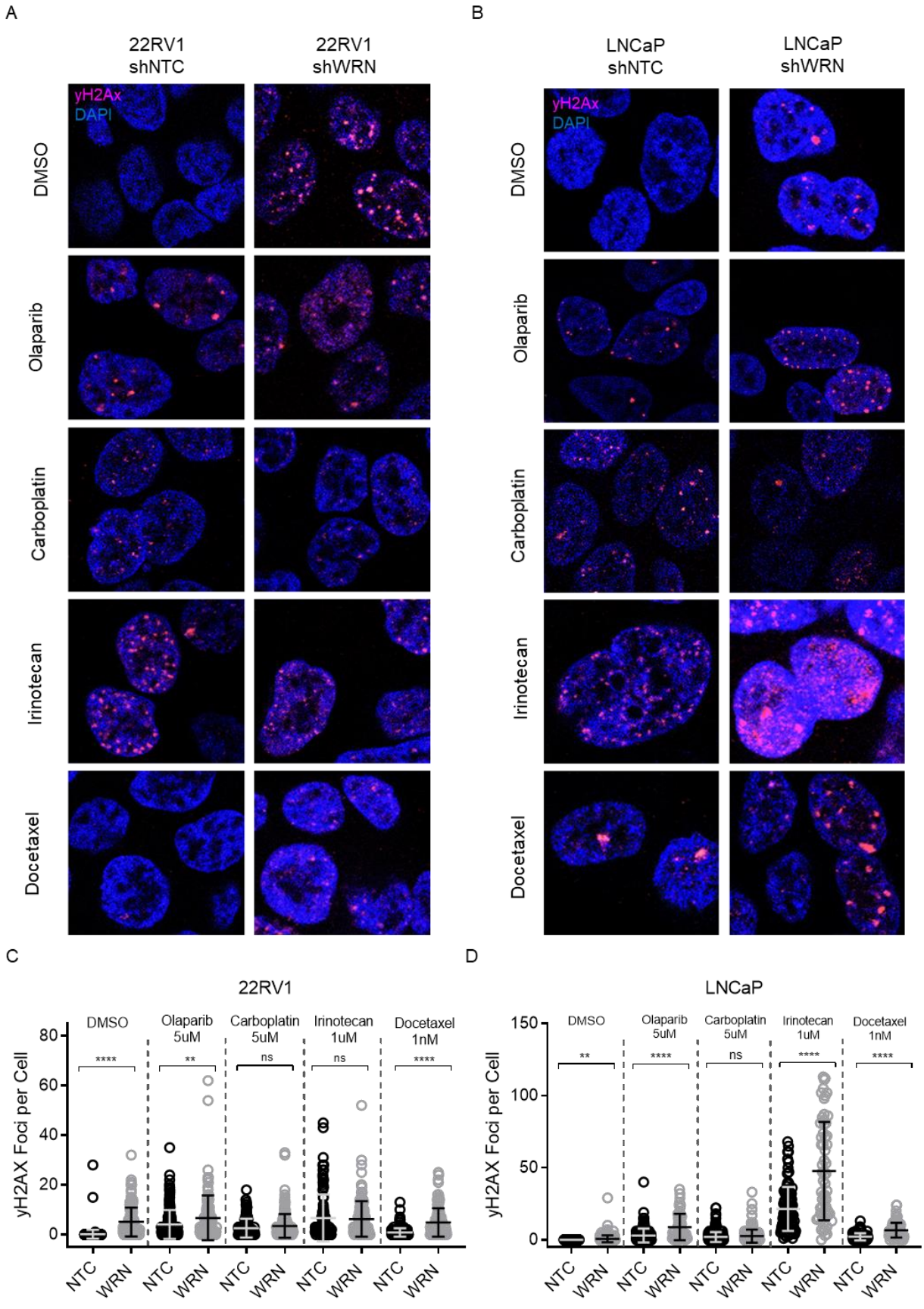
A
22RV1 shNTC
22RV1 shWRN
yH2Ax
DAPI
DMSO
Olaparib
Carboplatin
Irinotecan
Docetaxel
B
LNCaP shNTC
LNCaP shWRN
C
22RV1
yH2AX Foci per Cell
DMSO
Olaparib 5uM
Carboplatin 5uM
Irinotecan 1uM
Docetaxel 1nM
****
**
ns
NTC
WRN
D
LNCaP

Supplemental Figure 2.4. WRN knockdown lines have increased yH2Ax foci post-chemotherapeutic exposure. (A-B) Confocal immunostaining (63x) of γH2AX in 22RV1 and LNCaP shNTC versus shWRN cells 72 hours after treatment with growth media containing DMSO, 5 μM Olaparib, 5 μM Carboplatin, 1 μM Irinotecan, or 1nM Docetaxel. (C-D) Quantitation of γH2AX foci counts per cell in 22RV1 or LNCaP shNTC and shWRN cell lines exposed to DMSO, 5 μM Olaparib, 5 μM Carboplatin, 1 μM Irinotecan or 1nM Docetaxel. Original magnification for A and B: ×40. **P < 0.01 by Unpaired, Two-tailed T-Test.

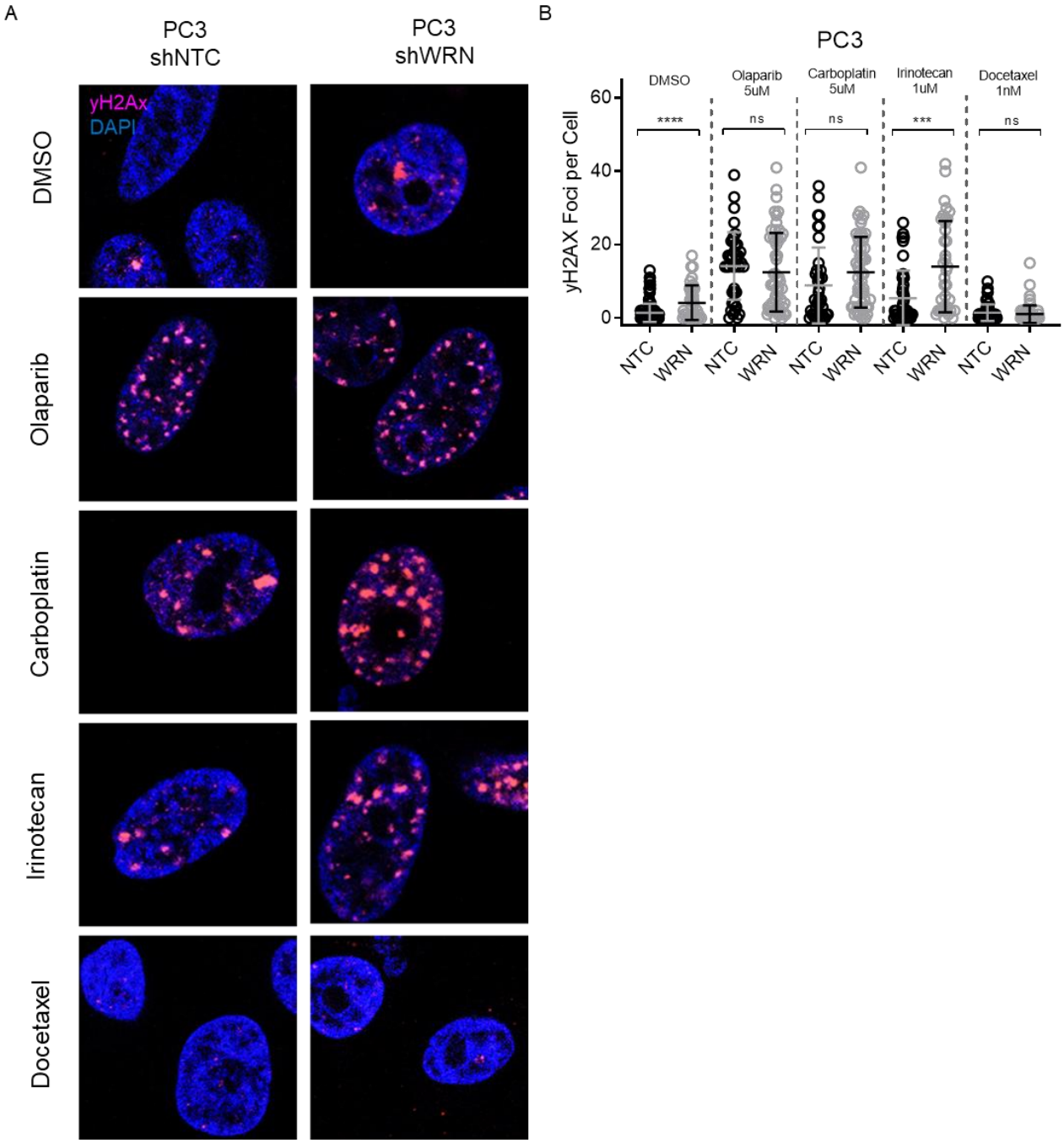
A
PC3
shNTC
PC3
shWRN
yH2Ax
DAPI
DMSO
Olaparib
Carboplatin
Irinotecan
Docetaxel
B
PC3
yH2AX Foci per Cell
DMSO
Olaparib 5uM
Carboplatin 5uM
Irinotecan 1uM
Docetaxel 1nM
****
ns
ns
***
ns
NTC
WRN

Supplemental Figure 2.5. WRN knockdown increases γH2AX foci in PC3 cells post-selected chemotherapeutics. (A) Confocal immunostaining (63x) of γH2AX in PC3 shNTC versus shWRN cells 72 hours after treatment with growth media containing DMSO, 5 μM Olaparib, 5 μM Carboplatin, 1 μM Irinotecan or 1nM Docetaxel. (B) Quantitation of γH2AX foci counts per cell in PC3 shNTC and shWRN cell lines exposed to DMSO, 5 μM Olaparib, 5 μM Carboplatin, 1 μM Irinotecan or 1nM Docetaxel. Original magnification for A and C: ×40. **P < 0.01 by Unpaired, Two-tailed T-Test.

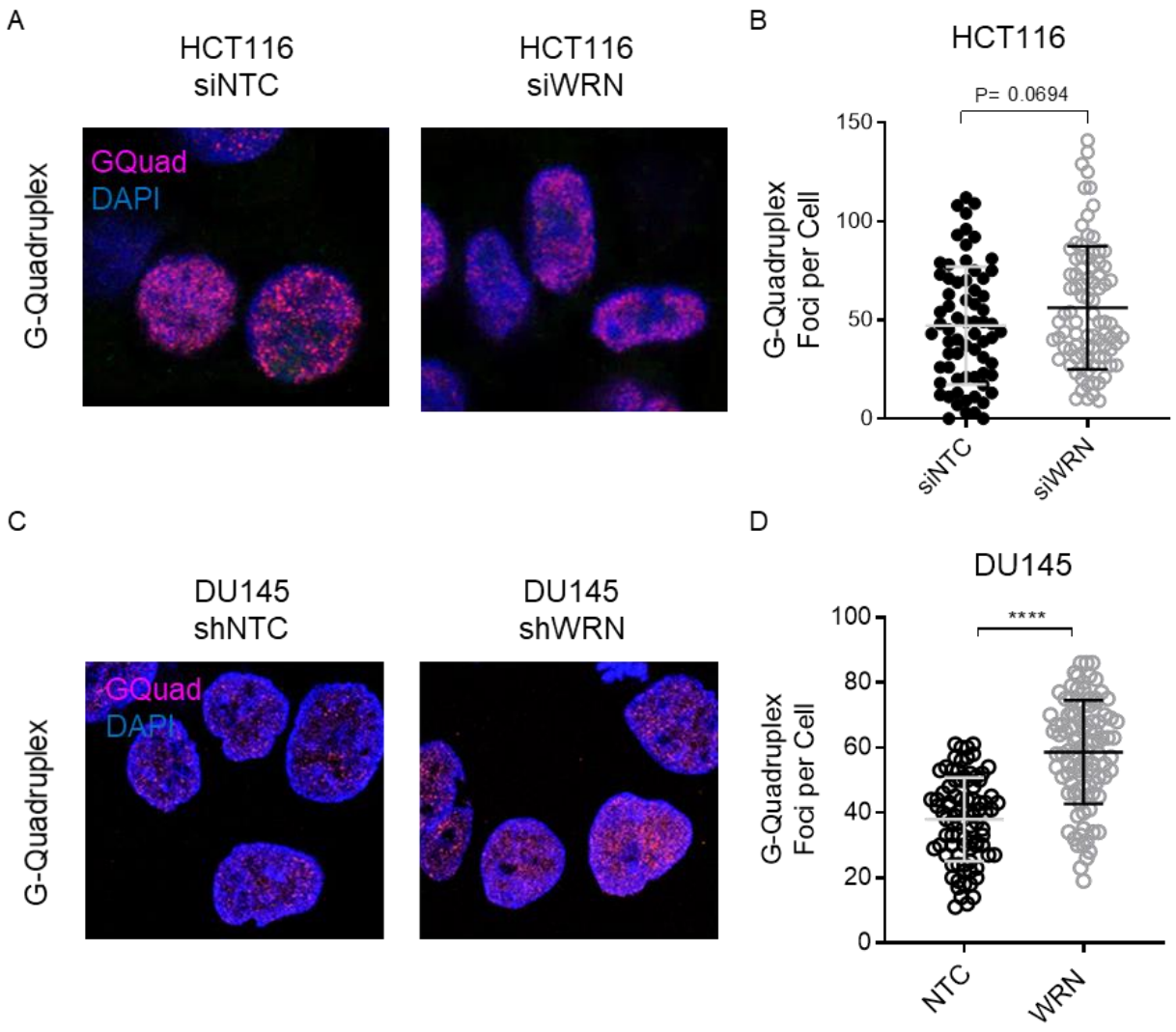

Supplemental Figure 2.6. G4-foci in MSI+ HCT116 and DU145 cells post-WRN knockdown. (A) Confocal immunostaining (A, C) (63x) and quantification (B, D) of G-Quadruplex foci in HCT116 grown in non-targeting siRNA media or siWRN knockdown (A-B) and DU145 shNTC versus shWRN isogenic knockdown cells (C-D) **P < 0.01 by Unpaired, Two-tailed T-Test.

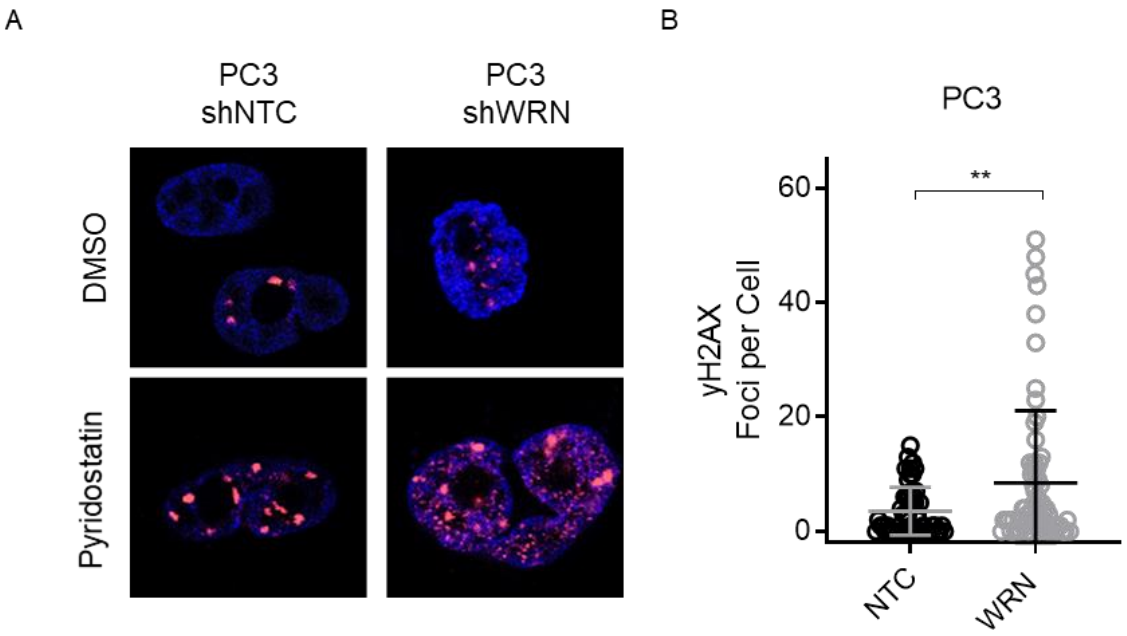

Supplemental Figure 2.7. WRN knockdown in PC3 cells increase γH2AX foci post-pyridostatin exposure. (A)Confocal immunostaining (63x) of γH2AX in PC3 shNTC versus shWRN cells, 72 hours after treatment with growth media containing DMSO, or 1 μM pyridostatin. (B) Quantitation of γH2AX foci counts per cell in PC3 shNTC and shWRN cell lines exposed to DMSO or 1 μM pyridostatin. **P < 0.01 by Unpaired, Two-tailed T-Test.

Chapter 3. Conclusions and Future Directions

3.1 Summary of Results

The series of studies included in this thesis examined the significance of RECQ-like DNA helicase 2, or WRN, in metastatic prostate cancer. Aberrations to *WRN* in mPC predominantly occur via homozygous deletion (homdel) alongside the 8p arm loss, and is responsible for regulating transcriptional expression. Tumors with *WRN* homdel in PRAD have lower overall survival and in mPC have a higher overall AR score and enrichment for Gleason score 8, but are not associated with NEPC or hypermutation. In mPC and across the entire TCGA dataset, tumors with *WRN* homdel did not overlap with hypermutated or MSI-high tumors and are mutually exclusive to the loss of driver MMR-mutations. As WRN is functionally required for eventual therapeutic targeting, we have established that *WRN* is rarely altered by homozygous deletion in MMRd or MSI tumors and is a promising target for chemotherapeutic inhibition.

In order to determine the effects on WRN therapeutic targeting on tumor cells, I used tumors excised from our established PDX xenograft line, the LuCaP series, disassociated them into 2D cultures and treated them with two doses of WRN inhibitor NSC 19630. I observed sensitivity to a lower dose of NSC 19630 in MMRd and HRRd tumors, including mPC MSI+ lines, suggesting that WRN inhibitors could have a more broad therapeutic impact than in MSI cancers alone. Expanding on this observation, I utilized an established dox-inducible BRCA2 knockdown LNCaP line and observed greater sensitivity to WRN-knockdown in the BRCA2-dox line than in control, as well as

more DNA damage from 53BP1 foci quantification after treatment with NSC 19630. In all, these promising results suggest that not only mPC MSI or MMRd patients could benefit from future usage of WRN-inhibitors, but also tumors with a wider range of DRD.

I then sought to establish isogenic cell lines to better study and characterize the effects of both WRN and MSH2-MSH6 complex knockdown individually and in tandem in mPC cell lines. MSI-high PC cell lines 22RV1 and DU145 were more sensitive to WRN depletion than other lines used in this study, LNCaP and PC3. I demonstrated that WRN knockdown induces DNA damage and senescent programming, but does not universally augment the effects of one specific chemotherapeutic. I then targeted the MSH2/MSH6 complex by knocking down MSH2 in 22RV1 and PC3, and MSH6 in MSH2-mutated LNCaP; interestingly loss of the MSH2 complex appeared to increase cell growth over time, especially in 22RV1. I then used RNAi to simulated a WRN-double knockdown condition, and observed that MSH2-loss was sufficient to induce further sensitivity to WRN-knockdown, but does not induce the synthetic lethality as observed in other cell lines such as HCT116. This suggests that a genomic effect, rather than MMR protein function itself, is mechanistically more likely responsible for the observed WRN synthetic lethality in large-scale CRISPR screens.

As WRN functionally resolves G-Quadruplex DNA knots during replication, I hypothesized that if the accumulation of these structures is observed, then their resolution may be a possible mechanism of WRN-destabilization in MSI cell lines. I then aimed to investigate the presence and variability of G4-DNA in mPC using the WRN and MSH2-complex knockdown lines, and observed an increase in G4 DNA across all lines post-WRN knockdown and in the WRN-MSH2 double knockdown condition. MSI

mPC cell lines 22RV1 was especially sensitive to G4 inhibitor pyridostatin, and all lines had increased DNA damage in the WRN knockdown grown in pyridostatin containing media. Importantly, I introduce an additional chemotherapeutic option for MSI tumors targeting G4 DNA, pyridostatin.

Our studies re-examine previous findings regarding synthetic lethality to WRN loss in MSI-high PC cell lines and demonstrate that, though not synthetically lethal, MSI mPC cells are still sensitive to WRN knockdown and provide evidence for the inclusion of prostate cancer MSI+ tumors in future studies. While these studies have provided insight into the pathology of WRN loss and mechanism of MSI-WRN sensitivity, several questions remain unanswered. These topics are discussed in the following sections.

3.2 Future Directions

The series of studies included in this dissertation provide evidence that WRN is a promising target in MMRd-MSI prostate cancers. During this process of scientific research, a number of key questions beyond the direct scope of this dissertation have emerged. Overarching questions that warrant future investigation include how the *WRN* focal deletion alters tumor progression versus the 8p chromosomal deletion as a whole, whether novel WRN inhibitors alone or in combination with other chemotherapeutic treatment improves survival of MSI and DRD mPC *in vivo* models, and if G4 DNA could be a clinically useful biomarker for WRN-targeted chemical inhibition. This section highlights critical avenues of research, as well as the results of initial experiments, that address these questions.

3.2.1 *WRN* deletion on 8p and gene dosage by copy number variation

This research has demonstrated the adverse outcomes associated with *WRN* homozygous deletion in mPC, though the breadth of new clinical associations remains to be explored. Further, it will be important to distinguish how the underlying circuitry is altered when both *WRN* and the entire 8p chromosomal arm is lost via homozygous deletion. To explore this, I looked for enrichment in co-occurring alterations in driver pathways with *WRN* homozygous deletion in mPC SU2C, and found that a *WRN* homdel co-occurs with *MYC*, *AMER1* (WNT signaling), *PIK3CA* and *STK3* (HIPPO pathway) amplification, as well as *TP53* and *PTEN* loss (Figure 3.1). This tumor-promoting circuitry contributes to the observed adverse outcomes as presented in mPC.

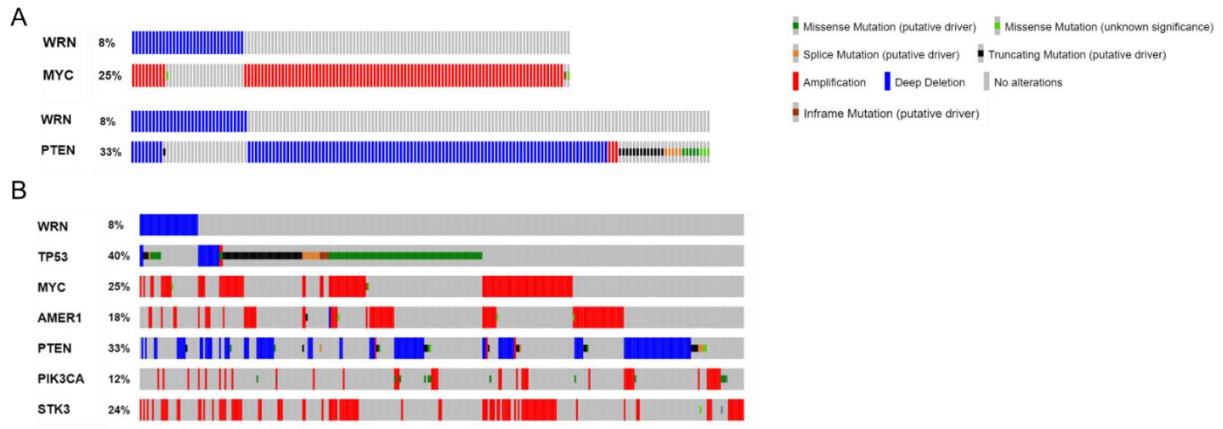

Figure 3.1. Co-occurring oncogenic pathway aberrations with *WRN* HOMDEL. (A) Oncoplot of tumors with *WRN* homozygous deletion, *MYC* and *PTEN* alterations in SU2C. Grey bars without alterations are omitted for space. (B) Oncoplot of tumors (columns) with *WRN* homozygous deletion with major pathway co-occurring alterations:

TP53, *MYC*, *AMER1* (WNT signaling), *PTEN*, *PIK3CA* and *STK3* (HIPPO pathway) alterations in SU2C. Grey bars without alterations are omitted for space.

This approach to characterizing *WRN* loss could be expanded to clinical associations based on WRN transcriptional status as well as 8p arm loss overall, in both mPC and PRAD. Further, it would be interesting to compare outcomes and gene circuitry changes to other cancers where *WRN* is lost, both via homozygous deletion or via additional means such as promoter methylation or pathogenetic mutation.

Overall, clinical genetic screens are structured by diagnostics using mutational aberrations, however, there are many ways gene expression can be dysregulated. Prostate cancer is driven by chromosomal rearrangements and alterations to genome copy number, and determining which genes are transcriptionally regulated by copy number variation may help to broaden the scope of personalized medicine.

To determine which dosage-sensitive genes are functional regulators of gene expression, I utilized the BROAD TCGA Firehose database (https://gdac.broadinstitute.org/) to compute overlaps with both RNA seq & CNV profiles in patient data. The associated software generated gene transcriptional expression vs copy number matrixes for available genes, and used a Pearson Correlation to rank linear relationship (Table 3.1). I then filtered out samples with missing data, filtered the correlation coefficient > 0, and filtered p & q statistic < .005. I then organized the results by cytoband, quantified the number of genes per region, and characterized what

transcriptional pathways the resulting genes were part of using PANTHRdb (http://pantherdb.org/) (Figure 3.1-3.4, Table 3.2).

	Copy Number	Expression	Common
Samples	492	497	491
Genes	24776	18274	15626

Table 3.1. Counts of the number of samples and genes with corresponding copy number and expression data sets.

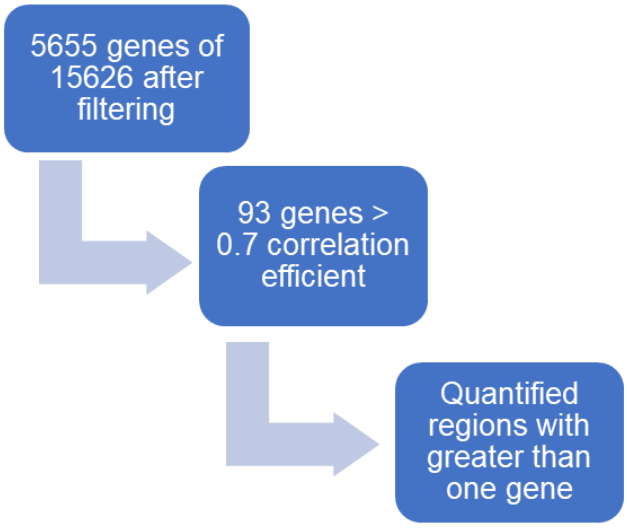

Figure 3.2. Gene expression versus copy number schematic.

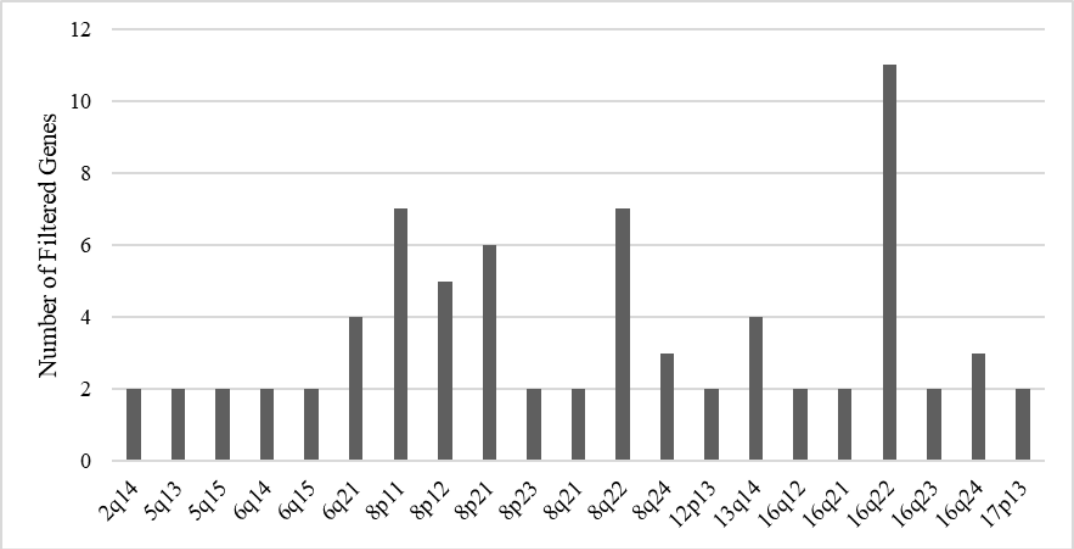

Figure 3.3. Where the top 20 gene-dosage genes are located in the genome.

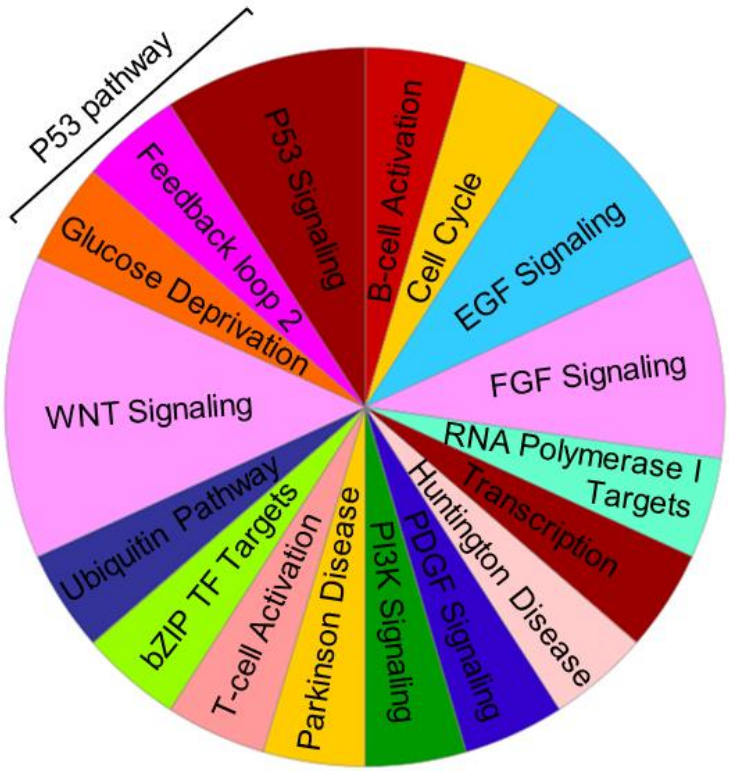

Figure 3.4. PANTHER analysis of 91 gene-dosage sensitive genes.

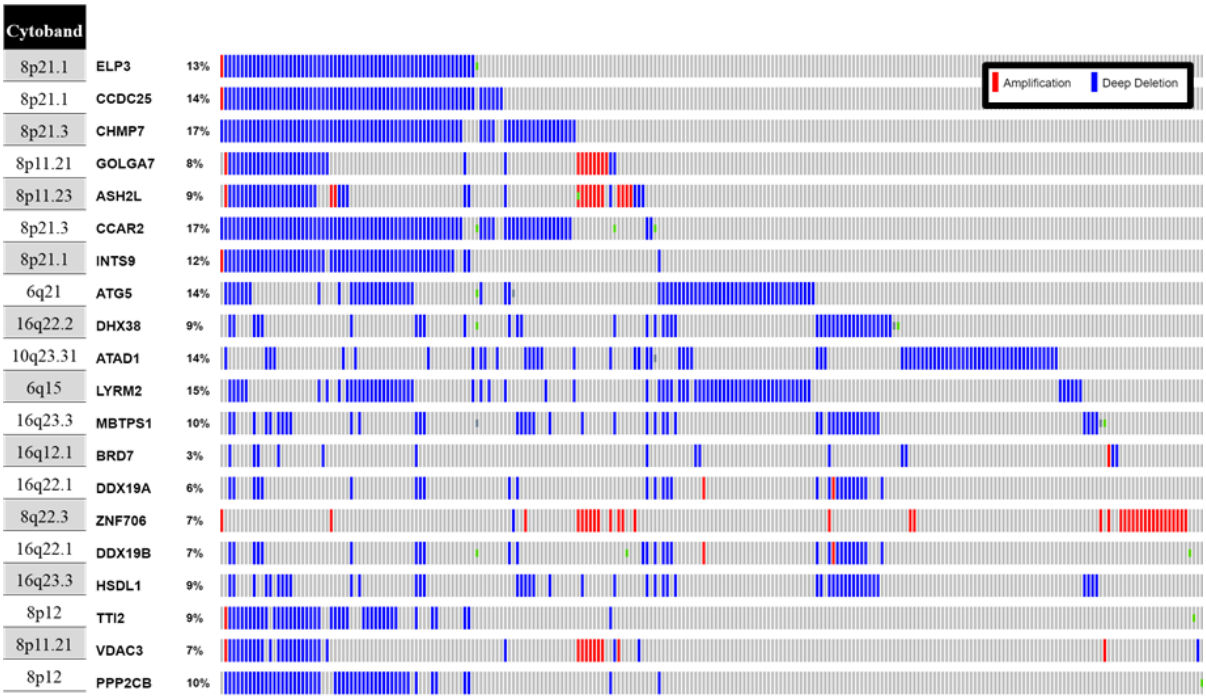

Figure 3.5. The top genes regulated by gene dosage and status in PRAD.

Gene Symbol	Cytoband	Correlation	Function	Relevent Pathway
ELP3	8p21.1	0.8665	Transcriptional Elongation	Histone Acetyltransferase
CCDC25	8p21.1	0.8467	Coiled Coil Domain	
CHMP7	8p21.3	0.8452	Spindle Dissasembly	Chromatin Remodeling
GOLGA7	8p11.21	0.8449	Golgi Transport	
ASH2L	8p11.23	0.8443	Histone Regulator	Histone Lysine Methyltransferase
CCAR2	8p21.3	0.8232	Transcriptional Elongation	Cell Cycle and Apoptosis
INTS9	8p21.1	0.8157	Transcriptional Regulator	RNA Processing
ATG5	6q21	0.8148	Autophagy and Apoptosis	Cell Response to Stress
DHX38	16q22.2	0.8094	DEAD box Helicase	RNA Helicase
ATAD1	10q23.31	0.7955	ATPase	
LYRM2	6q15	0.7943	Mitochondrial Protein	
MBTPS1	16q23.3	0.7874	Serine Protease	Protein Regulator
BRD7	16q12.1	0.7873	Chromatin Remodeling	p53-Dependent Senescence
DDX19A	16q22.1	0.787	DEAD box Helicase	mRNA Export
ZNF706	8q22.3	0.7813	Transcriptional Repressor	Gene Expression Regulator
DDX19B	16q22.1	0.78	DEAD box Helicase	mRNA Export
HSDL1	16q23.3	0.78	Hydroxysteroid Dehydrogenase	Oxidoreductase
TTI2	8p12	0.778	DNA Damage Response Regulator	DDR Resistance
VDAC3	8p11.21	0.777	Voltage-Dependent Anion Channel	Metabolism
PPP2CB	8p12	0.7759	Protein Phosphatase	Negative Regulator of Cell Division

Table 3.2. Top 20 genes with the highest Pearson's Correlation Coefficient in PRAD

We found that the 8p & 16q chromosomal regions were most enriched for genes regulated by CNV gene-dosage, including *WRN* along the chromosomal 8p arm. Pathway analysis suggests that these genes altered by CNV are involved in tumor promoting pathways such as WNT, PI3K and gene regulation, and many genes lost are involved in immune system activation, the cell cycle and the tp53 pathway. Further, I categorized key mPC drivers of progression with their gene-dosage correlation and significance, and illustrate that many driver genes of mPC progression may be transcriptionally regulated by CNV (Table 3.3).

Gene Symbol	Cytoband	Correlation	p-value	q-value
ASF1A	6q22.31	0.6245	0	0
TP53	17p13.1	0.5459	0	0
WRN	8p12	0.4884	0	0
EZH2	7q36.1	0.4264	0	0
CDK12	17q12	0.4249	0	0
RB1	13q14.2	0.4188	0	0
CHEK1	11q24.2	0.3746	0	0
ATR	3q23	0.3437	4.663E-15	6.004E-11
SIRT5	6p23	0.3082	2.899E-12	3.519E-08
RECQL4	8q24.3	0.2916	4.436E-11	5.224E-07
BRCA1	17q21.31	0.2896	6.099E-11	7.147E-07
LIG4	13q33.3	0.2835	1.59E-10	1.838E-06
SIRT1	10q21.3	0.2496	2.081E-08	0.0002227
SPOP	17q21.33	0.2384	9.004E-08	0.0009344
RECQL	12p12.1	0.2317	2.079E-07	0.002118
BRCA2	13q13.1	0.2152	1.556E-06	0.0150288
MYC	8q24.21	0.1761	8.777E-05	0.7410119

Table 3.3. Relevant driver genes to prostate cancer progression with significant gene dosage correlations.

Copy loss in key genetic regulators accelerates genome instability and tumor progression by the suppression of regulatory control, and may be a mechanistic explanation for the increased chromosomal aberrations and associated adverse outcomes frequently seen in advanced prostate cancer pathogenesis. As such, there is value to the further exploration of transcriptional control by CNV in mPC to broaden our understanding of disease progression.

3.2.2 Further expansion of LuCaP xenograft model characterization

Central to precision oncology is the expansion of knowledge of genetic subtypes and tumor models in order to better understand both intra-tumoral and intra-patient somatic heterogeneity. To further explore this somatic landscape, the LuCaP lines were generated from patient tumors propagated in immunocompromised mice as xenografts, where I then extracted and purified DNA libraries, and submitted them for whole exome and RNA sequencing. The samples were then analyzed for pathogenic variation, copy number alterations, fusions and mutational signatures to be distributed and utilized investigating specific molecular subtypes and their corresponding therapeutic sensitives.

Expanding the genomic characterization of this sample library is an essential step in understanding treatment response and resistance, as well as discovering novel subtypes that may be susceptible to new treatment strategies. To this end, I categorized transcriptional expression from RNAseq of the LuCaP tumors into key groups of cancer

driver pathways of prostate progression, to be used as a resource for future studies (Figure 3.6). Whole exome sequencing revealed many identified genes with recurrent aberrations, especially those involved in aspects of DNA repair, and a subset of samples exhibited a clear hypermutated phenotype (Figure 3.7). Full aberrational profiling is underway, with a greater number of tumors to expand the dataset, with the goal to eventually establish a more comprehensive profiling of the PDX genomic circuitry.

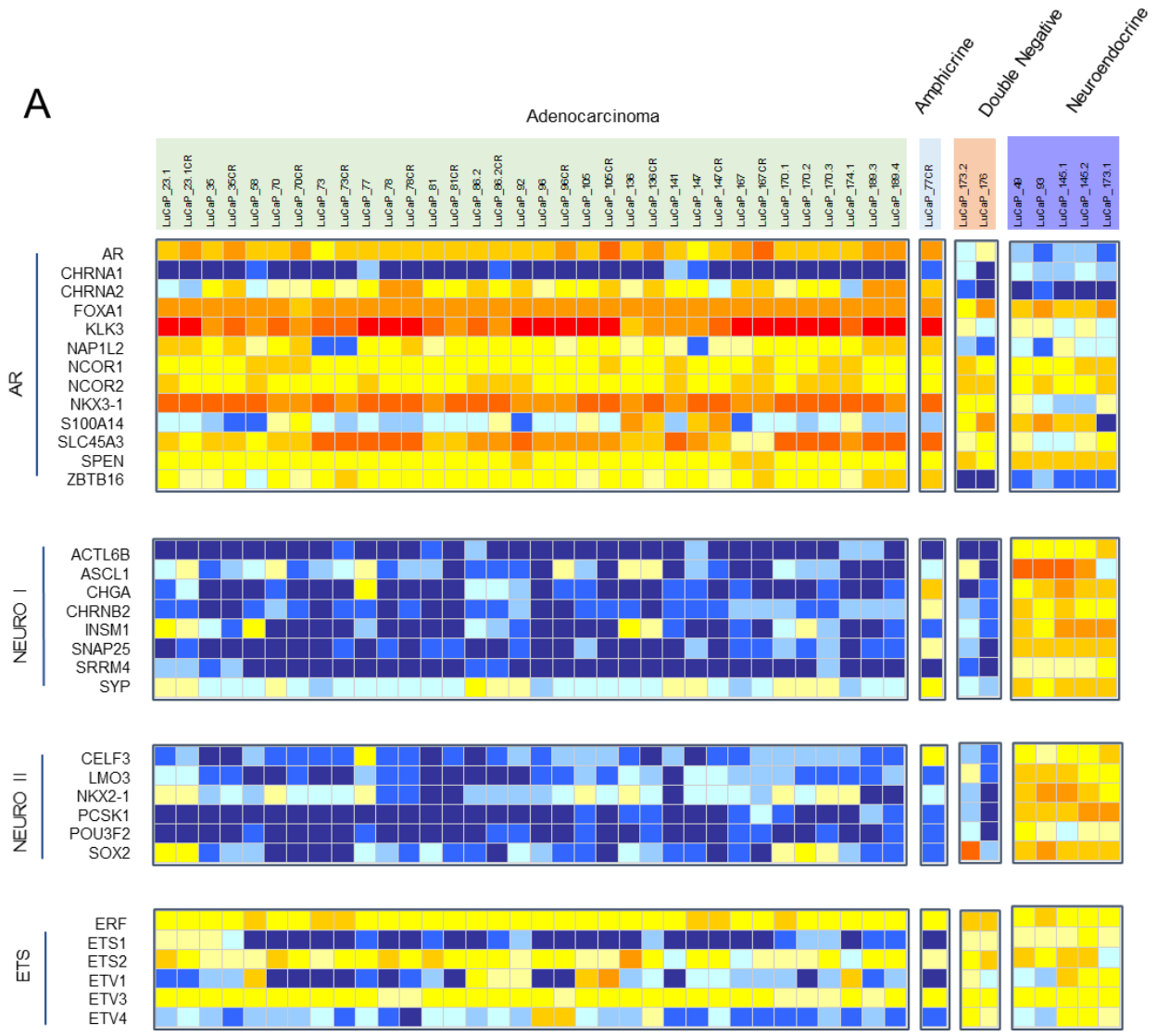
A
Adenocarcinoma
Amphicrine
Double Negative
Neuroendocrine
LuCaP_23.1
LuCaP_23.1CR
LuCaP_35
LuCaP_35CR
LuCaP_58
LuCaP_70
LuCaP_70CR
LuCaP_73
LuCaP_73CR
LuCaP_77
LuCaP_78
LuCaP_78CR
LuCaP_81
LuCaP_81CR
LuCaP_86.2
LuCaP_86.2CR
LuCaP_92
LuCaP_96
LuCaP_96CR
LuCaP_105
LuCaP_105CR
LuCaP_136
LuCaP_136CR
LuCaP_141
LuCaP_147
LuCaP_147CR
LuCaP_167
LuCaP_167CR
LuCaP_170.1
LuCaP_170.2
LuCaP_170.3
LuCaP_174.1
LuCaP_189.3
LuCaP_189.4
LuCaP_77CR
LuCaP_173.2
LuCaP_176
LuCaP_49
LuCaP_93
LuCaP_145.1
LuCaP_145.2
LuCaP_173.1
AR
AR
CHRNA1
CHRNA2
FOXA1
KLK3
NAP1L2
NCOR1
NCOR2
NKX3-1
S100A14
SLC45A3
SPEN
ZBTB16
NEURO I
ACTL6B
ASCL1
CHGA
CHRNB2
INSM1
SNAP25
SRRM4
SYP
NEURO II
CELF3
LMO3
NKX2-1
PCSK1
POU3F2
SOX2
ETS
ERF
ETS1
ETS2
ETV1
ETV3
ETV4

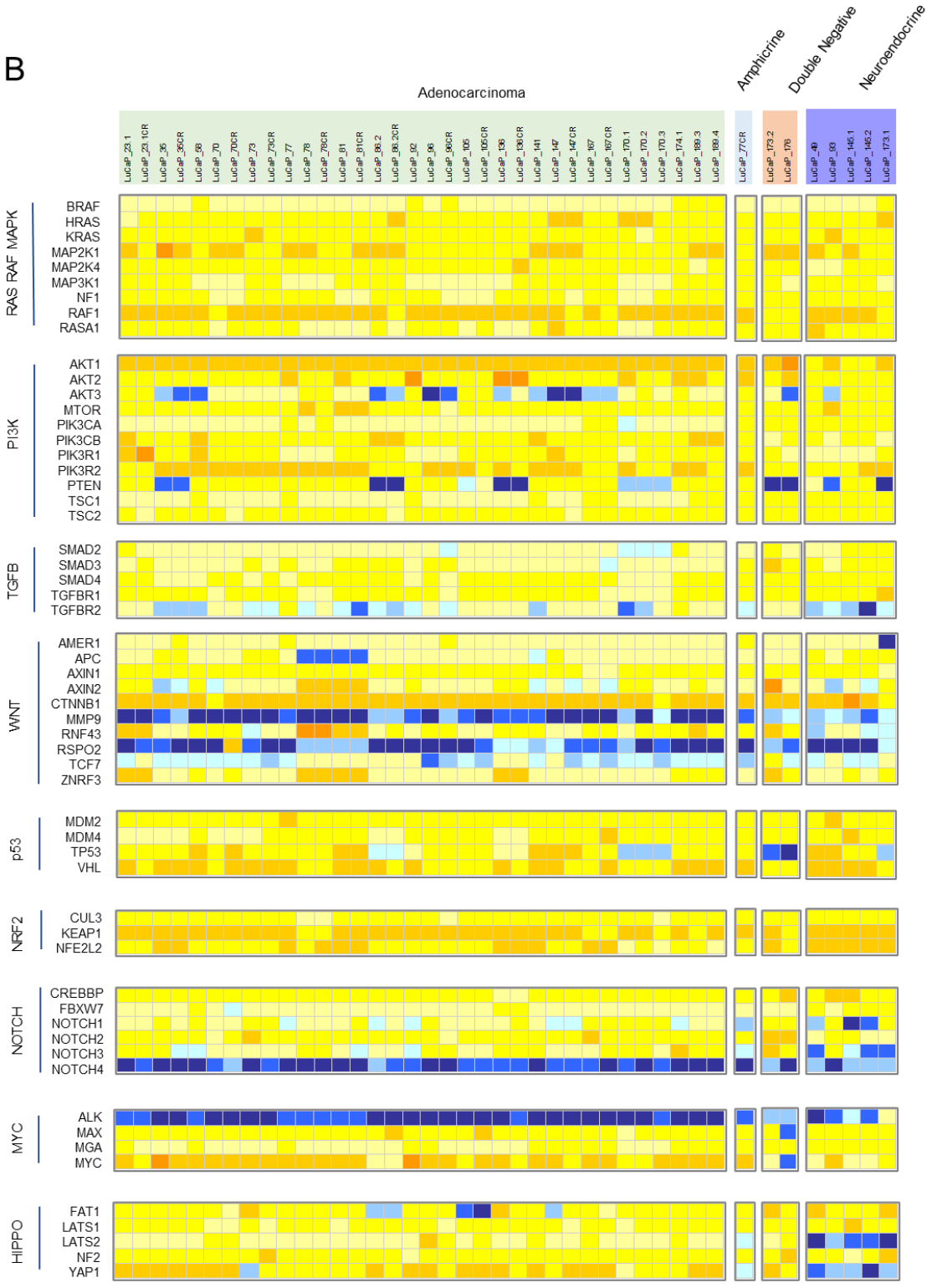
B
Adenocarcinoma
Amphicrine
Double Negative
Neuroendocrine
LuCaP_23.1
LuCaP_23.1CR
LuCaP_35
LuCaP_35CR
LuCaP_58
LuCaP_70
LuCaP_70CR
LuCaP_73
LuCaP_73CR
LuCaP_77
LuCaP_78
LuCaP_78CR
LuCaP_81
LuCaP_81CR
LuCaP_86.2
LuCaP_86.2CR
LuCaP_92
LuCaP_96
LuCaP_96CR
LuCaP_105
LuCaP_105CR
LuCaP_136
LuCaP_136CR
LuCaP_141
LuCaP_147
LuCaP_147CR
LuCaP_167
LuCaP_167CR
LuCaP_170.1
LuCaP_170.2
LuCaP_170.3
LuCaP_174.1
LuCaP_189.3
LuCaP_189.4
LuCaP_77CR
LuCaP_173.2
LuCaP_176
LuCaP_49
LuCaP_93
LuCaP_145.1
LuCaP_145.2
LuCaP_173.1
RAS RAF MAPK
BRAF
HRAS
KRAS
MAP2K1
MAP2K4
MAP3K1
NF1
RAF1
RASA1
PI3K
AKT1
AKT2
AKT3
MTOR
PIK3CA
PIK3CB
PIK3R1
PIK3R2
PTEN
TSC1
TSC2
TGFB
SMAD2
SMAD3
SMAD4
TGFBR1
TGFBR2
WNT
AMER1
APC
AXIN1
AXIN2
CTNNB1
MMP9
RNF43
RSPO2
TCF7
ZNRF3
p53
MDM2
MDM4
TP53
VHL
NRF2
CUL3
KEAP1
NFE2L2
NOTCH
CREBBP
FBXW7
NOTCH1
NOTCH2
NOTCH3
NOTCH4
MYC
ALK
MAX
MGA
MYC
HIPPO
FAT1
LATS1
LATS2
NF2
YAP1

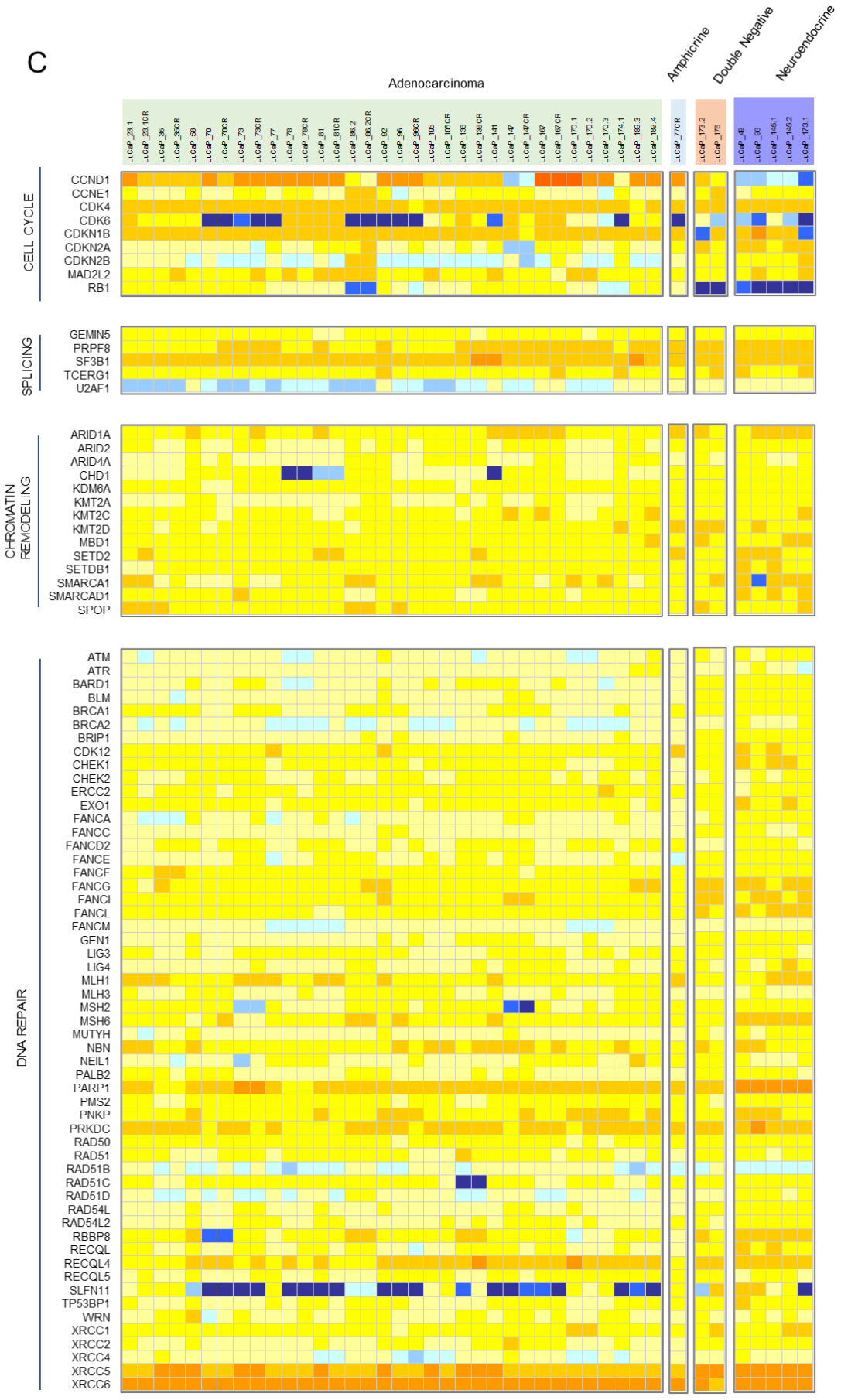
C
Adenocarcinoma
Amphicrine
Double Negative
Neuroendocrine
LuCaP_23.1
LuCaP_23.1CR
LuCaP_35
LuCaP_35CR
LuCaP_58
LuCaP_70
LuCaP_70CR
LuCaP_73
LuCaP_73CR
LuCaP_77
LuCaP_78
LuCaP_78CR
LuCaP_81
LuCaP_81CR
LuCaP_86.2
LuCaP_86.2CR
LuCaP_92
LuCaP_96
LuCaP_96CR
LuCaP_105
LuCaP_105CR
LuCaP_136
LuCaP_136CR
LuCaP_141
LuCaP_147
LuCaP_147CR
LuCaP_167
LuCaP_167CR
LuCaP_170.1
LuCaP_170.2
LuCaP_170.3
LuCaP_174.1
LuCaP_189.3
LuCaP_189.4
LuCaP_77CR
LuCaP_173.2
LuCaP_176
LuCaP_49
LuCaP_93
LuCaP_145.1
LuCaP_145.2
LuCaP_173.1
CELL CYCLE
CCND1
CCNE1
CDK4
CDK6
CDKN1B
CDKN2A
CDKN2B
MAD2L2
RB1
SPLICING
GEMIN5
PRPF8
SF3B1
TCERG1
U2AF1
CHROMATIN REMODELING
ARID1A
ARID2
ARID4A
CHD1
KDM6A
KMT2A
KMT2C
KMT2D
MBD1
SETD2
SETDB1
SMARCA1
SMARCAD1
SPOP
DNA REPAIR
ATM
ATR
BARD1
BLM
BRCA1
BRCA2
BRIP1
CDK12
CHEK1
CHEK2
ERCC2
EXO1
FANCA
FANCC
FANCD2
FANCE
FANCF
FANCG
FANCI
FANCL
FANCM
GEN1
LIG3
LIG4
MLH1
MLH3
MSH2
MSH6
MUTYH
NBN
NEIL1
PALB2
PARP1
PMS2
PNKP
PRKDC
RAD50
RAD51
RAD51B
RAD51C
RAD51D
RAD54L
RAD54L2
RBBP8
RECQL
RECQL4
RECQL5
SLFN11
TP53BP1
WRN
XRCC1
XRCC2
XRCC4
XRCC5
XRCC6

Figure 3.6. Characterization of onco-pathway expression in LuCaP PDX tumors.

(A) Transcriptional gene groups of drivers of prostate cancer progression (B) oncogenic transformation and (C) cell regulation and repair.

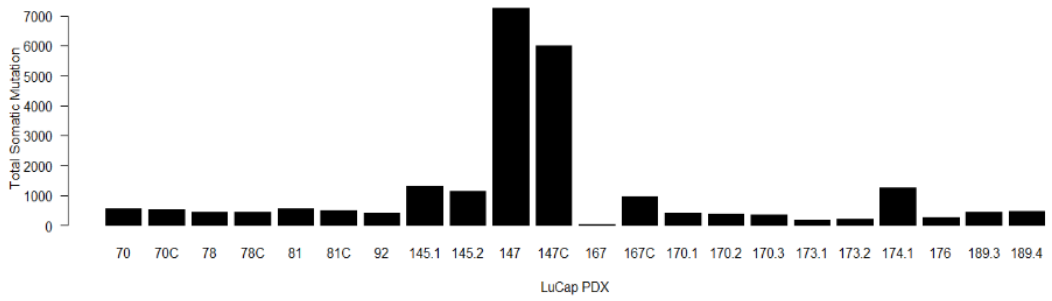

Figure 3.7. WES reveals hypermutated tumors within LuCaP PDX xenografts.

This generated exome dataset will allow us to discover novel drivers of cancer onset, map mutational variation throughout and between patients, highlight possible mechanisms of resistance and query how various genetic insults contribute to the surrounding genetic environment and ultimately disease progression.

Using a selection of excised LuCaP PDX tumors disassociated into single cells, I was able to demonstrate that available WRN inhibitor NSC 19630 was more effective reducing cell viability in DRD tumors, however this phenotype can be more deeply explored and expanded. Future research can further stratify LuCaP response by *WRN* and DNA repair gene status, and construct a more comprehensive panel of protein expression in order to better characterize this resource. To this end, we had variable success profiling WRN status via IHC of xenograft tumor slices and more work will be needed to establish concrete protein expression.

Future work will centralize on testing a broader sample set of LuCaPs with various iterations of WRN inhibitors; NSC 19630 was limited by its toxicity and more selective, less toxic, WRN inhibitors will need to be developed moving forward. It is likely that a greater subset of patient tumors could benefit from the development of WRN inhibiters, especially patients with homologous repair deficiency. We also were not able to test a larger drug panel on the xenografts, and associating treatment response to different therapeutics based on *WRN* status will be a key experiment moving forward.

3.2.3 Further development of WRN and MMRd knockdown cell models

The development of isogenic WRN and MSH2 knockdown cell models will allow for many future directions of research development. As *WRN* is lost clinically via a large chromosomal CNV, it will be imperative to compare *WRN* loss to 8p arm loss as a whole. Alternative methods such as CRISPR or TALEN gene editing could be applicable methodology to compare *WRN*-specific copy loss to a cell in comparison to entire 8p arm circuitry loss. These methods would also allow for “add-back” experimentation to determine if the rescue of gene expression reduces the observed cell death and senescent programming phenotypes in mPC cells.

Though we did not observe any universal augmentations of the effects of a specific drug to WRN loss, a more comprehensive drug screen panel will more thoroughly characterize any chemotherapeutic sensitivity caused by WRN knockdown. As MSI tumors are approved for anti-PD-1 treatment, the next step will be to test if WRN

knockdown alters susceptibility to available immune-therapeutics. To better translate WRN inhibitors to human tumors, future work will have to determine if WRN inhibitors synergize with the current standard of care for MSI tumors in order to bring less toxic, more effective treatment to patients.

WRN knockdown cell lines could also be further characterized by RNAseq, cell cycle phase analysis, markers of DNA damage and cell stress such as the TUNEL and COMET assay, as well as deeper analysis into the kinetics of stalled replication fork dynamics using DNA fibre. DNA fibre assays allow for quantifiable assessments of the DNA Helicase tracking and replication fork kinetics, and is a useful assay to visualize how the loss of replication fork proteins or exposure to fork-obstructing chemotherapeutics damage cellular DNA. I established a working DNA fibre assay to use for these future experiments on mPC cells, and specifically to quantify different means of replication fork dynamics post-WRN knockdown in control and MSI-high cells. This protocol will also be more widely applicable to research focusing on the mechanism of sensitivity or resistance to specific chemotherapeutics, and I demonstrate that method schematic using LNCaP cells grown in olaparib or carboplatin (Figure 3.8-3.9).

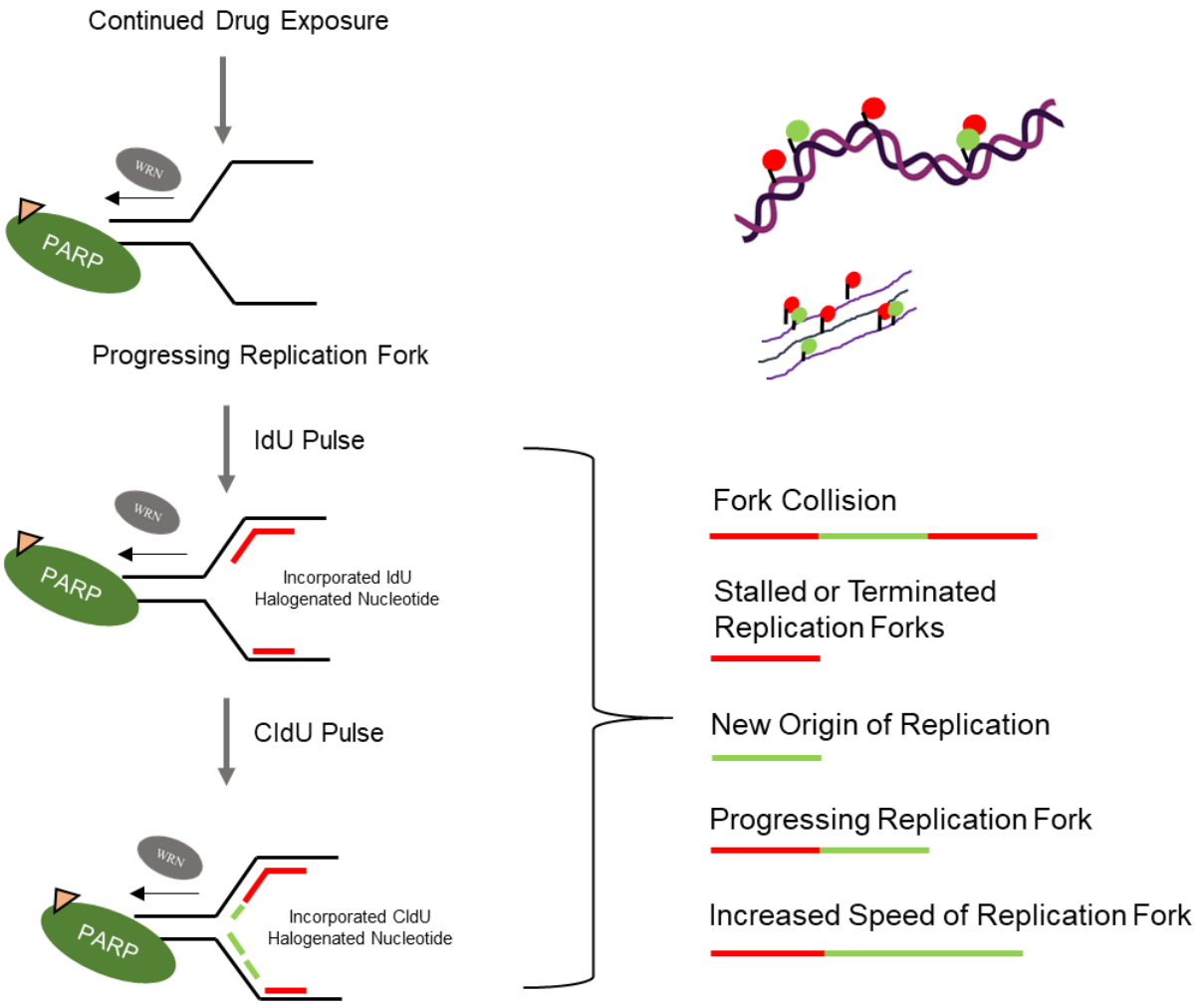

Figure 3.8. DNA fibre schematic for visualizing replication fork dynamics.

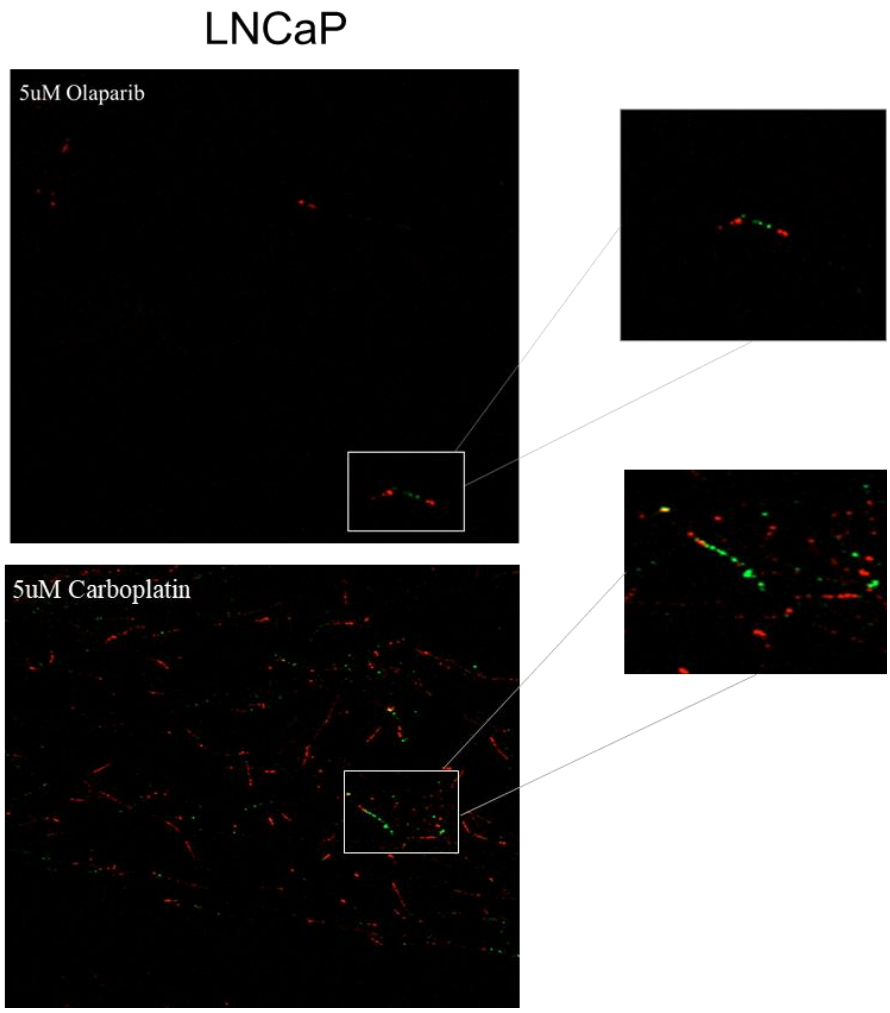

Figure 3.9. Replication fork collision and termination in LNCaP cells.

MSH2 has been established as the dominant driver of mismatch repair deficiency in mPC, and though we were able to successfully generate an isogenic knockdown cell line, we were unable to quantify the effect on mismatch repair capabilities. One such approach available utilizes fluorescent-tagged mismatch containing plasmids and allows for florescent output to be a by proxy measurement for mismatch repair capabilities[82]. This technology would be a useful assay to run on the MSH2 knockdown lines to

determine under what context MSH2, or other MMR proteins such as MLH1, impairs mismatch repair abilities.

Consistent with the observation that MSI-high mPC cell lines are not immediately effected to the same extent of synthetically lethality by WRN loss as observed in other cancers, it has been suggested that mPC may have an alternate MSI phenotype unique to the prostate. We have approached characterizing this novel phenotype of MSI mPC by preparing our selection of LuCaP tumors for MSI quantification via next generation analysis using mSINGS[83,84]. Further, we have generated LuCaP libraries for global methylation sequencing to determine alternate epigenetic signatures in both MSI as well as other models of DRD mPC. Once these assays and analyses are compete it will be useful to also run them on different passages of the MSH2 knockdown cells to quantify how loss of mismatch repair capabilities can drive genomic stress in a cancer cell. This dataset will expand the characterization of this model set, as well as explore novel avenues of disease progress and susceptibilities.

3.2.4 G4 DNA as a transcriptional regulator

Though we are the first to propose G4 DNA as a mechanism of MSI susceptibility to WRN loss, we are not the first to explore the functionality of G4 DNA as a transcriptional regulator. Genome-wide mapping has found G-quadruplexes to be enriched at regulatory sites such as oncogene promoters, key TSS and 5'UTRs, and alongside DNA methylation and histone modification, are features that regulate gene expression and genome function. Characterizing the epigenomic landscape has

increased our understanding of advanced disease, and incorporating G4-based ChIP-seq assays on mPC samples to globally map where the G-quadruplexes are would be a key next step to understanding how DNA secondary structures might regulate gene expression in mPC.

To investigate if WRN-mediated G4 DNA at transcription start sites (TSS) were present at any genes of prostate cancer progression, I compiled the previously curated gene list by Tang et al. of genes with G4 motifs near the TSS that overlapped in both Werner syndrome fibroblasts and WRN knockdown cells[69] (Figure 3.10-3.11). Using a similar methodology, I then utilized available mPC data from the SU2C dataset to generate a list of genes that were significantly transcriptionally co-expressed (positive linear correlation) with WRN. Excluding genes along the 8p locus that are co-homozygous deleted alongside *WRN*, this list was then compared to the aforementioned list of genes regulated by WRN-mediated G4 DNA near TSS (Figure 3.12).

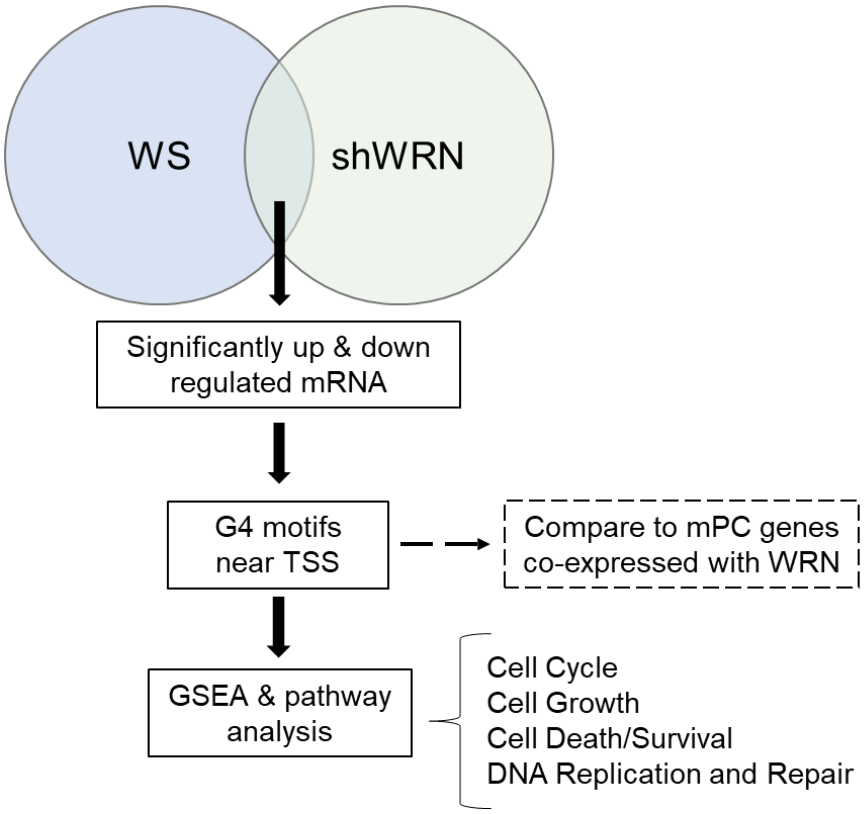

Figure 3.10. Establishing WRN transcriptional regulation by G4-motif resolution.

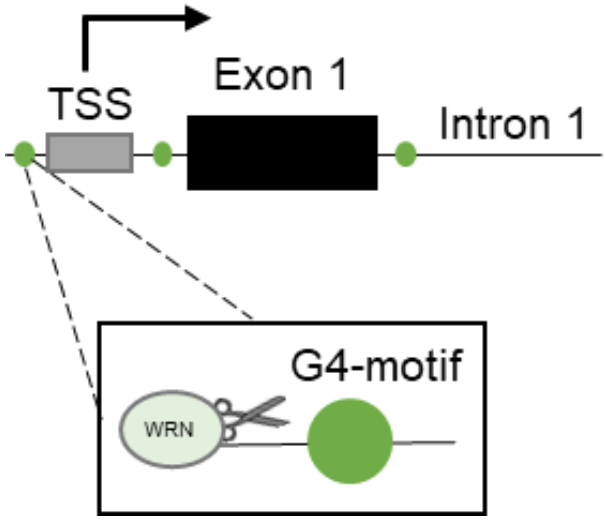

Figure 3.11. Mechanism of WRN mediated G4-motif resolution.

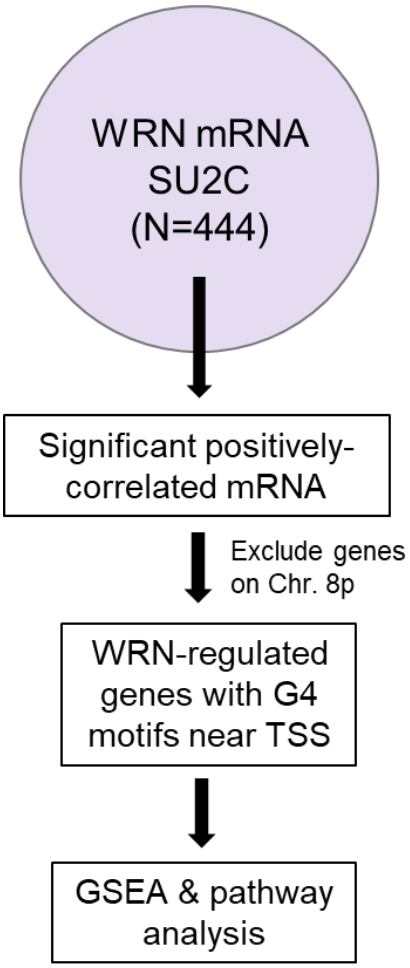

Figure 3.12. Determining WRN-regulated targets of transcriptional in mPC.

From this gene set, there were 42 genes that were previously determined to be WRN-regulated by the resolution of G4 DNA at the TSS, and are also possible candidates for WRN-transcriptional regulation by G4 mediation in mPC (Figure 3.13). Running GSEA pathway enrichment analysis (www.gsea-msigdb.org/) on these 42 genes indicated an overlap in cell pathways such as the cell cycle, cell growth and DNA replication (Table 3.4).

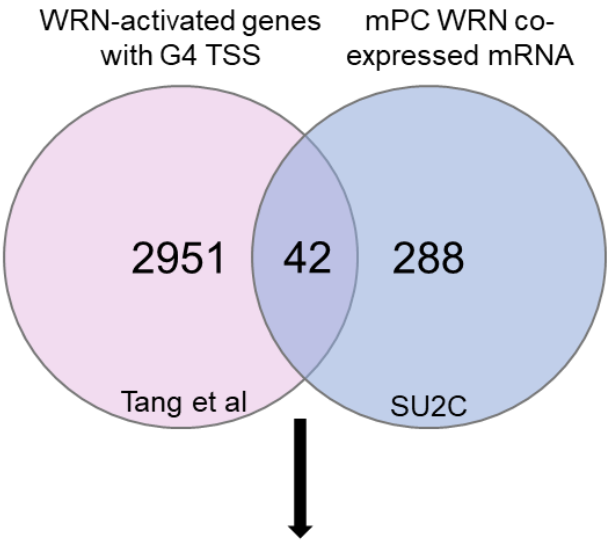

ACADM	CCP110	COMMD8	FANCI	KIF14	NCAPG
ARAP2	CENPE	DEPDC1	FBXO5	KIF20B	NCAPG2
BARD1	CENPF	DLGAP5	FERMT2	KIF23	NDUFB5
CASP3	CENPI	DONSON	GMNN	LBR	NREP
CCDC88A	CENPL	ECT2	HAUS4	MELK	PARPBP
CCNA2	CKLF	EIF5A2	HMGB2	METTL2B	PCID2
CCNB2	COG2	EZH2	INPP5B	MTG1	

Figure 3.13. G4 regulated genes in mPC.

Pathway	P value	Ratio
Cell Cycle	1.22E-16	15/693 (0.0216)
Cell Cycle, Mitotic	2.17E-16	14/561 (0.025)
M Phase	7.73E-15	12/417 (0.0288)
Mitotic Prometaphase	2.98E-11	8/203 (0.0394)
Signaling by Rho GTPases, Miro GTPases and RHOBTB3	1.02E-10	11/717 (0.0153)
Mitotic Metaphase and Anaphase	4.09E-09	7/236 (0.0297)
Cell Cycle Checkpoints	1.77E-08	7/292 (0.024)
Resolution of Sister Chromatid Cohesion	1.89E-07	5/126 (0.0397)
RHO GTPase cycle	3.05E-07	7/444 (0.0158)
Mitotic G2-G2/M phases	1.85E-06	5/200 (0.025)

Table 3.4. Top Canonical GSEA pathways of 42 WRN-regulated genes with G4-motifs near the transcription start site.

These results suggest a promising new avenue of gene regulation by the resolution of DNA secondary structures, such as G-quadruplexes, by replication fork moderators like WRN. We have demonstrated that G4 DNA can be detected via confocal microscopy and are enriched in MSI cancer cell lines, and future research will translate these findings into human samples and assess the potential of G4 DNA as a biomarker histopathologically. It will also be imperative to explore the applicability of G4-targeting pyridostatin or telomestatin in a greater range of tumors, especially other subtypes of DRD. Investigating G4 DNA enrichment in patient samples as a potential biomarker, target for drugs such as pyridostatin and target for TSS regulation will be central avenue to explore for potential novel to therapeutic development.

3.3 Conclusion

This body of work addresses the unmet need to characterize the DNA helicase WRN in metastatic prostate cancer patients and cell lines. *WRN* is lost via homozygous deletion in ~10% of prostate cancers, alongside many genes on chromosome 8p, and we address here for the first time the clinical outcomes associated with *WRN*-specific homozygous deletion in metastatic prostate cancers. Importantly, *WRN*-deletion does not co-occur in the same tumors with mismatch repair loss or MSI, and future WRN inhibitor development should focus on targeting the WRN protein in those tumors. To that end, MSI mPC cell lines are also sensitive to WRN loss, despite not demonstrating initial synthetic lethality as seen in other tumor types, and should not be excluded from future studies investigating WRN therapeutic targeting in MSI solid tumors. Though this mechanism of synthetic lethality between WRN and MSI-cell lines is still being explored at the time of writing, we present initial evidence that GC-region forming DNA secondary structures, G-quadruplexes, are targets of the WRN protein to resolve, and contribute to the lethal accumulation of genomic stress leading to cell death in MSI cells. G-quadruplex DNA structures also present a promising target for chemotherapeutics such as pyridostatin, especially in MSI and DRD tumor lines. In all, this research increases our understanding of DNA repair deficient diseases and tumor heterogeneity, and aims to help patients have access to better treatment strategies for personalized tumor treatment.

References

1. Attard, G. *et al. Prostate cancer*. *The Lancet* vol. 387 (Lancet Publishing Group, 2016).
2. Ku, S.-Y., Gleave, M. E. & Beltran, H. Towards precision oncology in advanced prostate cancer. *Nature Reviews Urology* (2019) doi:10.1038/s41585-019-0237-8.
3. Abida, W. *et al.* Genomic correlates of clinical outcome in advanced prostate cancer. *Proc Natl Acad Sci USA* **116**, 11428–11436 (2019).
4. Robinson, D. *et al.* Integrative Clinical Genomics of Advanced Prostate Cancer. *Cell* **161**, 1215–1228 (2015).
5. Armenia, J. *et al.* The long tail of oncogenic drivers in prostate cancer. *Nat. Genet.* **50**, 645–651 (2018).
6. Cheng, H. H., Pritchard, C. C., Boyd, T., Nelson, P. S. & Montgomery, B. Biallelic Inactivation of BRCA2 in Platinum-sensitive Metastatic Castration-resistant Prostate Cancer. *European Urology* **69**, 992–995 (2016).
7. Tryggvadottir, L. *et al.* Prostate Cancer Progression and Survival in BRCA2 Mutation Carriers. *JNCI Journal of the National Cancer Institute* **99**, 929–935 (2007).
8. van Dessel, L. F. *et al.* The genomic landscape of metastatic castration-resistant prostate cancers reveals multiple distinct genotypes with potential clinical impact. *Nat Commun* **10**, 5251 (2019).
9. Mateo, J. *et al.* DNA Repair in Prostate Cancer: Biology and Clinical Implications. *European Urology* **71**, 417–425 (2017).
10. Mateo, J. *et al.* DNA-Repair Defects and Olaparib in Metastatic Prostate Cancer. *N Engl J Med* **373**, 1697–1708 (2015).

11. de Bono, J. *et al.* Olaparib for Metastatic Castration-Resistant Prostate Cancer. *N Engl J Med* **382**, 2091–2102 (2020).

12. Helleday, T. The underlying mechanism for the PARP and BRCA synthetic lethality: Clearing up the misunderstandings. *Molecular Oncology* **5**, 387–393 (2011).

13. Lebel, M. & Leder, P. A deletion within the murine Werner syndrome helicase induces sensitivity to inhibitors of topoisomerase and loss of cellular proliferative capacity. *Proceedings of the National Academy of Sciences of the United States of America* **95**, 13097–102 (1998).

14. Lebel, M. & Monnat, R. J. Werner syndrome (WRN) gene variants and their association with altered function and age-associated diseases. *Ageing Research Reviews* **41**, 82–97 (2018).

15. Dhillon, K. K. *et al.* Functional role of the Werner syndrome RecQ helicase in human fibroblasts. *Aging Cell* **6**, 53–61 (2007).

16. Sidorova, J. M., Li, N., Folch, A. & Monnat, Jr., R. J. The RecQ helicase WRN is required for normal replication fork progression after DNA damage or replication fork arrest. *Cell Cycle* **7**, 796–807 (2008).

17. Agrelo, R. *et al.* Epigenetic inactivation of the premature aging Werner syndrome gene in human cancer. *Proceedings of the National Academy of Sciences of the United States of America* **103**, 8822–8827 (2006).

18. Chughtai, S. A. *et al.* Two novel regions of interstitial deletion on chromosome 8p in colorectal cancer. *Oncogene* **18**, 657–665 (1999).

19. Armes, J. E. *et al.* Candidate tumor-suppressor genes on chromosome arm 8p in early-onset and high-grade breast cancers. *Oncogene* **23**, 5697–5702 (2004).

20. Lutchman, M. *et al.* Loss of heterozygosity on 8p in prostate cancer implicates a role for dematin in tumor progression. *Cancer Genetics and Cytogenetics* **115**, 65–69 (1999).

21. El Gammal, A. T. *et al.* Chromosome 8p deletions and 8q gains are associated with tumor progression and poor prognosis in prostate cancer. *Clinical Cancer Research* **16**, 56–64 (2010).

22. Kluth, M. *et al.* Genomic deletion of chromosome 8p is an independent prognostic marker in prostate cancer. *Oncotarget* **6**, 27966–79 (2015).

23. Cai, Y. *et al.* Loss of Chromosome 8p Governs Tumor Progression and Drug Response by Altering Lipid Metabolism. *Cancer Cell* **29**, 751–766 (2016).

24. Masuda, K. *et al.* Association of epigenetic inactivation of the WRN gene with anticancer drug sensitivity in cervical cancer cells. *Oncology Reports* **28**, 1146–1152 (2012).

25. Shamanna, R. A. *et al.* Camptothecin targets WRN protein: mechanism and relevance in clinical breast cancer. *Oncotarget* **7**, 13269–13284 (2016).

26. Bosch, L. J. W. *et al. WRN* Promoter CpG Island Hypermethylation Does Not Predict More Favorable Outcomes for Patients with Metastatic Colorectal Cancer Treated with Irinotecan-Based Therapy. *Clin Cancer Res* **22**, 4612–4622 (2016).

27. Aggarwal, M., Sommers, J. A., Shoemaker, R. H. & Brosh, R. M. Inhibition of helicase activity by a small molecule impairs Werner syndrome helicase (WRN) function in the cellular response to DNA damage or replication stress. *Proceedings of the National Academy of Sciences* **108**, 1525–1530 (2011).

28. Aggarwal, M. *et al.* Targeting an Achilles ' heel of cancer with a WRN helicase inhibitor Targeting an Achilles ' heel of cancer with a WRN helicase inhibitor. **4101**, 3329–3335 (2016).

29. Chan, E. M. *et al.* WRN Helicase is a Synthetic Lethal Target in Microsatellite Unstable Cancers HHS Public Access. *Nature* **568**, 551–556 (2019).

30. Kategaya, L., Perumal, S. K., Hager, J. H. & Belmont, L. D. Werner Syndrome Helicase Is Required for the Survival of Cancer Cells with Microsatellite Instability. *iScience* **13**, 488–497 (2019).

31. Lieb, S. *et al.* Werner syndrome helicase is a selective vulnerability of microsatellite instability-high tumor cells. *Elife* **8**, (2019).

32. van Wietmarschen, N. *et al.* Repeat expansions confer WRN dependence in microsatellite-unstable cancers. *Nature* **586**, 292–298 (2020).

33. Graham, L. S. *et al.* Mismatch repair deficiency in metastatic prostate cancer: Response to PD-1 blockade and standard therapies. *PLoS ONE* **15**, e0233260 (2020).

34. Robinson, D. *et al.* Integrative Clinical Genomics of Advanced Prostate Cancer. *Cell* **162**, 454 (2015).

35. Ross-Adams, H. *et al.* Integration of copy number and transcriptomics provides risk stratification in prostate cancer: A discovery and validation cohort study. *EBioMedicine* **2**, 1133–1144 (2015).

36. Mateo, J. *et al.* Olaparib in patients with metastatic castration-resistant prostate cancer with DNA repair gene aberrations (TOPARP-B): a multicentre, open-label, randomised, phase 2 trial. *The Lancet Oncology* **21**, 162–174 (2020).

37. Macoska, J. A. *et al.* Evolution of 8p loss in transformed human prostate epithelial cells. *Cancer Genetics and Cytogenetics* **154**, 36–43 (2004).

38. Chaib, H. *et al.* Haploinsufficiency and reduced expression of genes localized to the 8p chromosomal region in human prostate tumors. *Genes Chromosom. Cancer* **37**, 306–313 (2003).

39. Luo, J. WRN protein and Werner syndrome. *N Am J Med Sci (Boston)* **3**, 205–207 (2010).

40. Julia M Sidorova1,&, Keffy Kehrli1, Frances Mao1,*, and Raymond Monnat Jr1, 2. Distinct functions of human RECQ helicases WRN and BLM in replication fork recovery and progression after hydroxyureainduced stalling. **12**, 128–139 (2013).

41. Zimmer, K. *et al.* WRN-Mutated Colorectal Cancer Is Characterized by a Distinct Genetic Phenotype. *Cancers* **12**, 1319 (2020).

42. Grady, L. B. R. M. W. WRn promoter cpg hypermethylation does not predict more favorable outcomes for mCRC patients. **22**, 1–23 (2017).

43. Chan, E. M. *et al. WRN helicase is a synthetic lethal target in microsatellite unstable cancers*. *Nature* vol. 568 (Nature Publishing Group, 2019).

44. Lieb, S. *et al.* Werner syndrome helicase is a selective vulnerability of microsatellite instability high tumor cells. *bioRxiv* 530659 (2019) doi:10.1101/530659.

45. Gao, J. *et al.* Integrative Analysis of Complex Cancer Genomics and Clinical Profiles Using the cBioPortal. *Science Signaling* **6**, pl1–pl1 (2013).

46. Cerami, E. *et al.* The cBio Cancer Genomics Portal: An Open Platform for Exploring Multidimensional Cancer Genomics Data: Figure 1. *Cancer Discovery* **2**, 401–404 (2012).

47. Ciriello, G., Cerami, E., Sander, C. & Schultz, N. Mutual exclusivity analysis identifies oncogenic network modules. *Genome Research* **22**, 398–406 (2012).

48. Bluemn, E. G. *et al.* Androgen Receptor Pathway-Independent Prostate Cancer Is Sustained through FGF Signaling. *Cancer Cell* **32**, 474-489.e6 (2017).

49. Labrecque, M. P. *et al.* Cabozantinib can block growth of neuroendocrine prostate cancer patient-derived xenografts by disrupting tumor vasculature. *PLoS ONE* **16**, e0245602 (2021).

50. Nguyen, H. M. *et al.* LuCaP Prostate Cancer Patient-Derived Xenografts Reflect the Molecular Heterogeneity of Advanced Disease an--d Serve as Models for Evaluating Cancer Therapeutics. *Prostate* **77**, 654–671 (2017).

51. Chatterjee, P. *et al.* Supraphysiological androgens suppress prostate cancer growth through androgen receptor–mediated DNA damage. *Journal of Clinical Investigation* **129**, 4245–4260 (2019).

52. Nyquist, M. D. *et al.* Combined TP53 and RB1 Loss Promotes Prostate Cancer Resistance to a Spectrum of Therapeutics and Confers Vulnerability to Replication Stress. *Cell Reports* **31**, 107669 (2020).

53. Luchini, C. *et al.* ESMO recommendations on microsatellite instability testing for immunotherapy in cancer, and its relationship with PD-1/PD-L1 expression and tumour mutational burden: a systematic review-based approach. *Annals of Oncology* **30**, 1232–1243 (2019).

54. Moles, R., Bai, X. T., Chaib-Mezrag, H. & Nicot, C. WRN-targeted therapy using inhibitors NSC 19630 and NSC 617145 induce apoptosis in HTLV-1-transformed adult T-cell leukemia cells. *Journal of Hematology and Oncology* **9**, 1–11 (2016).

55. Pritchard, C. C. *et al.* Complex MSH2 and MSH6 mutations in hypermutated microsatellite unstable advanced prostate cancer. *Nature Communications* **5**, 4988 (2014).

56. Kategaya, L., Perumal, S. K., Hager, J. H. & Belmont, L. D. Werner Syndrome Helicase Is Required for the Survival of Cancer Cells with Microsatellite Instability. *iScience* **13**, 488–497 (2019).

57. de la Chapelle, A. & Hampel, H. Clinical Relevance of Microsatellite Instability in Colorectal Cancer. *JCO* **28**, 3380–3387 (2010).

58. Oki, E., Oda, S., Maehara, Y. & Sugimachi, K. Mutated gene-specific phenotypes of dinucleotide repeat instability in human colorectal carcinoma cell lines deficient in DNA mismatch repair. *Oncogene* **18**, 2143–2147.

59. Kim, T.-M., Laird, P. W. & Park, P. J. The Landscape of Microsatellite Instability in Colorectal and Endometrial Cancer Genomes. *Cell* **155**, 858–868 (2013).

60. The Cancer Genome Atlas Research Network. Comprehensive molecular characterization of gastric adenocarcinoma. *Nature* **513**, 202–209 (2014).

61. Abida, W. *et al.* Analysis of the Prevalence of Microsatellite Instability in Prostate Cancer and Response to Immune Checkpoint Blockade. *JAMA Oncology* **5**, 471 (2019).

62. Hause, R. J., Pritchard, C. C., Shendure, J. & Salipante, S. J. Classification and characterization of microsatellite instability across 18 cancer types. *Nat Med* **22**, 1342–1350 (2016).

63. Boyiadzis, M. M. *et al.* Significance and implications of FDA approval of pembrolizumab for biomarker-defined disease. *J Immunother Cancer* **6**, (2018).

64. Wu, T.-H. *et al. Durable response to programmed death-1 (PD-1) blockade in a metastatic gastric cancer patient with mismatch repair deficiency and microsatellite instability* | *Elsevier Enhanced Reader*. *Journal of Cancer Research and Practice* (2017).

65. Le, D. T. *et al.* PD-1 Blockade in Tumors with Mismatch-Repair Deficiency. *New England Journal of Medicine* **372**, 2509–2520 (2015).

66. Hart, T., Brown, K. R., Sircoulomb, F., Rottapel, R. & Moffat, J. Measuring error rates in genomic perturbation screens: gold standards for human functional genomics. *Mol. Syst. Biol.* **10**, 733 (2014).

67. Yu, J. S. L. & Yusa, K. Genome-wide CRISPR-Cas9 screening in mammalian cells. *Methods* **164–165**, 29–35 (2019).

68. Ghandi, M. *et al.* Next-generation characterization of the Cancer Cell Line Encyclopedia. *Nature* **569**, 503–508 (2019).

69. Tang, W. *et al.* The Werner syndrome RECQ helicase targets G4 DNA in human cells to modulate transcription. *Hum. Mol. Genet.* **25**, 2060–2069 (2016).

70. Henderson, A. *et al.* Detection of G-quadruplex DNA in mammalian cells. *Nucleic Acids Research* **42**, 860–869 (2014).

71. Nishikawa, T., Kuwano, Y., Takahara, Y., Nishida, K. & Rokutan, K. HnRNPA1 interacts with G-quadruplex in the TRA2B promoter and stimulates its transcription in human colon cancer cells. *Scientific Reports* **9**, 1–13 (2019).

72. Wu, W. *et al.* HERC2 facilitates BLM and WRN helicase complex interaction with RPA to suppress G-quadruplex DNA. *Cancer Research* **78**, 6371–6385 (2018).

73. Yamamoto, H. & Imai, K. Microsatellite instability: an update. *Arch Toxicol* **89**, 899–921 (2015).

74. Lee, K., Tosti, E. & Edelmann, W. Mouse models of DNA mismatch repair in cancer research. *DNA Repair* 7 (2016).

75. Verma, R., Agarwal, A. K., Sakhuja, P. & Sharma, P. C. Microsatellite instability in mismatch repair and tumor suppressor genes and their expression profiling provide important targets for the development of biomarkers in gastric cancer. *Gene* **710**, 48–58 (2019).

76. Antonarakis, E. S. *et al.* Clinical Features and Therapeutic Outcomes in Men with Advanced Prostate Cancer and DNA Mismatch Repair Gene Mutations. *European Urology* **75**, 378–382 (2019).

77. Negrini, S., Gorgoulis, V. G. & Halazonetis, T. D. Genomic instability — an evolving hallmark of cancer. *Nat Rev Mol Cell Biol* **11**, 220–228 (2010).

78. Sansregret, L., Vanhaesebroeck, B. & Swanton, C. Determinants and clinical implications of chromosomal instability in cancer. *Nat Rev Clin Oncol* **15**, 139–150 (2018).

79. Hieronymus, H. *et al.* Tumor copy number alteration burden is a pan-cancer prognostic factor associated with recurrence and death. *eLife* **7**, e37294 (2018).

80. Wang, X. *et al.* Copy number alterations are associated with metastatic-lethal progression in prostate cancer. *Prostate Cancer Prostatic Dis* **23**, 494–506 (2020).

81. Xu, H. *et al.* CX-5461 is a DNA G-quadruplex stabilizer with selective lethality in BRCA1/2 deficient tumours. *Nature Communications* **8**, (2017).

82. Ito, S. *et al.* Fluorescence detection of DNA mismatch repair in human cells. *Scientific Reports* **8**, 1–9 (2018).

83. Hempelmann, J. A. *et al.* Microsatellite instability in prostate cancer by PCR or next-generation sequencing. *Journal for ImmunoTherapy of Cancer* **6**, 1–7 (2018).

84. Adam Waalkes, Nahum Smith, Kelsi Penewit, Jennifer Hempelmann, E. Q. K., Ronald J. Hause, Colin C. Pritchard & Salipante, S. J. Accurate pan-cancer molecular diagnosis of microsatellite instability by single molecule molecular inversion probe capture and high throughput sequencing. *Clin Chem* **64**, 950–958 (2018).